

© Anthony Selorm Kwesi Amable
University of Cape Coast

UNIVERSITY OF CAPE COAST

INVESTIGATIONS OF NATURAL RADIOACTIVITY, RADON LEVELS,
AND SOIL PROPERTIES IN KPANDO MUNICIPALITY, VOLTA
REGION, GHANA

BY

ANTHONY SELORM KWESI AMABLE

This thesis submitted to the Department of Physics of the School of Physical Sciences, College of Agricultural and Natural Sciences, University of Cape Coast, in partial fulfilment of the requirements for the award of Doctor of Philosophy degree in Physics

AUGUST 2023

DECLARATION

Candidate's Declaration

I hereby declare that this thesis is the result of my own original research and that no part of it has been presented for another degree in this university or elsewhere.

Candidate's Signature: Date:

Name: Anthony Selorm Kwesi Amable

Supervisors' Declaration

We hereby declare that the preparation and presentation of the thesis were supervised in accordance with the guidelines on supervision of thesis laid down by the University of Cape Coast.

Principal Supervisor's Signature:..... Date:.....

Name: Prof. Paul Buah – Bassuah

Co-Supervisor's Signature:..... Date:.....

Name: Dr. Francis Otoo

Co-Supervisor's Signature: Date:.....

Name: Prof. Anthony Kwabena Twum

ABSTRACT

This study measured natural radioactivity, indoor radon, radon exhalation rate and soil properties in the Kpando Municipality of Volta Region, Ghana. 120 dwellings, and 51 soil samples from Torkor, Agbenoxoe and Tsakpa in the Kpando Municipal were studied for indoor radon, radon exhalation rates, radionuclides and soil properties using CR – 39 detectors, gamma spectrometry and Gravimetric techniques. The radionuclides and radiation hazards associated with soil samples were found to vary as: ^{226}Ra (2.80 to 53.30 Bq/kg), ^{232}Th (3.40 to 58.80 Bq/kg), ^{40}K (62.70 to 421.60 Bq/kg), indoor absorbed dose rate (13.72 to 138.45 nGy/h), indoor effective doses (67.37 to 679.77 $\mu\text{Sv/y}$) and indoor excess lifetime cancer risk (0.24×10^{-3} to 2.38×10^{-3}). The radon exhalation varied from 1.00×10^{-5} to 15.00×10^{-5} Bq/m²h and the soil properties ranged from 1.11 to 1.66 Mg/m³ (bulk density), 0.10 to 0.65 (soil porosity), 6.00 to 19.00 % (moisture content), 30.21 to 52.00 % (silt), 35.00 to 55.00 % (sand) and 0.01 to 34.79 % (clay). The annual indoor radon concentrations in homes ranged from 23.50 Bq m⁻³ to 124.90 Bq m⁻³, the mean seasonal indoor radon levels are 60.54 ± 6.49 Bq/m³ (dry season), 63.85 ± 6.28 Bq/m³ (rainy season) with seasonal radon correction factors varying from 0.51 to 1.55. The results show that, soil properties have influence on the soil radionuclides and indoor radon. The results of Pearson's linear correlation analysis were in line with principal component analysis and cluster analysis. The findings of this studies are within the recommended limits proposed by International Commission on Radiological Protection, United Nations Scientific Committee on the Effects of Atomic Radiation and World Health Organization. Therefore, soil from these areas is safe and can be used as a construction material without posing any significant radiological threat to the population.

KEY WORDS

CR-39

HPGe

Indoor radon

Natural radioactivity

Seasonal variation

Soil properties



ACKNOWLEDGEMENTS

God alone is worthy of all the glory because He provided me with the strength and health, I needed to finish this study. To my supervisor, Prof. Paul Buah-Bassuah (UCC, Department of Physics), Dr. Francis Otoo (GAEC, RPI), and Prof. Anthony Twum (UCC, Department of Physics), I owe an immense debt of gratitude for all the support, advice and encouragement, they gave me as I worked to finish this major task. My heartfelt gratitude also goes to the Physics Department at UCC for their regular seminars (Dr. Peter Osei – Wusu Adueming, Prof. George Amoako – Head of Physics Department, Prof. Raymond Edziah, Prof. Benjamin Anderson and other lecturers), advice, encouragement, and the opportunity to pursue my studies.

For their help with the time-consuming tasks of installing and removing CR – 39 detectors and collecting soil samples in the investigated areas, I owe a great debt to Mr. Nicholas M. Gborse and Godwin Modzaka and, assemblymen and chiefs. The staff at the Radiation Protection Institute, GAEC, especially Madam Rita Kporzro and, Joseph Andoh at Soil Research Institute (CSIR, Accra), were extremely helpful and supportive throughout the entire process of analyzing the detectors and soil samples, and I am very grateful to them. Am also grateful for the managers of Ghana Atomic Energy Commission and Soil Research Institute for making their facilities available for this study.

My family and I went through a lot of hardship during this time, and I owe them a great deal because I could not have finished this project without their encouragement and guidance.

DEDICATION

To my wife Mrs. Florence Tenii Amable and my children Abigail, Bubune and Nuna.



TABLE OF CONTENTS

	Page
DECLARATION	ii
ABSTRACT	iii
KEY WORDS	iv
ACKNOWLEDGEMENTS	v
DEDICATION	vi
LIST OF TABLES	xiv
LIST OF ABBREVIATIONS	xix
CHAPTER ONE: INTRODUCTION	
Background to the study	1
Radon and natural radioactivity in Ghanaian soils and buildings	5
Natural radioactivity and radon concentration levels in soils and dwellings	5
Statement of the Problem	6
Objective of the Study	8
Specific objectives of the Study	8
Significance of the study	8
Scope and Limitations	10
Organization of the study	11
Chapter Summary	11
CHAPTER TWO: LITERATURE REVIEW	
Introduction	13
Radioactivity in the environment	13
Natural radionuclides in the soil	14
Radioactive decay and equilibrium	20

Radioactive decay equilibrium	25
Interaction of gamma rays with matter	28
Natural radioactivity detection	35
High purity germanium detector	35
NaI (TI) Detector	36
Radon in the Environment	37
Properties and origin of Radon	37
Decay products of Radon	38
Radon as a Health Hazard	39
Sources of Radon Exposure	39
Indoor Radon	39
Factors influencing indoor radon	40
Dwelling engineering	40
Meteorological parameters	41
Radon Detection	48
Tracks Formation	53
Chemical etching	53
Biological effects of Natural Radioactivity and Radon	54
Deterministic effects	54
Stochastic effects	55
Radiation Dose	55
Radiation exposure	55
Absorbed dose	56
Equivalent Dose	56
Effective Dose	56

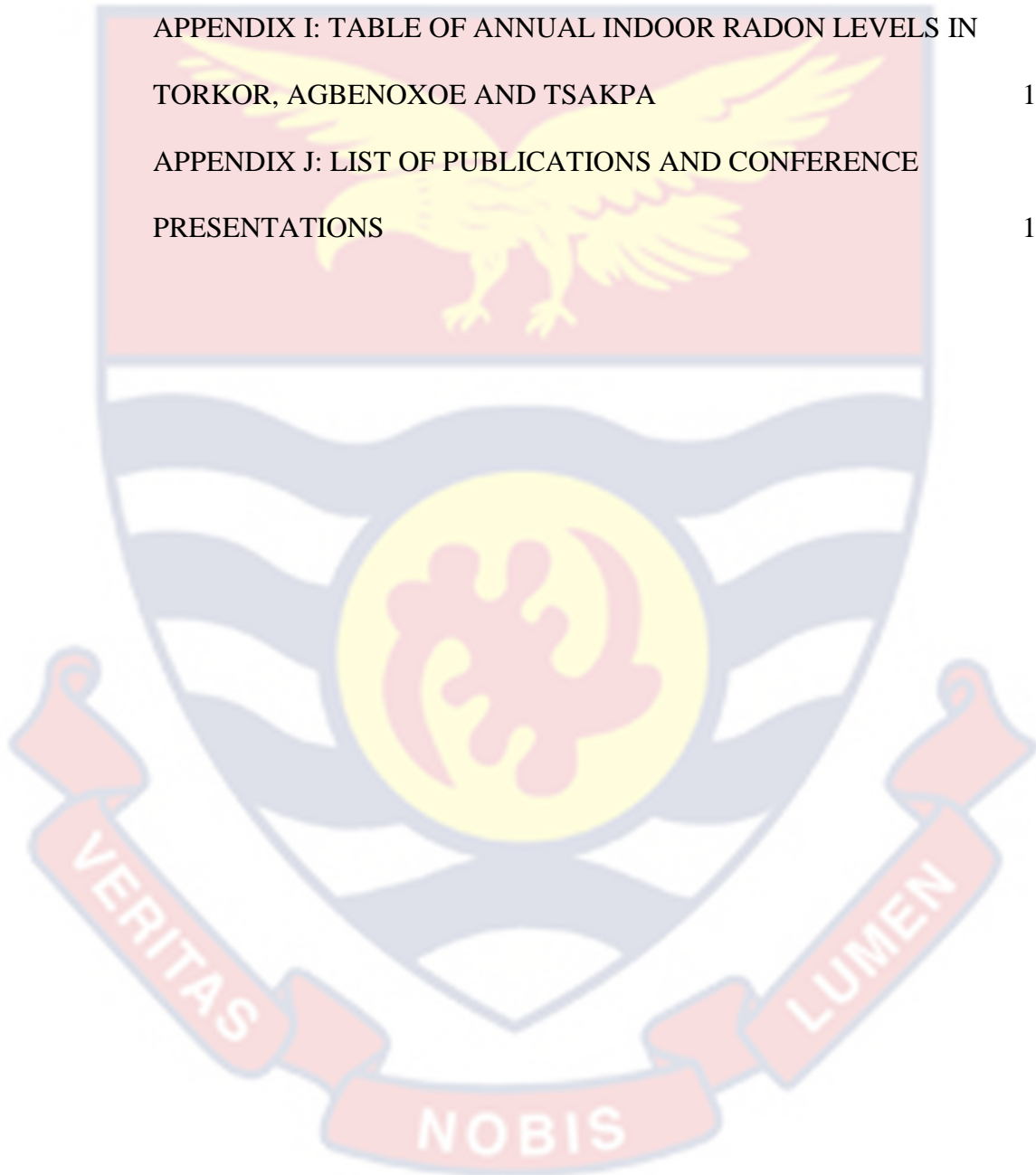
Radon generation and transport	57
Effect of some soil characteristics on Radionuclides and ^{222}Rn in soil and Dwellings	62
Lung Cancer Risk Associated with Radon	63
Radon Entry into dwellings	63
Seasonal radon correction factor	64
Chapter Summary	65
CHAPTER THREE: MATERIALS AND METHODS	
Introduction	67
Study Area	67
Geology of the study Area	68
Meteorology of the Study Area	69
Sample collection, preparation and analysis	69
Gamma Activity Measurement	71
Energy calibration of gamma-ray spectrometry system	71
Efficiency calibration of gamma-ray spectrometry system	72
Activity concentration estimation	74
Radiological hazards indices	75
Radium equivalent index	76
Internal and external hazards indices	76
Gamma index (I_γ)	77
Alpha index (I_α)	77
Absorbed and Effective Dose Rates	78
Absorbed Dose Rate	78
Annual Effective Dose Equivalent (AED)	78

Excess lifetime cancer risk (ELCR)	79
The Activity Utilization Index (AUI)	79
Annual gonadal equivalent dose (AGED)	80
Representative level index (RLI)	80
Physiochemical properties of Soil Samples	80
Radon Measurements	83
Characterisation of the Buildings	83
Distribution of the Radon Detectors in Buildings	83
Preparation, Collection and Chemical Etching of Radon Dosimeters	85
Detector Scanning and Counting Tracks	86
Evaluation of Radon Parameters	87
Radon Risk Assessment	88
Annual Effective Dose (AED)	88
Excess lifetime cancer risk (ELCR)	88
Effective Dose Equivalent	88
Seasonal variation of Radon	89
Seasonal Radon Correction Factors	89
Multivariate statistical analysis	89
Chapter Summary	90
CHAPTER FOUR: RESULTS AND DISCUSSION	
Introduction	92
Activity Concentrations in Soil samples	92
Radon exhalation rates	97
Soil characteristics	99
Regression Analysis of the Radionuclides	104

Radionuclide correlation with soil properties.	107
Effects of moisture, porosity and bulk density on radon exhalation rate in the soil.	108
Effects of soil texture on radon exhalation rate in the soil.	110
Comparing current results to national and international data.	111
Radiological characterization	115
Radium equivalent activity index	115
External and Internal Hazard Indices	116
Activity concentration indices (I_{γ} and I_{α})	119
Activity utilization index (AUI) and representative level index (RLI).	120
Absorbed and effective dose rates	121
Absorbed dose rate (D)	121
Annual Effective Dose Equivalent (AED)	124
Excess lifetime cancer risk (ELCR)	125
Annual gonadal equivalent dose (AGED).	130
Indoor Radon Concentration	130
Seasonal variability in indoor radon concentrations	135
The effects of building characteristics on the indoor radon levels	137
Seasonal Correction Factor	139
Dose Estimation	144
Annual effective dose (AED)	144
Evaluation of Lung Cancer Risk from the measured indoor radon levels	145
Multivariate Statistical Analysis	151
Principal component analysis (PCA)	151
Cluster analysis	155

Chapter Summary	156
CHAPTER FIVE: SUMMARY, CONCLUSIONS AND RECOMMENDATIONS	
Overview	162
Chapter Summary	162
Conclusions	164
Recommendations	165
Research institutions/Academia	165
Regulatory Authorities	166
Building Industries in Ghana	166
Residents/Dwellers	166
REFERENCES	167
APPENDICES	187
APPENDIX A: TABLE OF RADIONUCLIDES LEVELS AND RADON EXHALATION RATES IN SOIL OF TORKOR	187
APPENDIX B: TABLE OF RADIONUCLIDES LEVELS AND RADON EXHALATION RATES IN SOIL OF AGBENOX	188
APPENDIX C: TABLE OF RADIONUCLIDES LEVELS AND ^{222}Rn EXHALATION RATES IN SOIL OF TSAKPA	189
APPENDIX D: TABLE OF INDOOR RADON CONCENTRATION (Bq/m^3)	190
APPENDIX E: TABLE OF INDOOR ^{222}Rn LEVELS IN DIFFERENT	193
APPENDIX F: TABLE OF INDOOR ^{222}Rn LEVELS IN DIFFERENT LOCATIONS IN TSAKPA	194

APPENDIX G: TABLE OF INDOOR ^{222}Rn LEVELS IN DIFFERENT LOCATIONS IN AG	195
APPENDIX H: TABLE OF INDOOR ^{222}Rn LEVELS IN DIFFERENT LOCATIONS IN TORKOR	196
APPENDIX I: TABLE OF ANNUAL INDOOR RADON LEVELS IN TORKOR, AGBENOXOE AND TSAKPA	197
APPENDIX J: LIST OF PUBLICATIONS AND CONFERENCE PRESENTATIONS	198



LIST OF TABLES

	Page
1 Average Activity Levels (Bq kg ⁻¹) of ²²⁶ Ra, ⁴⁰ K and ²³² Th in Soil from Torkor.	94
2 Average Activity Levels (Bq kg ⁻¹) of ²²⁶ Ra, ⁴⁰ K and ²³² Th in Soil from Agbenoxoe.	95
3 Average Activity Levels (Bq kg ⁻¹) of ²²⁶ Ra, ⁴⁰ K and ²³² Th in soil from Tsakpa.	96
4 Radon Exhalation Rates of Torkor, Agbenoxoe and Tsakpa, Kpando Municipality	98
5 Properties of Soil Samples from Torkor	101
6 Properties of Soil Samples from Agbenoxoe	102
7 Properties of Soil Samples from Tsakpa	103
8 Pearson Correlation Matrix of Radionuclides Concentration and Radon in Soil and Dwelling, and some Soil Properties.	106
9 T – Test Comparison of the Activity Concentration Levels of Radionuclides in Torkor, Agbenoxoe and Tsakpa Soil Samples at 95 % Confidence Interval.	107
10 Comparing Current Results (²²⁶ Ra, ²³² Th and ⁴⁰ K activity levels) to National and International Data	114
11 Ra _{eq} (Bq/kg) in the Soil Samples from Torkor, Agbenoxoe and Tsakpa	116
12 H _{ex} , H _{in} , I _γ , I _α , AUI and RLI for Soil Samples from Torkor.	117
13 H _{ex} , H _{in} , I _γ , I _α , AUI and RLI for soil Samples from Agbenoxoe.	118
14 H _{ex} , H _{in} , I _γ , I _α , AUI and RLI for Soil Samples from Tsakpa.	119

15	External and Internal Absorbed Dose Rates and AED for Soil Samples from Torkor.	122
16	External and Internal Absorbed Dose Rates and AED for Soil Samples from Agbenoxoe.	123
17	External and internal Absorbed Dose Rates and AED for Soil Samples from Tsakpa.	124
18	ELCR and AGDE for Soil Samples from Torkor.	127
19	ELCR and AGDE for Soil Samples from Agbenoxoe.	128
20	ELCR and AGDE for Soil Samples from Tsakpa.	129
21	Annual Mean Indoor ^{222}Rn Levels in Torkor, Agbenoxoe and Tsakpa, Kpando Municipality	132
22	Minimum and maximum Indoor Radon-222 levels (Bq/m^3) in Different Seasons and Annual Measurement.	133
23	Mean Indoor radon-222 level (Bq/m^3) in Different Seasons and Annual Average Indoor Radon-222 Concentration.	137
24	^{222}Rn seasonal correction factors for dwellings with different building materials	141
25	^{222}Rn seasonal Correction Factors Based on the Towns	141
26	^{222}Rn Seasonal Correction Factors Based on the Locations	141
27	Building Code (DC) and Description of Building Materials.	142
28	Ratio of the Seasonal to Annual Indoor radon Concentration Levels of the Three Studied Locations.	143
29	Estimated Values for AED, AED_L and ELCR Dry Season.	148
30	Estimated Values for AED, AED_L and ELCR during Rainy Season.	149
31	Rotated Component Matrix ^a	152

LIST OF FIGURES

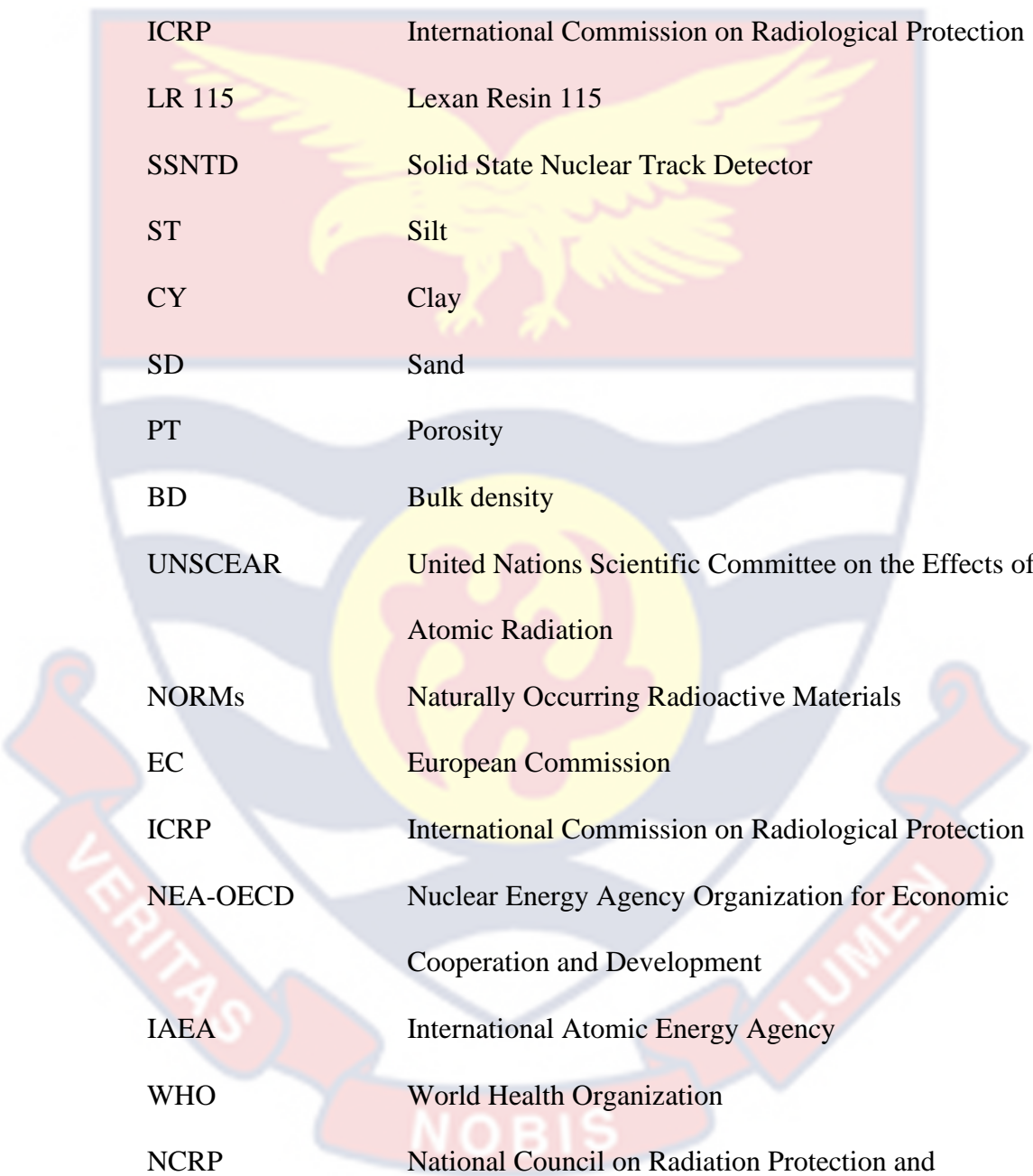
1	Comparison of Number of Deaths from Various Causes in U.S.A (U.S EPA, 2003).	4
2	Thorium Series (L'Annunziata, 2020)	17
3	Uranium – 238 Decay Series (L'Annunziata, 2020)	18
4	Uranium – 235 Decay Series (L'Annunziata, 2020)	19
5	Secular equilibrium between long-lived parent and short-lived daughter nuclei (Le et al., 2014)	27
6	Radioactive decay between parent and decay nuclei with time (Le et al., 2014).	28
7	Pair production (Le et al., 2014)	29
8	Diagram showing photoelectric effect (L'Annunziata, 2020)	30
9	Diagram showing Compton scattering (L'Annunziata, 2020)	31
10	Diagram showing mass attenuation of radionuclide, D. (Podgorsak, 2016)	35
11	Diagram showing radon generation and transport to atmosphere (Ishimori et al, 2013).	58
12	Diagram showing soil classifications (USDA, 1999)	63
13	Diagram showing the radon entry points in a building (Blanco-Novoa et al., 2018)	64
14	Map of Kpando Municipality showing the study locations	68
15	Graph showing energy calibration of gamma-ray spectrometry system	72
16	Graph showing efficiency calibration of gamma-ray spectrometry system	74
17	Experimental setup for radon exhalation measurement	85

18	Latent tracks formed on the CR-39 detector from one location (Torkor)	87
19	Average activity levels of ^{226}Ra , ^{40}K and ^{232}Th at Torkor, Tsakpa and Agbenoxoe.	97
20	Variation of soil moisture content with radon exhalation rate	109
21	Variation of soil porosity with radon exhalation rate	109
22	Variation of soil bulk density with radon exhalation rate	110
23	Variation of soil texture with radon exhalation rate	111
24	Radium-226 levels in soil and corresponding radon-222 level in dwellings.	134
25	Correlation between radium-226 levels and radon-222 exhalation rates.	134
26	Mean indoor ^{222}Rn concentration (Bq/m^3) for dry and rainy season.	137
27	The variability of indoor radon with dwellings in different materials during dry season.	139
28	The variability of indoor radon in dwellings with different materials during rainy season.	139
29	AED (mSv/y) due to radon-222 in different three towns of the Kpando Municipal.	145
30	AED (mSv/y) due to radon-222 in different seasons for the studied towns.	145
31	Bar chart of indoor Rn-222, AED, AED_L and ELCR of the studied area.	150
32	Bar chart of indoor Rn-222, AED, AED_L and ELCR of the studied locations.	150

33	Scree plot	153
34	Box plot for radionuclides and soil properties.	154
35	Box plot for only radionuclides	154
36	Dendrogram (Euclidean distance) using Ward linkage of hierarchical cluster analysis for 11 variables.	156



LIST OF ABBREVIATIONS

The background of the page features a large, semi-transparent watermark of the University of Cape Coast crest. The crest is a shield-shaped emblem with a yellow eagle with outstretched wings in the center. The shield is divided into three horizontal sections: a top red section, a middle white section with blue wavy lines, and a bottom yellow section. A red banner wraps around the bottom of the shield with the Latin motto 'VERITAS LIBERABIT VOS'.

DNA	Deoxyribose Nucleic Acid
EPA	Environmental Protection Agency
GAEC	Ghana Atomic Energy Commission
ICRP	International Commission on Radiological Protection
LR 115	Lexan Resin 115
SSNTD	Solid State Nuclear Track Detector
ST	Silt
CY	Clay
SD	Sand
PT	Porosity
BD	Bulk density
UNSCEAR	United Nations Scientific Committee on the Effects of Atomic Radiation
NORMs	Naturally Occurring Radioactive Materials
EC	European Commission
ICRP	International Commission on Radiological Protection
NEA-OECD	Nuclear Energy Agency Organization for Economic Cooperation and Development
IAEA	International Atomic Energy Agency
WHO	World Health Organization
NCRP	National Council on Radiation Protection and Measurements
MeV	Mega electron Volt
keV	Kilo electron Volts

Bq/m ² h	Becquerel per square meter hour
Bq/m ³	Becquerel per cubic meter
HPGe	High purity germanium detector
NaI	Sodium Iodide
PADC	Polyallyl Diglycol Carbonate
AED	Annual Effective Dose Equivalent
AED _L	Annual Effective Dose to the lungs
ELCR	Excess Lifetime Cancer Risk
RLI	Representative level index
AUI	Activity utilization index
RPI	Radiation Protection Institute
nGy/h	nano Gray per hour
μSv	micro sievert
Bq/kg	Becquerel per kilogram
mSv	milli sievert
Bq	Becquerel
$n(t)$	Parent Radionuclide at time
n	Number of Atoms in radionuclide
λ	decay constant of radionuclide
$t^{1/2}$	Half-life of radionuclide
α	Alpha particles
τ	Mean life of Radionuclide (years)
Q	Value is a term used to quantify the energy released during the decay process.
β^-	Negatron Emission of Radioactive nuclei

β^+	Positron Emission of Radioactive nuclei
γ	Gamma ray particles
C	Activity concentration of radionuclides
M_{sam}	mass of sample
N_{sam}	net peak area for the radioactive product in sample
$P(E)$	gamma emission probability
$T(C)$	counting time of decay product of sample
$\eta(E)$	photo peak efficiency
Ra_{eq}	Radium equivalent index
C_{Ra}	Concentration of Radium
C_{Th}	Concentration of Thorium
C_K	Concentration of Potassium
H_{ex}	External hazard indices
H_{in}	Internal hazard indices
I_α	Alpha activity Index
I_γ	gamma activity Index
D	Absorbed Dose Rates
C_{Rn}	Radon concentration
λ_{Rn}	Decay constant of radon
USEPA	United States Environmental Protection Agency

CHAPTER ONE

INTRODUCTION

Chapter one looks at the general overview of the research and previous studies on radionuclides, radon and soil properties, the problem under investigation, the importance, the objectives and the organization of the thesis are also presented.

Background to the study

Human populations are continuously subjected to background radiation from both man-made and natural sources (UNSCEAR, 2000). Natural radiation sources contribute through radiation from terrestrial, cosmogenic, cosmic rays and radioisotopes in the outer solar system. Whereas radiations of man - made origin are generally produced due to different kinds of human activities, such as nuclear research activities, nuclear weapon testing, medical diagnostic and therapeutic procedures, electricity generation from nuclear reactors, and nuclear reactor accidents (UNSCEAR, 2017). Since nuclear weapon testing, nuclear research, and nuclear fuel cycle activities in nuclear power plants have taken place over the years, radioactive particles have been released into the surroundings (IAEA, 2011).

Background radiation levels range globally between around 2.0 and 8.0 mSv/y and are primarily dependent on the geography and geology of the location (Ojovan et al., 2019). As a result of high levels of radioactive substances, countries such as Brazil, India, and China have the highest background radiation levels (Hendry et al., 2009). The external radiation levels that may reach up to 50 Gy/h come from the monazite sand deposits that are found along the shores of Brazil. Effective dosages of natural background

radiation from terrestrial gamma rays ranged from 0.3 to 1.0 mSv, with 0.48 mSv serving as the world mean (Ojovan et al., 2019). These exposure levels could, in some situations, be on par with or even higher than those caused by the utilization of ionizing radiation for medical and industrial purposes (UNSCEAR, 2010). Due to the difference in geology, the exposure of individuals to natural sources differs from one geological area to the other.

Gamma radiation exposure to humans predominately affects the entire body from external sources and the lungs from internal sources of alpha particles. Soil as the major building material and rocks in the earth can emit radon, a gas that when decays into daughter radionuclides can accumulate in the lungs (Belete & Anteneh, 2021). ^{226}Ra with a half-life of 1600 ± 0.44 % years and a product of the decay of ^{238}U found in uranium ore, is the source of radon. ^{222}Rn having a half-life of 3.82 days, disintegrates into a variety of transient progenies, including ^{218}Po , ^{214}Pb , ^{214}Bi , and ^{214}Po . Being an inert radioactive gas, when radon is ingested, it frequently exhales without causing any harm. However, owing to the fact that they are heavy metal atoms, the progenies of radon implant themselves in the human respiratory system and continuously irradiate the lining of lungs, which ultimately results in the lung cells suffering significant damage (Sahu et al., 2014).

On the basis of the findings of a number of epidemiological investigations that were carried out within houses, IARC has declared that radon is a human carcinogen that belongs in category 1 (Kim et al., 2016; Cheng et al., 2021; WHO, 2010). For lack of a threshold, the connection between exposure to radon and response may be most accurately described as linear, as stated in recommendations issued by the WHO in 2010 (WHO, 2010). The

increased relative risk is approximately 16 % per each 100 Bq/m³ rise in radon levels, in accordance with the results of an average long-term exposure to radon that lasted for thirty years. In most cases, members of the general public will either consume or breathe in radon. ²²²Rn is the major source of radiation exposure within a building, while background radiation levels, which include gamma particles, represent the outdoor source of radiation exposure. The activity levels of natural radioactivity that may be discovered in rocks, soil, and other materials that are similar to soil are the principal contributor to the background radiation that is present in the environment (Otoo et al., 2018).

Radon and its offspring are a serious health risk that cause thousands of deaths each year that may have been avoided (Corrales et al., 2020; Gogna et al., 2019; Lorenzo-Gonzalez et al., 2019; Khan et al., 2021). Elevated amounts of radon - 222 exposure (Above 100 Bq/m³, recommended by WHO) have had detrimental effects on the health of uranium miners (WHO, 2009). Every 100 Bqm⁻³ increase in radon concentration results in a 16 % increase in the risk of lung cancer. As radon exposure rises, lung cancer risk increases proportionately because of the linear dose-response relationship. Up to eight million dwellings in the United States (US) have recorded higher ²²²Rn gas levels, according to the United States Environmental Protection Agency (USEPA) (Kumar et al., 2011). The number of fatalities per year in the US due to different causes is shown in Figure 1, with radon being the major cause.

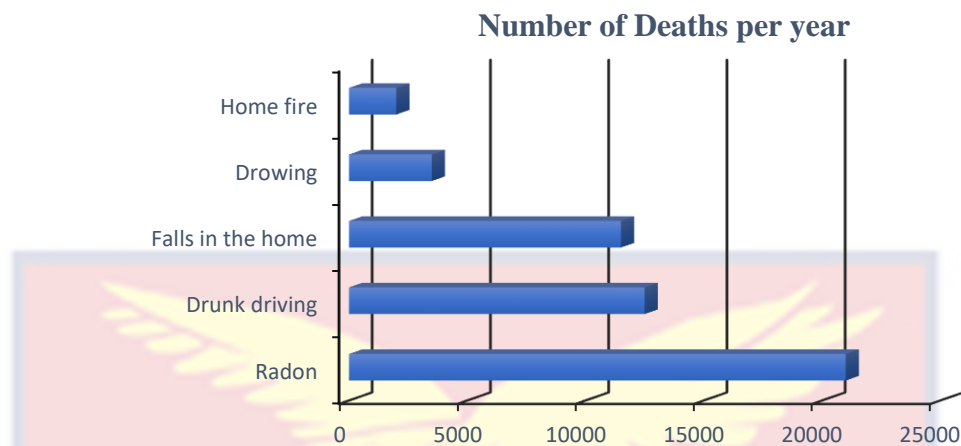


Figure 1: Comparison of Number of Deaths from Various Causes in U.S.A (U.S EPA, 2003).

Since background radiation from the environment is the primary source of radiation exposure for the general population, research into naturally occurring radioactive materials (NORMs) in geological building materials is very important (UNSCEAR, 2000). Building-related radiation exposure can be categorized into external or internal. The radiation dose to which people are exposed is strongly influenced by the radiation emission and attenuation caused by building materials. To figure out how much background radiation comes from the most common building materials and to lessen the effects of too high a dose, the size of this dose must be measured.

The majority of earlier investigations on environmental radioactivity in Ghana focused on specific regions and indicated significantly higher radiation levels in soil, water, and building materials (Amekudzie et al., 2011; Otoo et al, 2013; Otoo et al., 2018; Addo et al., 2020; Otoo et al., 2022). These measurements of ^{232}Th , ^{226}Ra , and ^{40}K activity levels were mostly made in Greater Accra and the mining towns of Ghana. The indoor radon measurement

in Ghana began as far back in 1970s, spearheaded by Aba Andam (Andam, 1993) and since then have seen a lot of researchers using various techniques to estimate indoor radon mostly in Ashanti Region, Greater Accra, Central Region, and Northern part of Ghana (Nsiah-Akoto et al., 2019). The measurement of indoor radon and activity concentration of terrestrial radionuclides in soils have not been done in the Kpando Municipality. This research set out to ascertain the indoor radon and radioactivity levels brought on by terrestrial radionuclides in soils and the influence of soil properties, so as to assess radiological hazards associated with the radionuclides.

Radon and natural radioactivity in Ghanaian soils and buildings

Several research have been conducted in Ghana to determine radionuclides and radon levels in soils and dwellings by different methods. The determination of radionuclides and radon concentration levels are mostly done in mining environments, in Ashanti and Greater Accra Regions and only a handful of investigations are done in other parts of Ghana.

Natural radioactivity and radon concentration levels in soils and dwellings

Since radon makes up about 60% of all-natural background radiation, exposure to it has emerged as a concern throughout the world (Otoo et al., 2018). It was recognized as a major cause of lung cancer in non-smokers and a considerable contributor to ionizing radiation exposure for the entire population. It causes 9 % of the lung cancer fatalities that occur each year in European Union (Darby et al., 2005). Several studies on radionuclides and radon levels in soil and dwellings have been done in Ghana. The majority of these studies focused on mining environments only. Extensive indoor radon measurements

have been conducted in Greater Accra Region, Ashanti Region, Central Region while the rest of the thirteen regions have seen little or no research on the radon concentration.

In 1989 to 1990, the first investigation into indoor radon was conducted in Kumasi metropolis and neighbouring towns using CR-39 SSNTD detectors (Adam, 1993). This study recorded average indoor radon concentration which was about 1.4 times higher than 100 Bq/m³ limit recommended by WHO (WHO, 2009). Later studies (Akortia et al., 2010; Nsiah-Akoto et al., 2019; Otoo et al., 2018; Kitson-Mills et al., 2019; Opoku-Ntim et al., 2020; Otoo et al., 2020; Otoo et al., 2022; Kporozro et al., 2022) had values greater than the 100 Bq/m³ proposed by WHO (WHO, 2009). Studies conducted on radionuclides in soil samples showed higher values of ²²⁶Ra, ²³²Th and ⁴⁰K (Faanu et al., 2010; Faanu et al., 2011; Amekudzie et al., 2011; Otoo et al., 2013; Faanu et al., 2016; Bekelesi et al., 2017; Otoo et al., 2018; Addo et al., 2020; Otoo et al., 2022) as compared to proposed reference levels by UNSCEAR (UNSCEAR, 2000 and 2008).

Statement of the Problem

Natural radioactivity and radon levels, as well as their decay products, have received a great deal of attention due to the health risks they pose. As a result, measurements of natural radioactivity and radon were carried out internationally at national levels, yielding extensive data that are publicly available (Almayahi et al., 2011). Many studies on indoor radon and natural radioactivity levels in Ghana, mostly focused on mines environment in Ghana. As a result, very few radiation data on the natural radioactivity and radon in the

environment in other parts of Ghana are available. The only study conducted in the Volta Region by Ansre et al. (2018) focused only on indoor radon level.

The correlation between radon and natural radioactivity levels, the influence of soil properties on radionuclides associated with Ghanaian soils as a major building material have not yet been evaluated (Otoo et al., 2018). Ghana primarily relies on global standards rather than national regulations that establish the acceptable levels of natural radionuclide and radon levels in local geological and manufactured construction materials (Otoo et al., 2018). ^{238}U , ^{226}Ra , ^{232}Th and ^{40}K concentrations were found to be greater than the global limits in most of the investigations conducted on soil, rocks, and other environmental samples (Darko et al., 2005; Otoo et al., 2013; Faanu et al., 2016; Otoo et al., 2018; Otoo et al., 2022).

Presently, there is no work that has been conducted on natural radioactivity, indoor and soil radon and, influence of soil characteristics in the studied locations to determine the background radiation. As a result, there are generally lack of enough knowledge on the potential hazards associated with radon and natural radioactivity. As a result of lack of information about the activity concentrations and harmful effects of radon, many people have continued to work in, and live-in places unaware of the problems posed to their lives. It is therefore essential to understand the facts on radionuclides and radon in the soil and accumulation in residences where humans spend a substantial amount of time, averaging 6 to 8 hours per day in the currently studied areas.

In order to address this issue, the current study sought to determine natural radioactivity, indoor radon, soil radon, soil characteristics, and to assess the radiological hazards associated with radiation.

Objective of the Study

The primary aim of this study was to determine the concentration levels of natural radionuclides of ^{226}Ra , ^{232}Th , ^{40}K and the radon level in soil and buildings and their dependence on soil properties in Kpando municipality of the Volta Region.

Specific objectives of the Study

The following specific objectives were defined to achieve the stated objectives of this study:

1. To determine activity of ^{226}Ra , ^{232}Th and ^{40}K in soil samples and their radiological impact.
2. To determine seasonal variation and correction factor for radon concentration in selected buildings in the study locations (Torkor, Agbenoxoe and Tsakpa).
3. To determine soil properties and their influence on radionuclides in the soil at Torkor, Agbenoxoe and Tsakpa.
4. To compare the radon and radionuclides concentrations data with other studies conducted locally and internationally, and with the proposed reference level by international radiological organizations such as WHO, ICRP and UNSCEAR.

Significance of the study

The United Nations Scientific Committee on the Effects of Atomic Radiation (UNSCEAR) stated in two comprehensive reports issued in 2000 and 2008 (UNSCEAR, 2000 and 2008) that inhaling radon and its decay products are known lung carcinogens. The International Committee on Radiological

Protection analyzed the scientific evidence of radon's health effects in several publications and made recommendations on how to safeguard against indoor radon exposure (ICRP, 1993). According to the WHO, the percentage of cancer cases caused by ^{222}Rn ranged from three to fourteen percent, depending on the country's average radon level and the calculating technique utilized. Radon has been recognized as the second leading cause of lung cancer after smoking (WHO, 2009).

Ghana and the majority of African nations do not have radiological regulatory control for dwellings. The population is not adequately informed about the radiological risks and exposure levels of NORMs, including radon (Darko et al., 2005), as a result of the lack of baseline data on NORMs. Several studies on radon exhalation rates and radon levels in dwellings have been conducted in communities throughout Greater Accra, Ashanti region, Central region, and northern part of Ghana. Other parts of Ghana had seen little or no research on NORMs and their health risks. Radon and natural radioactivity studies in the Volta Region is scanty and no studies have been carried out on radionuclides and radon levels and their dependence on soil properties in the Kpando Municipality. The environment that could be vulnerable to radioactive contamination must have baseline information on the background radiation (Jibiri and Bankole, 2006).

Therefore, there is the need to carry out radon, natural radioactivity and soil properties studies in these communities. This study will serve as the baseline studies for regulatory monitoring and further studies. It will also increase the interest in radon and radioactivity studies within the region. This study will assist in reducing and in some instances eliminate, possible issues

associated with radon and natural radioactivity. The findings of this study could be relevant for future radio-geochemical studies in the area, notably in the search for rare earth elements and the position of ^{40}K changes. The findings of this study will also serve as a baseline for monitoring and evaluating future radioactive contaminations in the environment caused by national accidental releases or those on a worldwide scale. Such information can also be used to assess the radiological health consequences of natural radiation in the environment, as well as to confirm and plan decisions about potential radiation-related health issues in the area.

Scope and Limitations

Due to time and resource constraints, the study was restricted to just three towns (Torkor and Agbenoxoe which are along the Volta Lake and Tsakpa on the hill) within Kpando Municipality. The study measured radionuclides, radon levels in soil and dwellings, and their dependence on soil properties to provide scientific reference data on environmental natural background radiations of Torkor, Agbenoxoe, and Tsakpa. 120 buildings (40 from each town) were utilized for indoor radon monitoring, and 51 soil samples (seventeen from each town) were used to quantify concentrations of ^{226}Ra , ^{232}Th , and ^{40}K using gamma spectroscopy, soil properties using Bouyoucos hydrometer and gravimetric techniques, and closed-can procedures with CR-39 detectors for radon exhalation rates and the study only covered a few households and localities in Kpando Municipality of Volta Region, Ghana.

Organization of the study

This thesis is divided into five sequential chapters. The first chapter explains the background of the study, studies done in Ghana on natural radioactivity and radon in soils and dwellings, objectives, significance, scope and organization of the study. The relevant literature on the topic were presented in chapter 2. The chapter includes the concept of radionuclides and radon in the soil and dwellings environments, some soil properties and their effects on radionuclide level in the soil. The radiation related health risks were also reviews. The third chapter outlines the research topic and the methods employed to attain the specified goals. This chapter covers sampling, sample preparation, radiological health hazard parameter evaluation, and various statistical studies on the data obtained. The fourth chapter focuses on data analysis and discussion of the findings, as well as the study's findings. The research outcomes and recommendations are presented in Chapter 5.

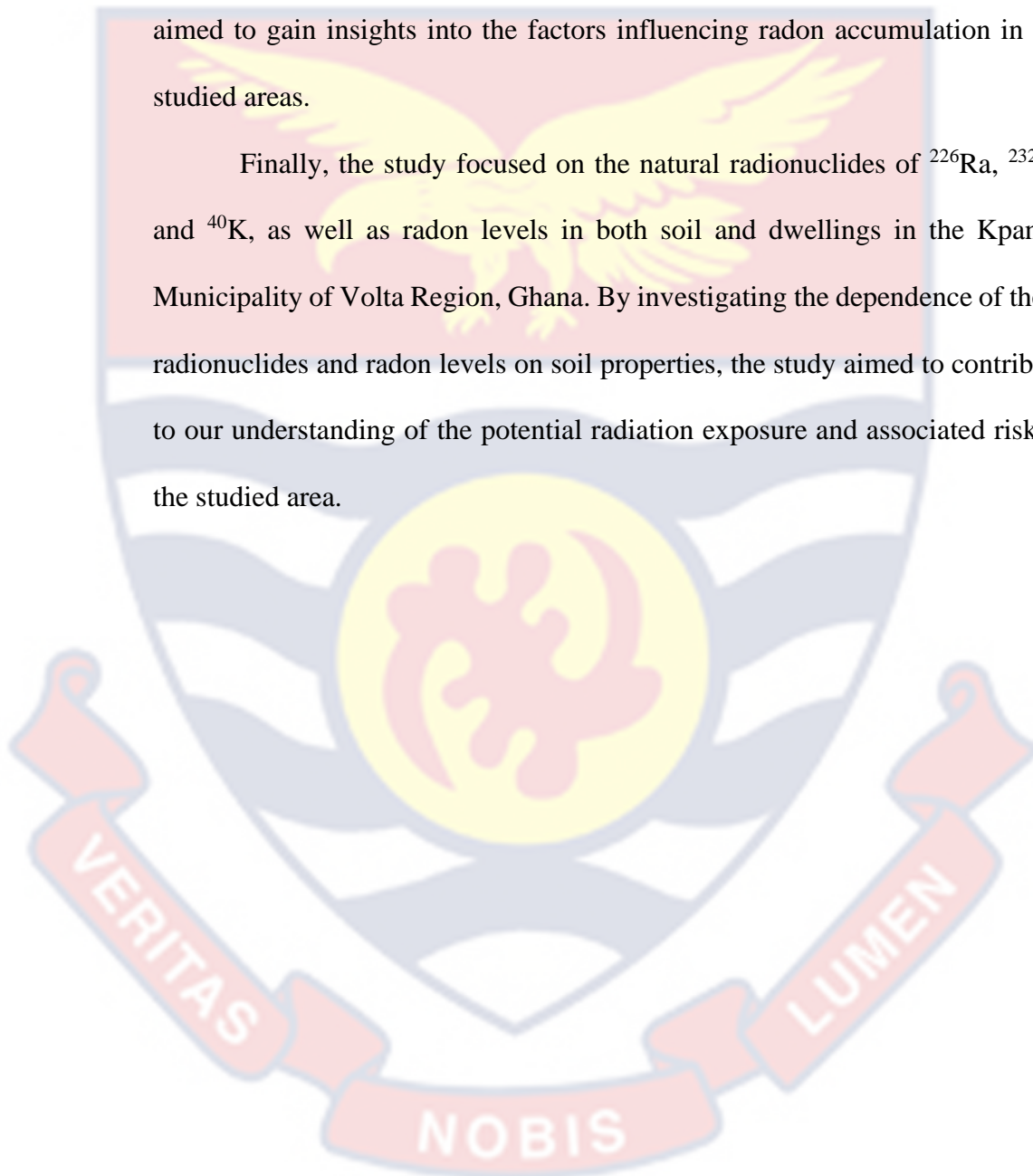
Chapter Summary

Natural radionuclides of ^{226}Ra , ^{232}Th and ^{40}K are naturally occurring radioactive materials (NORMs) found in soil, rocks, plants, air and water. These radionuclides emit radiation and can have potential health effects on human populations when present in elevated concentrations. This study focused on analyzing the levels of these radionuclides in the soil of the Kpando Municipality of Volta Region, Ghana.

Radon, a radioactive gas produced by decay of ^{226}Ra , can accumulate in an enclosed spaces and pose a health risk when inhaled. Therefore, the radon levels in both soil and dwellings within the studied areas was also investigated. The studied aimed to understand the dependence of radon levels in both soil and

dwellings, and activity concentrations of radionuclides on soil properties. Soil properties, such as texture, porosity, moisture content and bulk density, can influence the concentration and mobility of radionuclides in the soil. By examining the correlation between soil properties and radon levels, the study aimed to gain insights into the factors influencing radon accumulation in the studied areas.

Finally, the study focused on the natural radionuclides of ^{226}Ra , ^{232}Th and ^{40}K , as well as radon levels in both soil and dwellings in the Kpando Municipality of Volta Region, Ghana. By investigating the dependence of these radionuclides and radon levels on soil properties, the study aimed to contribute to our understanding of the potential radiation exposure and associated risk in the studied area.



CHAPTER TWO

LITERATURE REVIEW

Introduction

This chapter examines earlier research linked to this study. It looks at the broad overview of natural radioactivity, radioactivity theory, radon measuring methodologies, indoor radon measurement, radon exhalation rate, and various characteristics that might impact radon and radionuclide concentrations in soil samples.

Radioactivity in the environment

Cosmic rays and terrestrial radiations are the two types of natural radiation that reach the earth's surface. The latter component consists mostly of primordial radionuclides that were produced during early phases of development of the solar system. Uranium, actinium, thorium, and neptunium represent the four distinct series of natural decay (L'Annunziata, 2020). To avoid using the same name twice, the Actinium Decay Series is named after one of its members. Neptunium completely decayed in the first 50 million years because of the ^{237}Np isotope's short half-life in comparison to the age of the earth. Only three radioactive series are found in heavy elements (^{238}U , ^{235}U , and ^{232}Th). They gradually lose mass and change atomic number until they form stable lead (L'Annunziata, 2020).

Radiation exposure from naturally occurring radioactivity in soil was acknowledged as a significant source of lung cancer risk in early 1970s. The natural radioactive materials are ubiquitous chemicals found in the environment, including rocks, soil, water, air, and even tissues (Otoo et al., 2022). There is no way to prevent the existence of natural radionuclides since

they are a result of the earth's genesis. One of the main building materials known to contain radioactive elements that occur naturally is brick. Radiation dosage from ^{238}U , ^{232}Th , and their progenies, as well as ^{40}K , was imparted to residents by the natural radioactivity of bricks. The distribution of radionuclides ^{238}U , ^{232}Th , and ^{40}K in the soil, rock, air, plants and water varies globally (UNSCEAR, 2014).

Natural radionuclides in the soil

The nutrient requirements for plants are met by the complex physiochemical system that is organized in soil, which is composed of mineral and organic materials, water, and air. The inorganic component may belong to one of several textural groups, depending on the percentage of sand, silt, and clay in surface soils. Sand comprises particles ranging in size from 0.06 mm to approximately 2 mm and is primarily composed of primary minerals like quartz. Clay particles are smaller than 2 μm in diameter, while silt particles range in size from 2 to 0.06 mm (Van Wijngaarden et al., 2002).

The core of the Earth contains a good percentage of radionuclides. Uranium, Thorium, and Radium are all found in trace amounts in the earth's crust, along with radioactive isotopes of several other elements, including potassium. The soil, some building materials (such as bricks and concrete), and rocks all contribute to the radiation exposure (Chowdhury et al., 2004; Uosif et al., 2015). According to Chowdhury et al. (2004), natural radioactive materials in rocks and soils account for roughly 8 % of an individual's annual radiation dose, including medical exposure. Regarding radiological protection, radiation exposure from natural sources has become increasingly important. This is largely due to ^{222}Rn and its solid, short - lived progeny ^{218}Po , ^{214}Pb , and ^{214}Bi .

These radionuclides irradiate organs with Alpha, Beta, and Gamma rays. Other terrestrial radionuclides exist in nature, such as ^{235}U , ^{87}Rb , ^{138}La , ^{147}Sm , and ^{176}Lu , although their contributions to human dose are minimal. These radioisotopes can be found in the body and emit Alpha, Beta, and Gamma particles that irradiate organs. Trace levels of terrestrial radionuclides produce external exposures.

Radiation levels are greater in igneous rocks such as granite than in the sedimentary rocks. There are significant radionuclide concentrations in some phosphates and shales. The radioactive background concentrations in soils have been determined through a number of studies, and they may be related to airborne exposure rates. These results provide a more thorough assessment of background radiation exposure levels across different countries. All of these spectrometric studies show that the outdoor radiation from ^{238}U , ^{232}Th , and ^{40}K components contribute roughly equally to the externally incident dose of gamma radiation to people under typical indoor and outdoor conditions (Usikalu et al., 2021).

Potassium (^{40}K)

Sir Humphry Davy found potassium in 1807 by electrolyzing Potash (L'Annunziata, 2020). First electrolytically separated metal. Alkaline potassium (^{39}K) is silvery-white in nature only and contains potassium as ionic salts. It's in soil, rocks, animal tissues, and plants. The naturally occurring potassium isotopes are ^{39}K , ^{40}K , and ^{41}K , with 93.2581 %, 0.0117 %, and 6.7302 % abundances (L'Annunziata, 2020). Only ^{40}K is radioactive (most unstable) and is the most prevalent bioenvironmental and human body radioisotope. It has a 1.28×10^9 year half-life.

It is a component of all soils and rocks, and its amount varies by location. Potassium contents in rock layers range from 0.1 to 5 %, averaging 2.5 %. A 70 kg adult has 140 g of potassium and 0.017 g of ^{40}K . Potassium – 40 degrades at 266000 atoms each minute. 100 disintegrations yield 89 beta particles with 1.33 MeV and 11 gamma photons with 1.46 MeV. It decays to a stable ^{40}Ca (80 %) in time emitting a 1.314 MeV maximum via β^- - decay and ^{40}Ar via β^+ - decay or electron capture (K – capture). ^{40}K has an activity of $3.1 \times 10^3 \text{ Bqkg}^{-1}$ (L'Annunziata, 2020). The potassium content of rocks can range from 0 to 10 %, but it is usually 1 to 5 %, with an average value of 2 %.

Thorium series

Thorium ($_{90}\text{Th}$) occurs naturally and was discovered in 1828 by the Norwegian mineralogist Morten Thrane Esmark and named after Thor by the Swedish chemist Jöns Jacob Berzelius (Krebs, 2006). ^{232}Th with half-life of 14.1 billion years, making it one of the longest-lived radioactive elements on earth.

Soil typically contains a thorium content of 6 ppm. Thulium oxide has the highest melting point of any oxide at 3300 degrees Celsius. Starting with the radioactive ^{232}Th and ending with the relatively stable ^{208}Pb , this series is known as the $4n$ decay chain (L'Annunziata, 2020). The progenitor of this series also generates ^{234}Th , ^{230}Th , ^{231}Th , ^{227}Th , and ^{228}Th , along with other isotopes of ^{232}Th and ^{238}U decay series. These isotopes are found in the decay chains ($4n + 1$), ($4n + 2$), and ($4n + 3$) (L'Annunziata, 2020). There are approximately 30 thorium isotopes with mass numbers ranging from 209 to 238. Figure 2 illustrates the 9 membered ^{232}Th decay sequence, which culminates in ^{208}Pb following emissions of α and γ - decay products.

The ^{230}Th , ^{229}Th , ^{228}Th , ^{234}Th , and ^{227}Th are the most stable after ^{232}Th ($t_{1/2} = 75,380$ years). The liver, lungs, and skeleton store thorium after ingestion. The skeleton stores 70% of thorium intake. The gonads (1.0%), soft tissues (16.0%), and the liver (4.0%) all contain a few thorium (Sathyapriya et al., 2012)

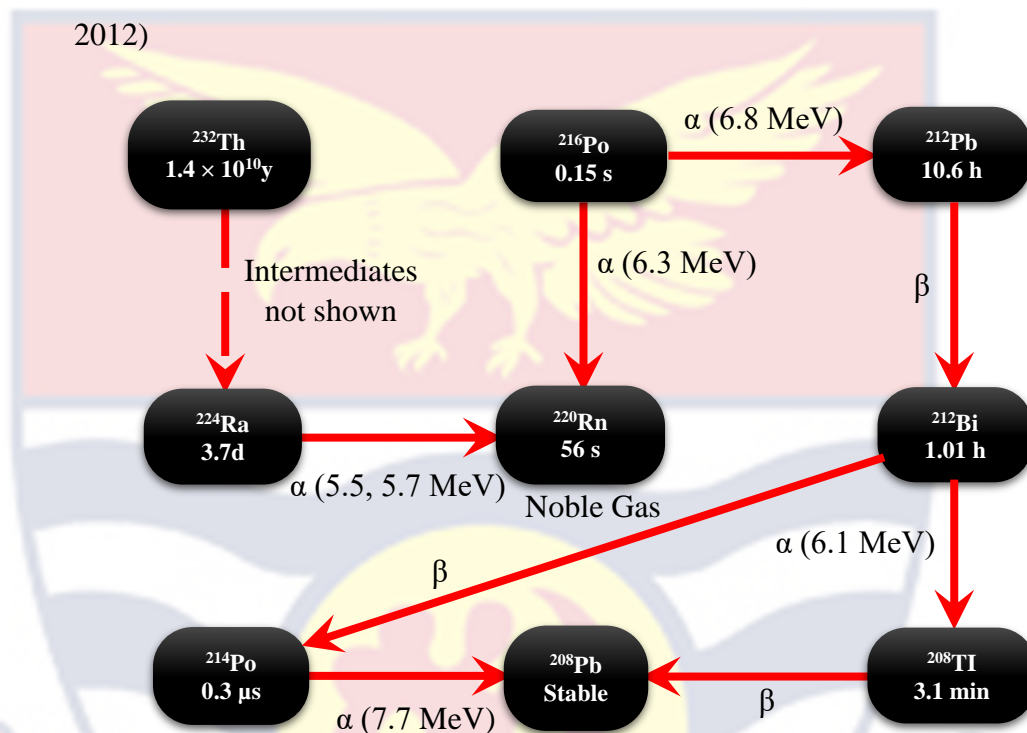


Figure 2: Thorium series (L'Annunziata, 2020)

Uranium ($^{238}\text{U}/^{235}\text{U}$) Decay Series

Uranium ($_{92}\text{U}$) is the heaviest of the primordial elements and is naturally radioactive but decay very gradually by emitting an alpha particle. Uranium-238 has a 4.5×10^9 year half-life, thus it is not very radioactive. The relative abundances of uranium in its natural forms are 99.2739 to 99.2745 %, 0.0050 to 0.0059 %, and 0.7198 to 0.7202 % for ^{238}U , ^{234}U , and ^{235}U , respectively (L'Annunziata, 2020). The parents of two radioactive decay series are ^{238}U and ^{235}U , with ^{238}U being the most long-lived member of the $4n + 2$ series, which also includes ^{234}U as a member and has n ranging from 52 to 59. While n varies

from 51 to 58, the ^{235}U is the most durable member and naturally occurring parent of the $4n + 3$ series (L'Annunziata, 2020).

Figures 3 and 4, illustrate 8 each membered ^{238}U and ^{235}U decay sequences, which culminates in ^{214}Pb and a stable ^{207}Pb following emissions of α and γ - decay products, respectively in each case. Terrestrial uranium is transferred by water, plants, and vegetables, and eventually through swallowed dietary supplements. Uranium and its derivatives are exceedingly harmful from both a radiological and chemical standpoint since they release highly ionizing alpha radiation. It is thought that just 15% of absorbed uranium comes through food, while 85% comes from drinking water.

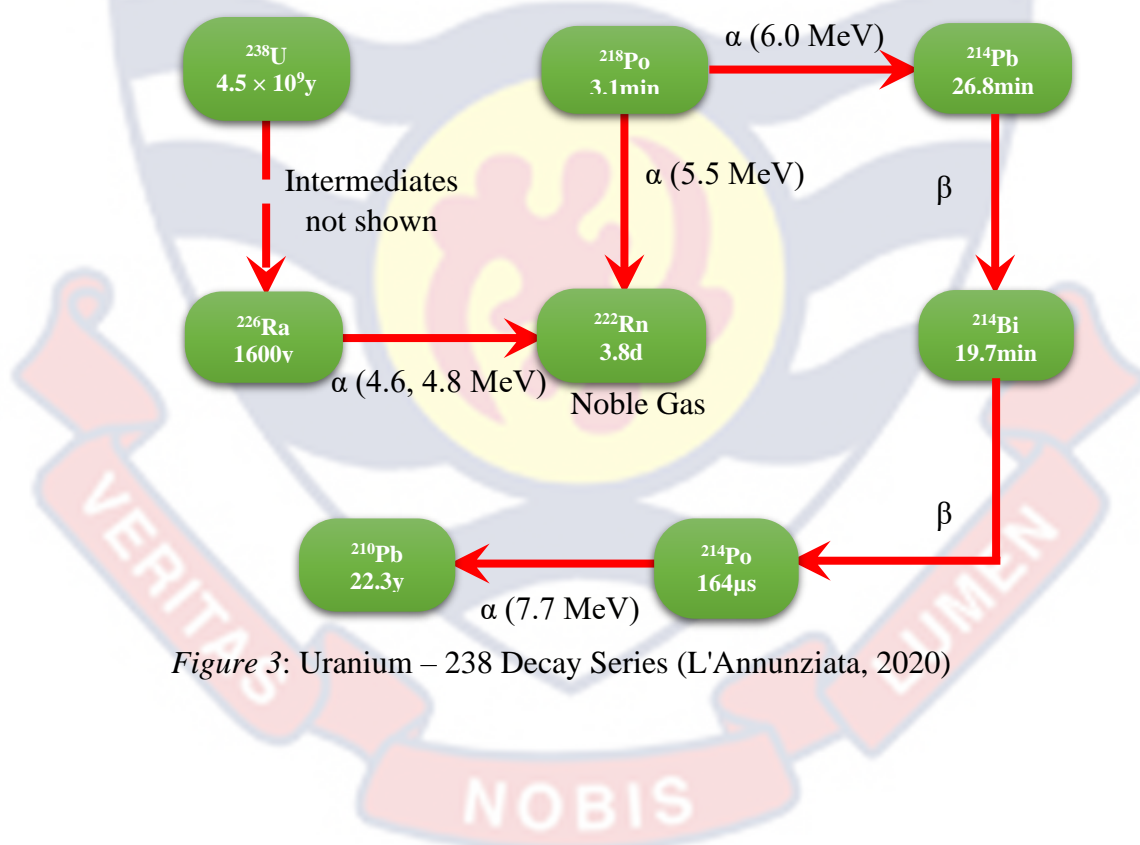


Figure 3: Uranium – 238 Decay Series (L'Annunziata, 2020)

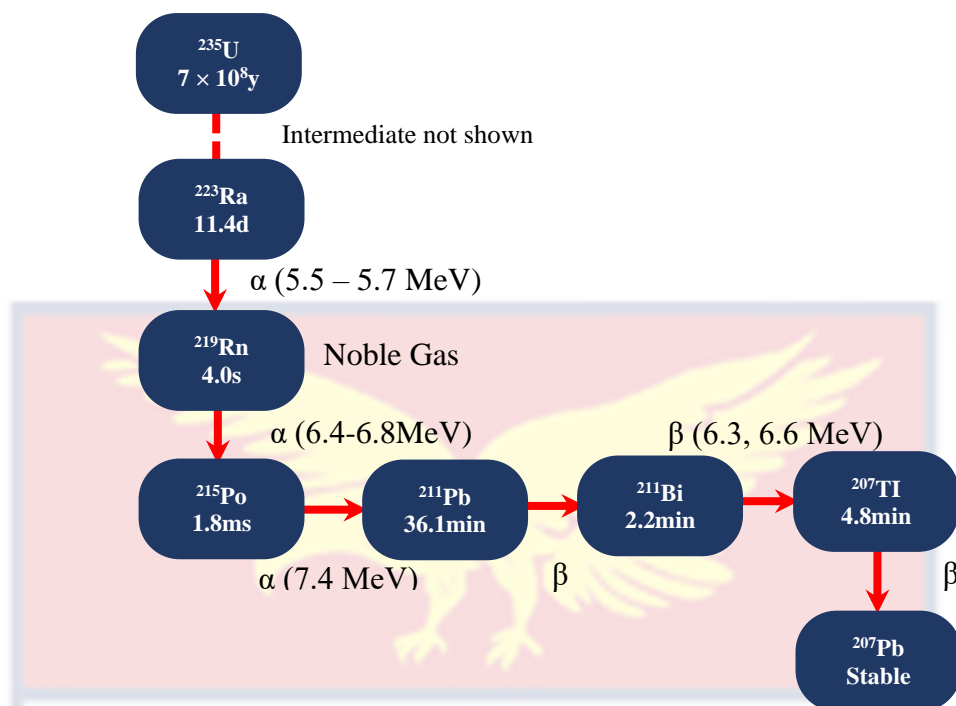


Figure 4: Uranium – 235 Decay Series (L'Annunziata, 2020)

Radium (²²⁶Ra)

Due to its radioactive characteristics, radium was one of the first materials found and was therefore inextricably linked with the discovery of radioactivity (Nisti et al., 2015). It is a radioactive element with chemical traits resembling those of barium and calcium. It contains thirteen radioisotopes, the most prevalent of which are the radioactive series ²³⁸U, ²³⁵U, and ²³²Th's decay products, ²²³Ra, ²²⁴Ra, ²²⁶Ra, and ²²⁸Ra. The remaining isotopes are produced synthetically (Olszewski et al., 2016).

²²⁶Ra is a radioisotope of radium with the highest environmental concern owing to its significant radiotoxicity and contribution to the population's internal dosage. It releases alpha and gamma radiations and has a half-life of 1600 years. Throughout the 20th century, ²²⁶Ra was utilized for a variety of industrial and medical applications. Consumer goods like toothpaste, hair treatments, and even food are included in the latter group due to their alleged

health benefits. These things were subsequently banned in a number of nations due to the possible health dangers such as lung cancer (Olszewski et al., 2016).

Bitumen slate, shale, volcanic, and phosphate rocks have the highest concentrations of ^{226}Ra . While sedimentary phosphate rocks correlate with uranium-rich minerals, bituminous slate and shale have high levels of ^{226}Ra that are most likely the result of organic-clay linkages (Nisti et al., 2015). Human activities have raised the quantities of ^{226}Ra in the environment, requiring the development of appropriate analytical processes capable of emulating their natural behaviour in the environment (soil, sediment, biota, and water).

Radioactive decay and equilibrium

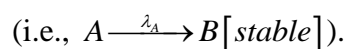
Radioactive substances emit β , α and γ particles. Artificial nuclei can spontaneously fission, emit neutrons, and emit protons and heavy ions. Radioisotopes form more stable atoms. Radioactive decay slows exponentially over time. Radioactive decay obeys a statistical law; Hence it is difficult to anticipate when an atom would disintegrate (L'Annunziata, 2020). Rutherford and Soddy gave the law that governs the decay and growth of radioactive materials. The law proposed that, when the number of nuclei in the sample is n , concentration (K) of a radioactive element is given by (L'Annunziata, 2020):

$$K = n\lambda \quad (1)$$

where λ = decay constant ($\lambda \neq 0$).

Considering the decay equation between parent and daughter nuclides:

1. Parent nuclide that disintegrates to produce a stable daughter nuclide



The rate of transition in parent nuclei A to stable daughter nuclei B per time is:

$$\frac{dn_A}{dt} = -n_A \lambda_A \quad (2)$$

From the differential equation 2, if the decay constant, λ is positive, it's termed the continuous growth rate; if it's negative, it's called the continuous decay rate.

If time, t is zero, magnitude of parent nuclei is n_A^0 and n_A at time, t , then the solution of equation 2 yields:

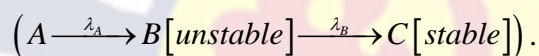
$$n_A = n_A^0 e^{-\lambda_A t} \quad (3)$$

Or

$$K_A = K_A^0 e^{-\lambda_A t} \quad (4)$$

where K_A^0 = activity at time, $t = 0$.

- The parent nuclide 'A' disintegrates to an unstable offspring nuclide 'B', which decays further to a stable nuclide C



The daughter nuclide's decay rate is determined by both its own decay rate and the rate at which it is created by the parent nuclide, and is expressed as:

$$\frac{dn_B}{dt} = \lambda_A n_A - \lambda_B n_B \quad (5)$$

Transposing equation 3 and 5 as a first-order linear differential equation, gives:

$$\frac{dn_B}{dt} + \lambda_B n_B = \lambda_A n_A^0 e^{-\lambda_A t} \quad (6)$$

The general form of equation 6 is called the Leibnitz equation (Ahmed, 2007; Cetnar et al., 2021), given by:

$$\frac{dy}{dx} + p = Q \quad (7)$$

and having its general solution as:

$$y = e^{-\int p dx} Q e^{\int p dx} dx + C e^{-\int p dx} \quad (8)$$

Solving for magnitude of atoms of daughter nuclide, n_B as a function of time, t from equation 6, we have:

$$n_B = \frac{\lambda_A}{\lambda_B - \lambda_A} n_A^0 (e^{-\lambda_A t} - e^{-\lambda_B t}) + n_B^0 e^{-\lambda_B t} \quad (9)$$

Equation 9 could be generalised for a substance that undergoes many decays if all initial nuclide concentrations are zero. Using Bateman equation (Ahmed, 2007; Cetnar et al., 2021), the i th radionuclide concentration is:

$$n_{B_i}(t) = \lambda_{B_1} \lambda_{B_2} \dots \lambda_{B_{(i-1)}} n_{A_1}^0 \sum_{j=1}^i \frac{e^{-\lambda_{B_j} t}}{\prod_{k=1, k \neq j} (\lambda_{B_k} - \lambda_{B_j})} \quad (10)$$

provided $n_{B_i}^0 = 0$ for $i > 1$. In the form of activity, n , Bateman equation (Ahmed, 2007; Cetnar et al., 2021) can be expressed as:

$$K_{B_i}(t) = \lambda_{B_1} \lambda_{B_2} \dots \lambda_{B_{(i-1)}} K_{A_1}^0 \sum_{j=1}^i \frac{e^{-\lambda_{B_j} t}}{\prod_{k=1, k \neq j} (\lambda_{B_k} - \lambda_{B_j})} \quad (11)$$

Alpha Particles

During an experiment with uranium in 1899, Ernest Rutherford discovered alpha particles for the first time. Alpha particles are helium nuclei with two protons giving them a double positive charge, as Rutherford showed in 1909 (L'Annunziata, 2020; Knoll, 2010). Alpha particles are a type of radiation with a very low penetrating power (L'Annunziata, 2020). An alpha particle emitted by a nucleus has discrete energy which is characteristic of the particular nucleus. Because of their electric charge and enormous mass, particles lose energy quickly when they pass through matter and do not go very far in the environment (relative to beta particles). Alpha particles are

characterized by low permeability with high ionizing power (L'Annunziata, 2020). Paper or skin can easily stop alpha particles with a few MeV.

An α -particle is thought to be travelling in the potential well of a strong attractive interaction (Abbasi, 2013). The alpha decay of the parent nucleus

$({}^A_Z X_N)$ to daughter nucleus ${}^{A-4}_{Z-2} Y_{N-2}$ could be expressed as (Duppen & Andreyev, 2018):



where A, N, and Z are the alpha decaying nucleus' mass, proton, and neutron numbers. Q_α - value reflects the negative of parent nucleus' alpha particle binding energy and quantifies decay energy. This release of kinetic energy is exothermic. Q-value predicts nuclear escape. Q-values range from 4 to 10 MeV for alpha emitters.

Beta Decay

In 1900, Henri Becquerel discovered the beta particle (Knoll, 2010). When a neutron (or proton) within the nucleus turns into a proton, the process of radioactive decay known as beta decay occurs (Abbasi, 2013). The neutron to proton ratio beta decays to produce a proton to neutron ratio, an electron to positron ratio, and an electron antineutrino/neutrino: $n \longrightarrow p + e^- + \bar{\nu}$ and $p \longrightarrow n + e^+ + \nu$. A beta particle is a charged particle that resembles an electron and is discharged from the nucleus of an unstable radioactive atom with an abnormal neutron-to-proton ratio (L'Annunziata, 2020).

A beta particle, a rapid electron emitted from the nucleus, and a neutrino, an electrically neutral subatomic particle, are also produced (L'Annunziata, 2020). Beta decay can be classified into three types: negatron emission, positron

emission, and electron capture (L'Annunziata, 2020). The atomic number (Z) and number of neutrons (N) of a nucleus vary by one unit during beta decay, but the overall mass number (A) remains constant ($A = N + Z$) (Knoll, 2010).

Because the beta particle is much lighter than the alpha particle, it can penetrate much deeper for the same amount of energy (Knoll, 2010).

Positron Emission

C. D. Anderson discovered the positron, a beta particle (β^+) with a positive charge, in 1932 (L'Annunziata, 2020). It has the same mass as an electron but one unit more positive charge. A positron emission occurs when a proton in a proton-rich nucleus ejects a positive electron (β^+) and so becomes a neutron [${}_1^1P \longrightarrow {}_0^1n + \beta^+$] (L'Annunziata, 2020). It usually happens when the proton to neutron ratio is greater than that of the chain's most stable isobar (Knoll, 2010).

Negatron Emission

Negatron emission is a negative-charged beta particle (β^-) that can arise only if the daughter nucleus is more energetically stable than the parent nucleus. According to theory, as a neutron spontaneously transforms to a proton and an electron, the neutron-to-proton ratio increases (L'Annunziata, 2020).



When the mass M (Z, A) of the parent nucleus exceeds the mass M (Z+1, A) of the daughter nucleus by more than one electron rest mass, Me, β^- decay can occur (Podgorsak, 2016). The proton remains in the nucleus, while the electron becomes a β^- particle. This occurs when the neutron-to-proton ratio exceeds the isobaric chain's stable ratio. This decreases neutrons while increasing protons

by one (Knoll, 2010). As a result, the energies of β^- particles range from zero to the Q limit (end point energy).

Electron Capture

Electron capture is a weak-interaction nuclear reaction. In this reaction, a free or bound proton captures an electron, resulting in an electron neutrino (Langanke et al., 2021). In electron capture decay, an unstable proton-rich (or neutron-deficient) nucleus reduces its proton excess by grabbing an orbiting electron from the same atom (L'Annunziata, 2020). In electron capture, Q is provided totally to the released neutrino, resulting in monoenergetic neutrinos (L'Annunziata, 2020).

The parent nuclide must be heavier than its neighboring isobar by an amount equal to the binding energy of the electron in the shell from which capture occurs. When an electron is captured, the disintegration energy over the electron's shell binding energy is squandered as neutrino and nucleus kinetic energy. In electron capture transitions, a bound proton absorbs an electron to become a neutron.



Radioactive decay equilibrium

Depending on their decay constants, daughter and parent nuclides may reach equilibrium after some time. Three factors can lead to long-term states of a radioactive substance (L'Annunziata, 2020):

1. Secular equilibrium;
2. Transient equilibrium
3. State of no equilibrium

Secular equilibrium

When the half-life of the parent exceeds that of the daughter, then the parent and daughter radionuclides reach secular equilibrium (Otoo et al., 2013) as shown in Figure 5. The parent radionuclide decays slowly to maintain equilibrium, while the daughter nuclide decays quickly. The decay of long-lived isotopes of uranium, such as ^{238}U and ^{235}U , and thorium, such as ^{232}Th , as well as the daughter decay products of these isotopes, are typical examples of secular equilibrium. Thus, the parent's activity equals that of daughter nuclide, and the ratio of their decay constants is the inverse of their equilibrium concentration (L'Annunziata, 2020). If parent's half-life is longer than daughter's $\left[\left(T_{\frac{1}{2}}^A \gg T_{\frac{1}{2}}^B\right) \text{ or } \lambda_A \ll \lambda_B\right]$ and the half-life of the decay product is higher, allowing the in-growth of the decay products. These two conditions promote the secular equilibrium state. For the condition of equal activity, the second term of equation 15 is neglected and hence, the daughter activity is given as:

$$A_B \approx \frac{\lambda_B}{\lambda_B - \lambda_A} A_A^0 e^{-\lambda_A t} = \frac{\lambda_B}{\lambda_B - \lambda_A} A_A^0 \quad (15)$$

Or

$$\frac{A_A}{A_B} \approx 1 - \frac{\lambda_A}{\lambda_B} \quad (16)$$

Since $\lambda_A \ll \lambda_B$, ignoring the second term on the right side of the equation 16, hence, we have $A_A = A_B$.

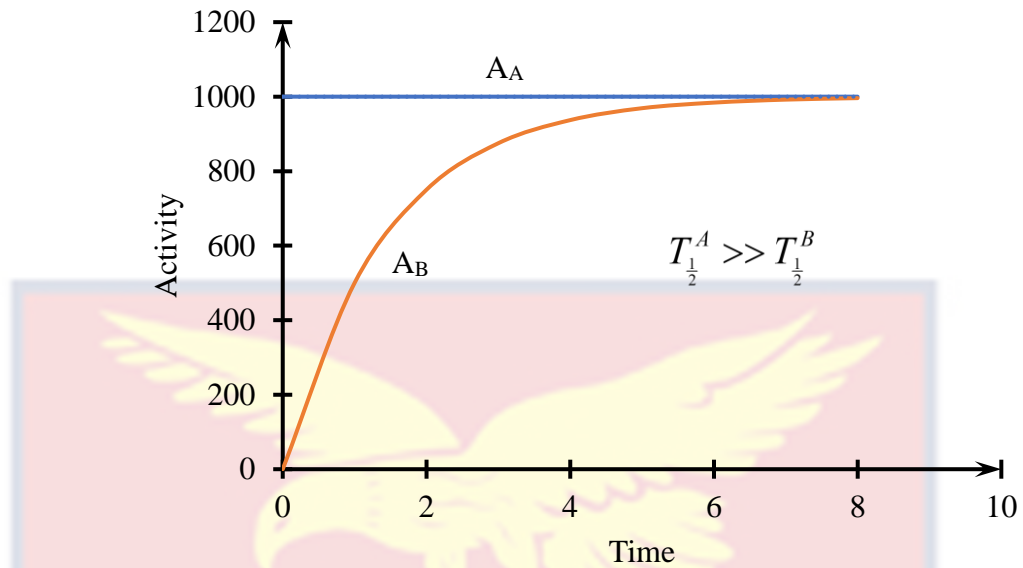


Figure 5: Secular Equilibrium between Long-lived Parent and Short-lived Daughter Nuclei (Le et al., 2014)

Transient equilibrium

Transient equilibrium occurs when the half-life of the parent nuclide is only slightly higher than that of the daughter nuclide, $T_{\frac{1}{2}}^A > T_{\frac{1}{2}}^B$ or $\lambda_A < \lambda_B$. As a result, the parent and daughter nuclides reside in a temporary state of equilibrium in which their activity diverge by a fixed proportion rather than being equal (L'Annunziata, 2020). The preceding approximation activity equation 2.16 is still true in this case, but the second term on the right side cannot be ignored. The common example of transient equilibrium decay is the decay of ${}_{82}^{212}\text{Pb}$ into ${}_{83}^{212}\text{Bi}$.

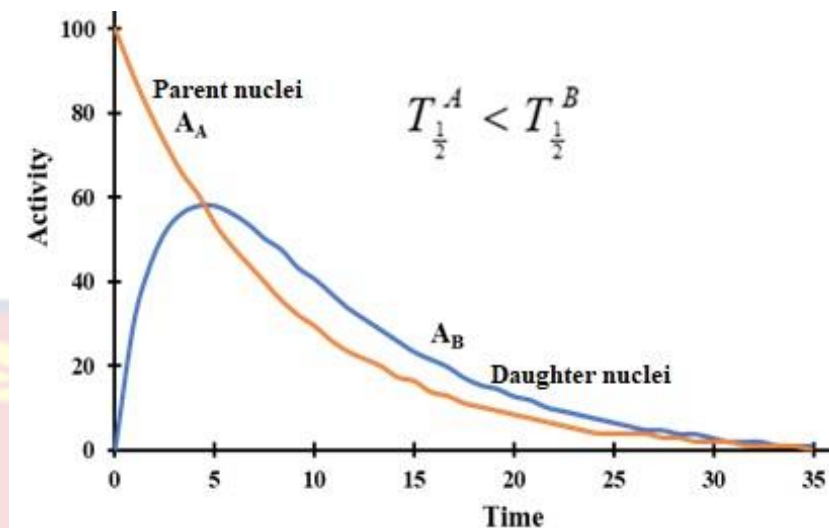


Figure 6: Radioactive Decay between Parent and Decay Nuclei with Time (Le et al., 2014).

Interaction of gamma rays with matter

When electromagnetic radiation passes through matter, it might do so passively or by transferring energy to the medium through which it is traveling (IAEA, 2010). The way electromagnetic photons, which are units of electromagnetic radiation, are absorbed by matter is determined by both the energy of the input photon and the composition of the target substance. Gamma rays interact with matter in three ways in the energy range of 0.01 to 10 MeV: the photoelectric effect, Compton scattering, and pair production (Knoll, 2010). These reactions are more likely to occur based on the material's atomic number, Z , and gamma-ray energy. At low energies, the photoelectric effect dominates, while pair production and the Compton effect dominate at high and intermediate energies, respectively.

Pair production

As shown in Figure 7, the full photon energy can be absorbed in the material and used up in the production of an electron-positron pair with total energy

equal to the photon energy, and the photon vanishes in the process (IAEA, 2010). The energy balance can be stated as follows:

$$E_\gamma = (T_{e^+} + m_{e^+}C^2) + (T_{e^-} + m_{e^-}C^2) \quad (17)$$

where T_{e^+} = kinetic energy of positron, T_{e^-} = kinetic energy of electron, m_{e^+} = rest mass of positron and m_{e^-} = rest mass of electron with $m_{e^+} = m_{e^-}$. Since $m_{e^+}C^2$ = rest energy of positron and $m_{e^-}C^2$ = rest energy of electron.

$$m_{e^+}C^2 = m_{e^-}C^2 = m_0C^2 = 0.511MeV \quad (18)$$

Equations 17 and 18 demonstrate that pair production is only possible if the gamma ray energy exceeds the total rest energies of positron and electron, or $2m_0C^2 = 1.022MeV$. The pair production method has a threshold energy requirement of 1.022 MeV. Pair formation is only significant for maximum-energy photons, and its contribution to the overall absorption cross section rises sharply beyond 1.02 MeV. (L'Annunziata, 2020).

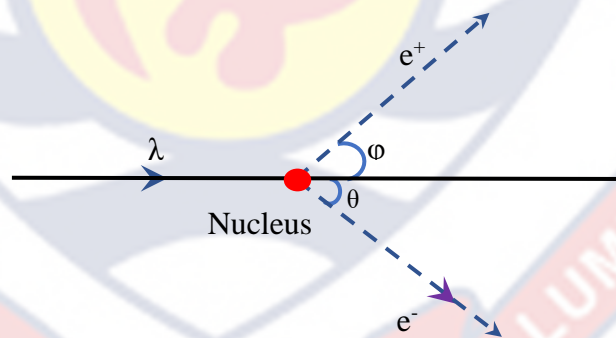


Figure 7: Pair Production (Le et al., 2014)

Photoelectric effect

As shown in Figure 8, photoelectric effect is a process in which a photon interacts with an inner bound shell electron in the medium's atom. This can happen if the incident photon energy exceeds the binding energy in the L or K

shell. The photon's transmission of kinetic energy to the electron causes the electron to be ejected from the atom (Knoll, 2010). When an electron is evacuated, an atom is left in an excited state, leaving a vacancy in that shell. An electron from the outer shell steps in to fill this void, emitting electromagnetic radiation (L'Annunziata, 2020). To calculate the kinetic energy (K.E) of a liberated electron, subtract the electron's binding energy from the photon energy. Which is:

$$\frac{1}{2}mv^2 = h\nu - E \quad (19)$$

where $h\nu$ = incident photon energy and E = ejected photo electron binding energy.

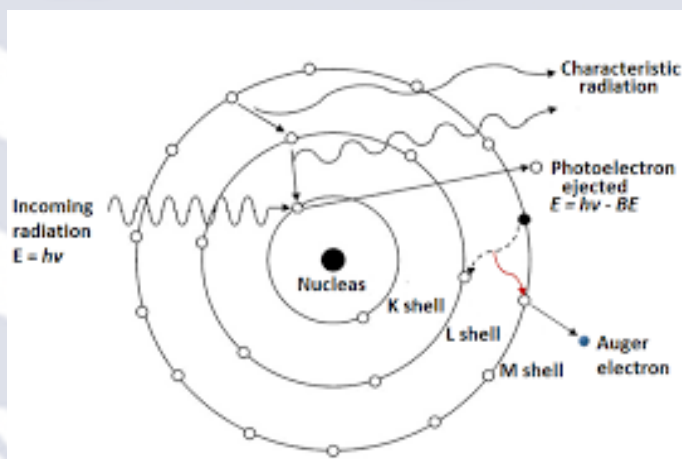


Figure 8: Diagram Showing Photoelectric Effect (L'Annunziata, 2020)

Gamma - ray with low energy interact primarily through the photoelectric effect in absorbing materials with higher atomic number Z . For shielding purposes in gamma ray spectroscopy, high- Z materials like lead are employed (Knoll, 2010). The photoelectric cross-section (δ_i) can be computed by detecting the K-shell X-ray energy and is approximated by equation 20:

$$\delta_t \cong C \frac{Z^n}{E_\gamma^{3.5}} \quad (20)$$

where C = constant, E = incident gamma photon energy, Z = target atom atomic number, and n is a number that changes between 4 and 5 depending on intruding photon's energy.

Compton scattering

In this process, as represented in Figure 9, an electron in the absorbing material's outer orbit interacts with a photon with energy E. The incident photon interacts with the atomic electron in this way, transferring energy to it and forcing the electron to leave the atom. After then, the photon experiences a deflection through an angle with regard to its initial direction. The recoiling electron receives some of the energy that the photon originally had. The energy given to the electron can range from zero to a significant fraction of the gamma radiation energy (IAEA, 2010).

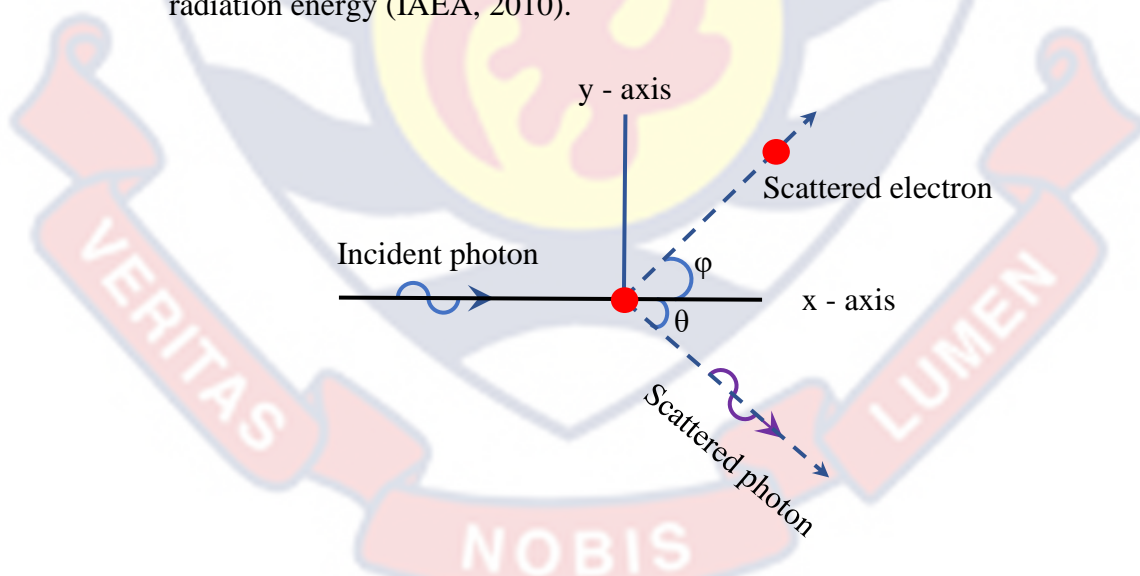


Figure 9: Diagram Showing Compton Scattering (L'Annunziata, 2020)

The relation between incident and scattered photon energy is denoted as:

$$\lambda_f - \lambda_i = \Delta\lambda = \frac{hc}{m_0c^2}(1 - \cos\theta) \quad (21)$$

where m_0c^2 represents an electron's 0.511 MeV rest mass energy

λ_f = scattered photon wavelength

λ_i = incident photon wavelength

Gamma ray attenuation

Becquerel identified three types of natural radioactivity in 1896, and a French chemist first saw it in 1900 when examining radiation from radium radiation with substantially higher penetrability than alpha and beta particles (L'Annunziata, 2020). Gamma decay can be represented by (L'Annunziata, 2020): ${}^A_ZX' \longrightarrow {}^A_ZX + \gamma$. Gamma radiations are electromagnetic radiations, with a very short wavelength of less than 0.1nm emitted by photons, which are radioactive nuclei.

The probability that gamma photons will interact with atoms, electrons, or nuclei as they pass through a material determines the attenuation of photons passing through it. The measured γ -ray intensity will be lower than the original emitted radiation's absolute intensity (Knoll, 2010). Despite the fact that the primary isotopes of uranium and plutonium generate gamma rays at constant energy and rates, the intensity of gamma rays measured outside a sample is constantly reduced due to gamma ray interactions with the sample. In gamma ray measurements involving large quantities of samples, this attenuation must be carefully considered. The transmitted gamma rays would be recognized and quantified if they pass through the sample without attenuation.

Linear attenuation coefficient

Gamma ray photons attenuate in any medium. Each photon in this package will pass in front of it without causing adsorption or excitation. As

photons interact, the resultant beam attenuates (Hasan et al., 2019). The wave's intensity and energy attenuate. As the path shortens, the intensity decreases (L'Annunziata, 2020). Gamma ray penetration is assessed using the linear attenuation coefficient (μ) (Otoo et al., 2013; L'Annunziata, 2020). The linear attenuation coefficient depends on:

1. energy of photon ($h\nu$);
2. atomic number, Z ;
3. absorber material effective density and
4. thickness of the sample.

Because of its reliance on density of absorbing medium, linear attenuation coefficient is the simplest absorption coefficient to determine experimentally, but it is rarely tabulated. Water, ice, and steam, for example, have distinct linear attenuation coefficients at different energies, although being the same chemical composition. Linear attenuation is the radiation interaction probability per unit length (Knoll, 2010; L'Annunziata, 2020). The linear attenuation coefficient indicates the empirically observed rate of radiation intensity drop (L'Annunziata, 2020):

$$I = I_0 e^{-\mu t} \quad (22)$$

where I (MeV/s) = intensity with no shielding in place

I_0 (MeV/s) = intensity with shielding material present

t (cm) = thickness of shielding material present and μ = linear attenuation coefficient.

The cross section characterizes the probability of interaction, which is true since the linear attenuation coefficient may be written in terms of cross section, σ as:

$$\mu = \sigma \frac{\rho K}{Z} \quad (23)$$

where K = Avogadro's number

ρ = weight density of the material and

Z = atomic number

Mass attenuation coefficient

The mass attenuation coefficient is a ratio of linear attenuation coefficient to density of an absorber and has the dimensions of area per mass (cm^2/g) and expressed mathematically as (L'Annunziata, 2020):

$$\mu_m = \left(\frac{\mu}{\rho} \right) (\text{cm}^2 \text{g}^{-1}) \quad (24)$$

where μ_m has unit of $\text{cm}^2 \text{g}^{-1}$ and ρ is the physical density. The mass attenuation coefficient is independent of the absorber density. The value of μ_m can be obtained from the measured values of incident and transmitted gamma-ray intensities. Density and photon energy govern mass attenuation coefficient calculations (Knoll, 2010). Bragg's rule gives the mass attenuation coefficient for multi-element materials:

$$\mu_m = \sum_k C_k (\mu)_k \quad (25)$$

where C_k = weight fraction of constituent element k and $(\mu)_k$ is mass attenuation coefficient of this element. The emission of the alpha particles decreases the mass of the parent nucleus as shown in Figure 10. The mass attenuation coefficient can be written in terms of cross section as (Podgorsak, 2016):

$$\mu_m = \sigma \frac{N_A}{Z} \quad (26)$$

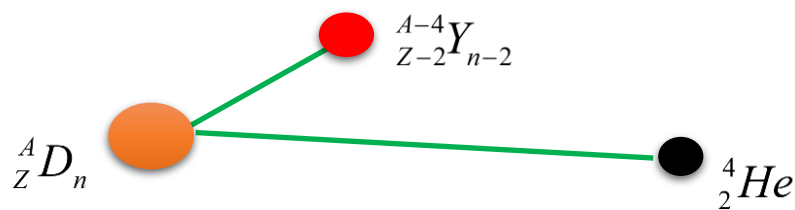


Figure 10: Diagram Showing Mass Attenuation of Radionuclide, D.
(Podgorsak, 2016)

Natural radioactivity detection

When radiation penetrates the detector material, a significant number of low-energy electrons are liberated from their atomic orbits, depending on how much of the energy is dissipated (Knoll, 2010). The released electrons are collected and transformed into a voltage or current pulse before being examined by an electrical system. The vast majority of nuclear radiation detectors operate on these core principles. The type of radiation, for example, influences the selection of a radiation detector. A number of detectors can be used to detect radionuclides.

High purity germanium detector

The intrinsic germanium or Hyper Pure Germanium (HPGe) detector is the one that is most frequently used for spectrometry. A built-in preamplifier in this HPGe amplifies the extremely tiny electrical pulses. The detector consists of a semiconductor diode with an n-type base, p-type emitter, and collector transistor. For an electric field to cross the intrinsic or depleted zone, the detector is reverse biased.

When radiation from a soil sample interacts with germanium atoms in a detector's depletion chamber, ion pairs (positrons and electrons) are formed, and these ion pairs are then accumulated at the P and N poles by the electric field.

The incident photon's energy is turned into electrical signals when it interacts with the crystal, and these signals are proportional to the charges created (Knoll, 2010). Because the electrical pulses are not particularly strong, a preamplifier is included. In order to precisely identify the signals, another amplifier is used to change the peak forms of each gamma line in accordance with their energy levels.

A multichannel analyzer is a device that monitors the electric potential of pulses and records them in channels corresponding to the amplitude of each signal (MCA) (Gilmore, 2008). The signals are then displayed on the screen. In order for the channel to match the energy that has been deposited, heights must be included in the channel allocation. Through calibration, common radionuclides like Cs-167 and Co-60 provide the link between energy and channels. Since the band gap of germanium is so tiny (about 0.7 eV), cooling detectors is necessary to adequately limit the heat effect from generated leakage currents (Gilmore, 2008). Leakage current, a source of noise, has the potential to negatively impact the detector's ability to resolve energy. Therefore, the detector is usually cooled using a source of liquid nitrogen at a temperature of -196°C .

NaI (TI) Detector

A crystal, a photomultiplier tube (PMT), a pre-amplifier, an amplifier, a multichannel analyzer (MCA), and spectrum data gathering and analysis software comprise a NaI (TI) detector. Gamma rays from an unknown radionuclide in a sample excite NaI (TI) atoms. Atoms de-excite by emitting visible photons (scintillations) whose strength is proportionate to the intensity of the gamma radiation. A photocathode, positively charged dynodes, and an

anode comprise the PMT. Light photons from the NaI (Tl) crystal interact with the photocathode, releasing photoelectrons.

At the first dynode, photoelectrons interact and release additional electrons. These electrons release more electrons as they reach the second dynode. The electron pulse intensifies down the dynode series until it hits the PMT's anode. The pre-amplifier converts the electron pulse from the anode into a voltage pulse. The relationship between voltage and scintillator gamma energy is directly proportional.

Radon in the Environment

Properties and origin of Radon

Radon is a colorless, odorless, and tasteless radioactive gas with a half-life of 3.82 days which decays into alpha particles (Podgorsak, 2016). It is a monoatomic gas with a density of 9.73 kg/m^3 at standard pressure and temperature, which is about 7.5 times the density of the Earth's atmosphere at sea level (1.217 kg/m^3), making it the heaviest of the noble gases (Khan, 2019). Radon has an atomic number of 86 and a boiling point temperature of -61.8 degrees Celsius. Radon is relatively soluble in water and readily diffuses with water vapour and gases.

Radon, a major component of natural radiation, is undetectable without special equipment. This is generated by naturally occurring decay chains of uranium and radium. 36 radon isotopes of mass numbers from 193 to 228 are known. ^{222}Rn has the longest half-life. Half-lives of ^{211}Rn , ^{210}Rn , and ^{224}Rn are an hour. ^{222}Rn , ^{220}Rn , and ^{219}Rn are the only natural isotopes of radon. ^{238}U (uranium), ^{232}Th (thorium), and ^{235}U (actinium) decay into these. The isotope ^{220}Rn , also known as thoron, has a half-life of 55.6 seconds, while ^{219}Rn ,

commonly known as action, has a half-life of 3.96 seconds (L'Annunziata, 2020). One molecule of radium is present in 1021 molecules of air, and 1 gramme of radium decays into ^{222}Rn in 6 inches of soil per square mile.

All soils contain radon in different amounts. Geophysical and geochemical factors affect its emission, whereas hydro-meteorological circumstances control it. It can also be present in the air, both indoors and out. Radon released from soil, on the other hand, is more than that released from water and construction materials (Hussein et al., 2013). The quantity of uranium and thorium in rocks and soil, the ground's ability to release radon, the soil's porosity, the soil-air pressure differential, and soil wetness all affect radon gas diffusion from soil into the air (Hussein et al., 2013). Along with earth, water, and air, building materials can emit radon. Different building materials release radon differently. Radium-226 particular activity is utilised to determine radon exhalation from soil (Bqkg^{-1}). The quantity is equal to the product of the radium (^{226}Ra) specific activity, A_s , and radon gas exhalation coefficient, η :

$$A_{\text{eff}}(^{226}\text{Ra}) = \eta \times A_s(^{226}\text{Ra}) \quad (27)$$

Decay products of Radon

Radon is an inert gas having atomic number 86 and three natural isotopes of mass numbers 222, 220 and 219 (Abbasi, 2013). These radioisotopes are members of ^{238}U , ^{232}Th and ^{235}U series respectively. Radon undergoes radioactive decay as intermediate radioactive decay product in the ^{238}U (^{222}Rn), ^{235}U (^{219}Rn), and ^{232}Th (^{220}Rn) decay chains (Figures 2 to 4). The daughter products of ^{222}Rn (^{218}Po , ^{214}Pb , ^{214}Bi , ^{214}Po) have an aggregate mean life of 71.57 minutes, while the ^{220}Rn (^{216}Po , ^{212}Pb , ^{212}Bi , ^{212}Po) and ^{219}Rn (^{215}Po ,

^{211}Pb , ^{211}Bi , ^{207}Tl) have aggregate mean lives of 16.81 hours and 1.03 hours, respectively (Mostafa et al., 2015). The Figures 2 to 4 also show the half-lives, decay mode, energy of emission (alpha, decay, and gamma), and yield of nuclear decay for the ^{238}U , ^{235}U , and ^{232}Th series, respectively.

Radon as a Health Hazard

The fact that radon is a human carcinogen is well recognized. Lung cancer is enhanced when people are exposed to higher radon concentrations for longer periods of time. Like many other environmental contaminants, the extent of radon's health hazards is unknown. Researchers, on the other hand, are more convinced about the dangers of radon than they are about the dangers associated with other cancer-causing environmental substances. The inhalation of radon as well as its offspring, followed by the deposition of energy and particles in the lining of the lungs, causes cancer. These particles are emitted by the short-lived decay products from ^{218}Po , ^{214}Pb , ^{214}Bi , and ^{214}Po (Esan et al., 2020).

High radon concentrations within homes could provide a serious health danger in the form of an elevated risk of cancer. Radon decay products attach to dust particles in the air or are deposited on room surfaces in the indoor environment. Inhaled radon decay products with a short half-life are deposited in lung tissues. Radon decay products irradiate sensitive cells in lung tissue, and these cells could be the bronchial epithelium's basal cells.

Sources of Radon Exposure

Indoor Radon

Radon is partially emitted once it is generated in soil-rock grains. Radon that has been emitted moves via the existing pore space and migrates across

short or long distances. The soil beneath the building and the building materials, which contain radium, are the primary sources of radon in structures. In comparison to the ground, buildings typically have slightly lower indoor air pressure.

Radon gas generally penetrates buildings through a variety of methods, including diffusion and pressure-driven flow from the ground beneath and next to the building. Radon gas typically enters buildings through gaps around cables and pipes, as well as cracks and holes in floors and walls. Most buildings with high indoor radon concentrations are recognized for using pressure driven flow as their primary method of entry. Exhalation also introduces radon from the soil and other building materials into the indoor environment. Outside air has relatively low levels of radon, which are of small concern (WHO, 2009), but when it is unable to disperse, it accumulates to a higher level inside the environment. The materials holding radium (the immediate parent of radon in the decay chain) components (such as soil, rocks, mining ores, and so on) and the materials carrying radon are examples of radon sources (such as water, natural gas etc.). Principal factors such as dwelling engineering and meteorological parameters affect the indoor radon concentration.

Factors influencing indoor radon

Dwelling engineering

The amount of radon present inside a structure is significantly affected by its architecture. Air enters a structure through fractures and gaps, as well as ceilings, floors, and walls, and sanitary devices (Ahad, 2004). The amount of air exchange provided by mechanical ventilation will be affected by fan positioning. Other situations involving the chimney and stack effects have been

recorded, in which radon concentrations on the first or second floors are higher than in the basement (Lewis et al., 2021; Gulan et al., 2022). Other sources include loose fitting pipes that go through walls or floor drains that are connected to weeping tiles and provide a direct access into the basement. A sump without a cover or a loose-fitting cover has been a common entrance pathway for water-borne radon gas.

Meteorological parameters

As ^{226}Ra decays in particles, radon atoms must escape to fluid-filled pores due to recoil. Radon gas diffuses through pores and reaches the surface before decomposing. Diffusion or convection transfer particles through pores to the atmosphere. Exhalation rates and infiltration owing to climatic variations affect indoor radon concentration. Some of these meteorological quantities that affect the transport of radon gas are pressure, temperature gradient, wind speed and moisture.

Pressure

Pressure affects radon exhalation. Due to the sucking action of falling pressure, a 1.0 mm drop in pressure generates a 5 - 10 % increase in radon exhalation. Radon-222 flux from soil and soil gas concentration alter inversely with barometric pressure. Theoretical and experimental data on flow and diffusion during barometric pressure fluctuations accord well.

Temperature gradient

Because of the stack effect, infiltration is highly dependent on temperature variations, especially during the winter season. The greater inside

temperature indicates a pressure across the building shell that changes with the height, including a convective loop that takes air into the building near the bottom and out toward the top of the building. (Zhang & Sun, 2019). As part of the infiltration model, the driving force has been parameterized in a straightforward model:

$$Q_{stack} = A_0 \cdot f_s \cdot T^{\frac{1}{2}} \quad (28)$$

where, A_0 = effective leakage area of the building

T = absolute value of the temperature difference between indoors and outdoors and

f_s = stack parameter.

Moisture

The amount of moisture in a substance increases the rate of radon emanation. Pearson found a substantial change in emanation with soil moisture over a duration of weeks (Zhang & Sun, 2019). Moisture appears to have three primary impacts that cause an increase in radon exhalation:

- (a). When there is fluid in the material's internal pores, the direct recoil portion of the emanation power increases.
- (b). The fluid may prevent radon gas from being absorbed by the material's internal surfaces.
- (c). Active radon transport on water molecules may occur if the sample has a moisture content gradient.

The sample will absorb more water before the pores are entirely filled if the porosity is high, and maximum radon exhalation rate will occur at a greater moisture content than low porosity materials. As moisture content increases, it

is seen that the rate of radon diffusion in soil and sand decreases and is lowest close to saturation (Zhang, 2019).

Wind speed

Wind speed enhances radon emission. For very low wind speeds detected between grass blades 125 cm above the ground, emanation does not vary with wind speed infiltration models such as:

$$Q_{wind} = A_0 f_w V \quad (29)$$

where V = Wind velocity, A_0 = Effective leakage area of the building and f_w = Wind parameter. The specifics of how wind speed varies with height close to the ground are crucial for describing how radon entrance is influenced by this component.

Occupancy behaviour

The occupants' living patterns largely affect the amount of radon gas in the indoor air (Yang et al., 2020). Human actions including opening and closing doors and windows, using air conditioning, fans, and other similar activities influence the air exchange rate, causing the radon level in a residence to fluctuate. Ventilation is also affected by the location and operation of fans. People, in reality, have a say in how much natural and mechanical ventilation are employed to boost air exchange rates (Senitkova & Kraus, 2019; Yang et al., 2020).

The amount of water and natural gas used in a home differs from one to the next. The quantity of radon released into indoor environment as a result of water use is determined by the amount, time, and location of water consumed. Cleaning, bathing, dish and cloth washing, and toilet flushing all discharge

water. The amount of radon in a house varies depending on whether it is used in the winter or summer, where it is used, and how long it is used.

Seasonal variability

Geological and meteorological fluctuations cause seasonal changes in soil-gas radon concentration (Yarmoshenko et al., 2016). Seasonal variations are related to topography, water saturation and moisture retention. A layer of water-saturated surface soil traps radon during the rainy season (the capping effect). During the dry season, as the earth got drier and more permeable, it breathed more easily. For sites with low permeability, the wet layer becomes thinner than the monitoring depth, and capping increases radon levels during the rainy season; radon levels begin to decline several months later as the wet layer expands. For sites with high permeability, the wet layer spreads rapidly beneath the monitoring depth, resulting in the lowest concentrations during the rainy season (Otoo et al., 2018).

Soil

Soil is typically regarded as the third most important environmental component, after air and water. In practice, soil provides the foundation, both literally and figuratively, for a significant portion of the earth's collected life through the capture of solar energy by green plants. Soil pollution can be defined as the failure of soil as an environmental component as a result of contamination, especially as a result of human activities. Because plant roots are one of the methods to incorporate contaminants into the food chain, determining their presence in soil is critical.

The presence of radium in the earth, as well as its ultimate precursor uranium, is linked to radon emanation. Although these elements can be found in almost any type of rock or soil, their concentrations vary depending on the location and geological nature. If radon is produced near the surface, it can escape rather than being trapped underneath. The level of radium in the soil, water, natural gas, and air pressure are all factors that influence the rate of radon emission from soil (Elzain, 2017).

Radon enters the air – largely by radon atom recoil and disintegration of ^{226}Ra – and fills soil pores. The percentage of ^{222}Rn created in the soil that penetrates the pores is known as emanating power. The rate of radon emission from the earth's surface is around 0.5 picocuries per m^2 per second ($0.0185 \text{ Bq m}^{-2} \text{ s}^{-1}$), or 160 Ci ($5.92 \times 10^{12} \text{ Bq}$) per km^2 per second. As soil allows about 10 % of radon to escape into the atmosphere, the annual amount of radon escaping from the total land area of $1.50 \times 10^{18} \text{ km}^2$ is $7.57 \times 10^{16} \text{ Ci}$. The amount of radium in soil, as well as permeability of soil, influence the rate of emission. Exhalation rates of ^{222}Rn from soil range from 0.0002 to $0.07 \text{ Bq m}^{-2} \text{ s}^{-1}$ (L'Annunziata, 2020).

If the earth material is regarded as a semi-infinite porous mass of homogeneous material, ^{222}Rn flux density at surface J_D ($\text{Bq m}^{-2} \text{ s}^{-1}$) is given by (Taapopi et al., 2017):

$$J_D = C_{Rn} \lambda_{Rn} f \rho \left[\frac{D_c}{\lambda_{Rn}} \varepsilon \right]^{0.5} \quad (30)$$

where:

C_{Rn} = Activity concentration (Bq/kg) of ^{226}Ra in the earth material

λ_{Rn} = disintegration constant ($2.1 \times 10^{-6} \text{ s}^{-1}$)

f = emission fraction

ρ = density (kg/m^3) of the material

D_e = effective diffusion coefficient (m^2s^{-1}) for the earth material

ε = porosity of the earth material

The first four factors in equation 31 define the volumetric production rate of radon ($\text{Bqm}^{-3}\text{s}^{-1}$) and the terms within the square brackets represent the diffusion length.

Building Materials

Radionuclides that are found in the earth's crust are present in building materials consisting of soil and rocks. As a result, building materials can be a source of ^{222}Rn , particularly if radium level is greater than 37 Bqkg^{-1} . Some industrial goods are also used to prepare building materials and contain a significant amount of radium (Amin, 2015).

The rate of radon emission is influenced by the material utilized as well as the surrounding environment. Surveys have compared the ^{226}Ra content and ^{222}Rn emission rates of building materials. The fluctuation in the emanation rate of radium-containing materials is due to physical characteristics such as ambient pressure and humidity. Furthermore, it has been discovered that concrete emits the most radon, with sand being the largest emitter and cement being the least among the concrete components (Abbasi, 2017). If a building unit, such as a wall or a floor, is modeled as a semi-infinite-thickness slab of porous materials, the radon flow density from one side is:

$$J_D = C_{Ra} \lambda_{Rn} f \rho \left[\frac{D_e}{\lambda_{Rn}} \varepsilon \right]^{0.5} \tanh \left(d \rho \left[\frac{D_e}{\lambda_{Rn}} \varepsilon \right]^{-0.5} \right) \quad (31)$$

where:

D = the half-thickness in meters of the building unit

The other symbols represent the same parameters as in equation 31, but the values are for the construction materials. The hyperbolic term in equation 31 accounts for the slab's finite thickness and is always smaller than unity.

Ground Water

Radon emanation from ground water sources is the second most significant source of radon. When ground water comes into contact with crustal rock, it dissolves the radon that has been released into the pores and voids of the rocks and soils due to ^{226}Ra decay. In most cases, water transport rather than diffusion governs the movement of radon in water. Several research have been undertaken to investigate the relationship between ^{222}Rn levels in water supplies and indoor radon levels in typical houses (Al Zabadi et al., 2012). The majority of these research produced semi-empirical relationships indicating that the indoor-to-aquatic radon ratio is on the order of 10^{-4} . Equation 32 is derived from a steady-state derivation of link between indoor radon and radon emitted from drinkable water supplies:

$$C_a = \frac{C_w f V_w}{X_h V_h} \quad (32)$$

Where:

C_a = concentration of ^{222}Rn air

C_w = concentration of ^{222}Rn water (pCi/L)

f = transfer efficiency of ^{222}Rn from water to air

V_w = water use rate (liters/hours)

X_h = ventilation rate of air change per unit hour

V_h = volume of house = volume of air change.

Natural Gas

Radon is combined with natural gas as a result of the presence of ^{226}Ra in the surrounding soil of the gas-well. ^{222}Rn gas travels with the natural gas until it reaches a point where it can be used in the home. Radon concentrations in wells have been observed ranging from undetectable levels to around $5.4 \times 10^4 \text{ Bqm}^{-3}$. Generally, the ^{222}Rn concentrations in natural gas stated as 1000 Bq/m^3 with an entry rate of about $0.3 \text{ Bq/m}^3/\text{h}$ into indoor environments. In general, ^{222}Ra is carried along with natural gas to gas plants, in which the natural gas is processed to eliminate pollutants and collect the less volatile hydrocarbons that naturally separate out in pipes. Natural gas that is delivered often comprises gas that was extracted from a number of different wells and fields. Due to this, the quantities of natural gas that are extracted from various sources might fluctuate over time (UNSCEAR, 1993).

Radon Detection

When radiation impacts the detector material, a large number of low-energy electrons are liberated from their atomic orbits, depending on how much energy is dissipated (Knoll, 2010). The released electrons are collected and converted into a voltage or current pulse in order to be examined by an electrical circuit. The vast majority of nuclear radiation detectors operate on these core principles. ^{222}Rn measurements are frequently described in terms of short-term or long-term measurements. Three characteristics were used to describe the radon measuring methods:

- (i). Whether the method measures ^{222}Rn or its offspring;
- (ii). Temporal resolution; and

- (iii). Radioactive detection of radioactive decay-produced emissions such as alpha, beta, or gamma radiation.

The most popular approaches rely on alpha particle detection (Knoll, 2010). For detecting radon concentrations in subterranean, occupational, indoor, and outdoor settings, a variety of equipment and procedures are available. When it comes to choosing the appropriate measuring method and methodology, factors such as dependability, resources, availability, sensitivity, time commitment, and cost all play a part. The two types of radon gas measuring procedures that are most often employed are time integrated/passive and active/instantaneous.

Passive techniques

The function of passive radon measuring equipment is not dependent on the presence of electricity. Because radon and its progeny's activity levels change over time owing to the impacts of seasonal, weather, and environmental variables in homes, concentrations must be determined over a longer period.

Time integrating detectors are devices that use passive approaches to calculate average concentrations over long periods of time. These are often less costly and are recommended for estimating a dwelling's average yearly radon gas concentration they do not require any particular training to use for a variety of applications (Khan et al., 2019). Activated charcoal detectors, electret ion chambers, thermo-luminescent dosimeters, and solid-state nuclear dosimeters are some of the most common passive radon detection techniques used to monitor radon gas concentration (WHO, 2009).

Solid State Nuclear Track Detectors (SSNTDs)

The majority of SSNTD applications employ two types of detecting media. First, polymeric or plastic detectors used for radiation monitoring and measurement in health physics, radiation protection, environmental research, and applications such as measuring radon levels in residences or outdoors, among other nuclear physics and radioactivity fields. The second type of detector consists of natural mineral crystals (and glasses) that retain their radiation (and temperature) histories (Kpordzro, 2018). They are utilized most commonly in geology, planetary sciences (especially lunar and meteoritic materials), oil drilling, and other related fields.

The plastic detector's chemical or chemical pattern increases the alpha channels, allowing them to be counted manually or automatically using optical microscopy. The primary distinction between filtered and unfiltered alpha track detectors is that unfiltered alpha track detectors lack a filter to separate radon progeny and other alpha particle ejectors. The laboratories in Ghana at GAEC can read CR-39 and LR-115 detectors.

CR – 39 Detector

The CR-39 detector (made of poly-allyl-diglycol-carbonate), is one of the widely used nuclear track detectors (Sabbarese et al., 2020). CR-39 detectors are tiny piece of specially formulated plastic made of CR-39, also known as polyallyl diglycol carbonate ($C_{12}H_{18}O_7$). A sturdy plastic measuring 1.0 cm by 1.0 cm that was sensitive to alpha particle tracks served as the detector. It is the most popular and regarded as an effective detector for measuring radon (IAEA, 2003). The exposure duration for nuclear-track detectors typically ranges from one to twelve months. The Radon measurement chamber has a tiny internal volume and high

sensitivity. Radon is more sensitive as a result of this circumstance.

Additionally, the unique construction of the chamber prevents sensitivity from varying with humidity and temperature. Until it is time to utilize the detector, it is enclosed in a radon diffusion-resistant material.

LR – 115 detectors

Cellulose nitrate ($C_6H_8O_9N_2$) film (LR – 115 type II) designed and produced by the Kodak Pathe, Dosirad Co., France is another widely utilized nuclear track material. The LR – 115 type II or polycarbonate (Makrofol) (Wasikiewicz et al., 2019), the most well-known detector in this category, is available commercially. It is a plastic track detector that has been used all around the world to monitor radon, thoron, and their offspring. The LR – 115 type II detector is red coloured based on cellulose nitrate with a thickness of approximately $12.0 \mu m$ deposited on $100 \mu m$ thick nondetachable clear polyester-based substrate. It is free of self-plate out effect and does not record tracks owing to self-plating daughters, - particles of energy 6.0 MeV (^{218}Po) and 7.69 MeV (^{214}Po). This detector has been widely utilized for long-term integrated measurements because it is sensitive to α – particles and provides a very useful and less expensive approach, which emits in the energy range of $1.9 - 4.2 \text{ MeV}$ α – particle traces can be seen via etched holes. This is a passive detector that does not require any power to operate.

Active techniques

Active techniques, also known as immediate techniques, require electricity to operate and are primarily employed for short-term measurements.

These are based on a single-point grab sampling of the air, followed by radon concentration determination by α -particle activity. Because Grab samples provide rapid results, they can be tested in the lab or on the spot with portable equipment. There are several instruments that employ active approaches. Scintillation cells or Lucas cells, Ionization chambers and surface barrier detectors are some of the most common alpha particle detectors employed by researchers today. The AlphaGUARD and Sarad 7 radon monitoring detectors are two active detectors used in RPI laboratory (GAEC), Ghana.

Alpha Guard

The AlphaGUARD, is a portable radon monitoring detector which is a continuous active radon sampling sensor. It is one of the most used commercial ionization chambers and detects radon concentration levels using an alpha spectroscopy to detect radon and has an optimal sensitivity. It is the most widely used portable radon measurement active equipment (Mostafa et al., 2015). ^{222}Rn and ^{220}Rn are the two common isotopes of radon that are recognized through their respective energies from the alpha decays (Tokonami, 2020). A digital output is created from the signal produced by the alpha detection. The AlphaGUARD, dataloggers, or a PC are all capable of reading this output. The AlphaGUARD is primarily used for radon measurements in water storage, indoor and outdoor settings, in mining environments, and in radon soil-gas.

Sarad 7 Radon Monitoring

Sarad 7 radon monitoring detector is active radon and thoron monitoring equipment that quantifies radon and thoron activity concentration in soil gas based on continuous or timed collecting of soil gas samples through a packer probe in a properly sized bore-hole and sealed with regard to ambient air. The radon and thoron detector RTM 2200 can operate sampling equipment like

pumps, valves, and positions. One radon and thoron monitor can measure radon in multiple rooms. Pressure and temperature sensors can be used to sample radon movement in buildings and facilities. The apparatus measures progeny and environmental and geological parameters like humidity, pressure, temperature, and soil flow rate. Sarad 7 includes built-in software that computes and stores concentration instantly.

Tracks Formation

During exposure, alpha particles from radon and its decay products strike the detector, generating minuscule areas of damage inside the plastic known as latent tracks. When ^{222}Rn or its decay products release alpha particles in close proximity to the detecting material, this damage occurs. Radon exposure, or the average concentration over time, is inversely related to track density, which is expressed as a number per unit of surface. The dimensions and shapes of these tracks disclose information about the mass, charge, energy, and travel direction of the particle. The detectors (CR-39) discriminate between different types and energy of particles (Khalil & Al – Jubbori, 2020).

Chemical etching

The size of the alpha tracks is increased by chemically etching the detector (CR-39), which makes it easier to count the tracks manually or automatically and to see the tracks created by the interaction of radon and its decay products with alpha radiation. The ratio of tracks to surface area is directly related to the integrated radon concentration after background counts are removed.

Track density can be transformed into radon concentration using a conversion factor established through controlled exposures at a calibration facility. The radon exposure, or the average concentration over the course of the exposure time, is inversely related to the track density, which is given as the number per unit of surface. The type of the chemical solution, its concentration, the length of the etching process, and the temperature vary depending on the type of detector. Chemical etching typically uses solutions of potassium hydroxide (KOH) or sodium hydroxide (NaOH) in varying concentrations at temperatures ranging from 40 °C – 100 °C (Durrani and Ilic, 1997).

Biological effects of Natural Radioactivity and Radon

Ionizing radiation and radioactive materials can be seen in our surroundings naturally. The risk of radiation exposure can only be minimized, not entirely eliminated. Radiation exposure can have both deterministic and stochastic negative impacts on health.

Deterministic effects

When a certain exposure threshold has been exceeded, negative consequences may result. The threshold is usually low and might change from person to person depending on how body cells are formed. The severity of an effect, however, increases with dose when exceeded. Erythema of the skin, sterility, hair loss, cataracts, and prenatal abnormalities are examples of deterministic effects. Delay in cell division or cell death is predictable in response to extremely high radiation doses. If the exposed tissues are sufficiently exposed, these impacts may impair their ability to function.

Stochastic effects

These are the effects of radiation exposure that have a delayed onset. This induction occurs over the whole dose range, without regard to a threshold level. These could result from a cell's change after radiation exposure. After a protracted wait, the altered cell can transform into cancer. There is no dose effect threshold below which cancer cannot develop. Higher doses increase the risk of cancer development, although radiation exposure has no effect on the severity of any cancer that could arise. Numerous hereditary disorders may arise in the offspring of a radiation-exposed person if a germ cell that transmits information to genes to offspring is destroyed.

Radiation Dose

The radiation dose is the amount of energy a person absorbed over a period of time (usually a day). The time, type, and amount of radiation all play a role in how radiation affects an individual. Dosimetry is the measuring of such doses, and the quantity is known as a dosage. It is measured using either the exposure or dose of radiation. Measuring the dose (quantity of energy absorbed in a system) is the best way to assess irradiation absorption (IAEA, 2010).

Radiation exposure

Radiation exposure is calculated using radiation's ability to ionize air at normal temperature and pressure. Many radiation detectors detect radiation exposure, such as the Geiger-Mueller counter. The previous exposure unit was the Roentgen (R), with 1 R equaling 2.58×10^{-4} Ckg⁻¹ air. Coulombs per kilogram (Ckg⁻¹) is the international system unit of exposure. The exposure unit only applies to air and cannot be used to calculate tissue dosage (IAEA, 2010).

Absorbed dose

The quantity of energy from any type of radiation that is absorbed by a given mass of tissue is regarded as absorbed dose. The mean absorbed dosage (D_A) caused by ionizing radiation of type R and averaged well over volume of a certain organ or tissue is provided by (L'Annunziata, 2020);

$$D_A = \frac{dE}{dm} \quad (33)$$

Absorbed dose rate is in a unit of Gy and $1.0 \text{ Gy} = 1.0 \text{ Jkg}^{-1}$.

Equivalent Dose

For radiation protection and occupational exposure purposes, equivalent dose is used to assess the biological effectiveness of various radiation types to tissues. It is the sum of absorbed dose and radiation weighting factor W_R for ionizing radiation of type R (L'Annunziata, 2020):

$$H = \sum_R W_R D_A \quad (34)$$

Equivalent dose is measured in Sievert (Sv).

Effective Dose

To assess the human radiation risk, the effective dose is employed. It is the result of adding the tissues' weighting factors W_t and the equivalent dose to each organ or tissue, H_T . Organ susceptibility to cancer brought on by radiation is expressed using tissue weighting factors (L'Annunziata, 2020):

$$E = \sum_t W_t \sum_R W_R D_A \quad (35)$$

The Sievert is S.I unit for effective dose (Sv). Additionally, neither effective dose nor its measure, the Sievert, are purely physical quantities. The

definition of effective dose takes into account radiobiological and radio-epidemiological weighting elements to balance the physical quantity of absorbed dose. So, the effective dosage is a protection number that combines radiobiology, radio-epidemiology, and physics (Theunis, 2017).

Radon generation and transport

The generation and transport of radon in soil and construction materials, along with the distribution of radon within a dwelling by airflow, are two types of radon transport in residences. Radon gas is produced by radium ^{226}Ra soil grains, and radon atoms that reach the pores space when ^{226}Ra decays can be taken to the soil surface and breathed into the atmosphere, as shown in Figure 11. ^{222}Rn gas generation rate, R_t is:

$$R_t = \frac{\lambda_{Rn} E_c C_m \rho}{\varepsilon} \quad (36)$$

where λ_{Rn} = radon decay constant, E_c = emanation coefficient, C_m = concentration of ^{226}Ra (Bq/kg), ρ = soil bulk density (kg/m^3) and ε = soil porosity.

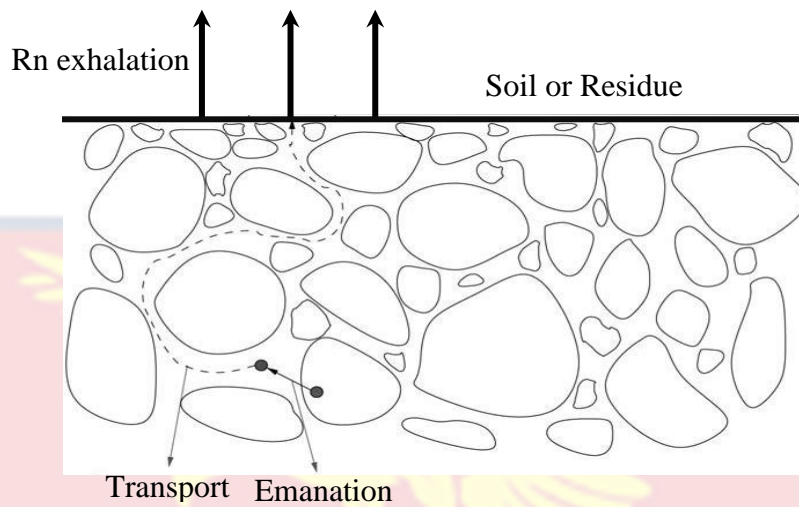


Figure 11: Diagram Showing Radon Generation and Transport to Atmosphere (Ishimori et al, 2013).

Once in the pore volume, ^{222}Rn can diffuse or advected to the surface. Moisture, porosity, and tortuosity affect radon diffusion, which can be expressed as a diffusion coefficient using Fick's equation. Radon gas flow in soil is likely to be slower than in homogeneous medium for the following reasons:

1. Tortuous flow path around particles (Tortuosity = τ) and
2. A volume of fluid that is relatively less in size (Porosity = n).

Considering these two factors, radon flow density can be expressed as (Baskaran, 2016):

$$J^d = -\varepsilon_s \tau D_m \nabla C_{Rn} \quad (37)$$

where ε_s is the porosity of the soil. The flux density ($J^d, \text{Bqm}^{-2}\text{s}^{-2}$) brought about by random mobility of molecules, as stated by Fick's law, which says that

the ^{222}Rn flux density is directly proportional to its concentration gradient under the assumption of a steady state and given as:

$$J^d = -D_{cm} \nabla C_{Rn} \quad (38)$$

where D_{cm} is the molecular diffusion coefficient measured in meters per second and is the radon concentration measured in Bq/m^3 .

Diffusion of radon gas from a higher concentration to a lower concentration is indicated by the negative sign (Baskaran, 2016). The radon diffusion coefficient is determined by the kind of soil, the amount of water present in the soil, the level of soil compaction, the soil's location, and the pore size distribution (Baskaran, 2016). The product of molecular diffusion coefficient and tortuosity is the effective bulk diffusion coefficient, D_e of the soil and expressed mathematically as:

$$D_e = \tau D_{cm} \quad (39)$$

Effective bulk diffusion coefficients for radon in mill tailing, silty sandy clay, compacted silt sands, clayey sands, compacted inorganic clays, varved clays, mud, loams, and alluvial-detrital granite deposits range from $2.2 \times 10^{-10} \text{m}^2 \text{s}^{-1}$ (mud with 85% water content) to $7.2 \times 10^{-6} \text{m}^2 \text{s}^{-1}$ (Mill tailing) (Baskaran, 2016). Combining equations 36 and 38, equation 39 results as:

$$J^d = -\varepsilon_s D_e \nabla C_{Rn} \quad (40)$$

Radon is transported from soil to indoor environment via diffusion and viscous movement in the soil, as well as the transfer of radon-rich air from cavities and channels beneath and around building foundations to the building interior (Rybalkin, 2012). Radium content, emission power, and soil moisture all affect radon concentrations in soil pores. In addition to air that originates

directly from building materials and other sources, atmospheric pressure fluctuations, thermal gradients in fractured rocks, and air instabilities owing to temperature differences cause air with high radon content to enter living space in houses.

There are two main processes that account for the transport of radon gas through any porous media (Otoo et al., 2013):

- (a). Diffusive transport due to the differences in radon concentration and
 - (b). Convective transport due to the pressure gradient induced by air flow
- Darcy's law in terms of air permeability describes how soil air permeability, moisture, and pressure gradient influence effective radon transmission. Darcy's law states that the apparent velocity of fluid flow through soil is proportional to the pressure gradient:

$$\vec{K} = -\frac{x_d}{\mu} \nabla Y \quad (41)$$

where \vec{K} is the surface velocity vector (m/s), x_d is the soil's Darcy's permeability (m^2), ∇Y is the pressure gradient (Pa), and μ is the gas-phase viscosity of the soil pores (kg/ms). Multiply Darcy's velocity by the radon activity concentration (C_{Rn}) in the soil pores and divide by the soil porosity:

$$\phi_{Rn} = -\frac{C_{Rn} x_d}{\varepsilon \mu} \nabla Y \quad (42)$$

A general differential equation can be used to characterise soil radon transport, accounting for diffusion and advection, radon formation, and radioactive decay (Munoz et al., 2017):

$$\frac{\partial C_{Rn}}{\partial t} = D_e \nabla^2 C_{Rn} + \frac{\nabla C_{Rn} x_d}{\varepsilon \mu} \nabla Y + G - \lambda_{Rn} C_{Rn} \quad (43)$$

Radon exhalation rate of soil

The ^{222}Rn exhalation rate in soil is used to estimate environmental radon levels. pressure, temperature, ventilation conditions, and building materials affect radon and its decay product concentration. Radium and radon exhalation rates in soil or construction materials are crucial for assessing radiological threats and health risks. Exhalation rate is the amount of radon released per unit of time and depends on:

1. Radium concentration in the material which in turn depends on the uranium concentration in the material,
2. The porosity and density of the material,
3. Diffusion coefficient of radon in the material and
4. Emanation factor of radon from the material.

Mass exhalation rate is used to express indoor radon emitted by ornamental and construction materials (Abbas et al., 2020). Emanation and transport drive radon exhalation from soil. Soil variables affect these mechanisms. Equations 44 and 45, compute radon surface E_x and mass E_m exhalation rates (Abbas et al., 2020; Jasaitis & Peciuliene, 2021):

$$E_x = \frac{\lambda V C_{Rn}}{A_s \left[t + \lambda^{-1} \left(e^{-\lambda t} - 1 \right) \right]} \quad (44)$$

$$E_M = \frac{\lambda V C_{Rn}}{M \left[t + \lambda^{-1} \left(e^{-\lambda t} - 1 \right) \right]} \quad (45)$$

where C_{Rn} = radon concentration measured in (Bqm^{-3}), M = mass (kg), t = exposure time (hours), V = hollow volume (m^3), A_s = surface area from which the radon exhaled (m^2) and λ = radon decay constant (per hours).

Effect of some soil characteristics on Radionuclides and ^{222}Rn in soil and Dwellings

Soil Bulk Density

The bulk density determines the aggregate particle's overall volume as well as the volume of the sample's water content. The aggregate particle is solely included in the mass measurement.

Bulk specific gravity will be less than apparent density because it contains the water permeable void volume. Bulk is defined as the mass of a unit volume of aggregate, including water permeable spaces, at a certain temperature divided by the mass of an equal volume of gas-free distilled water at that same temperature.

Soil Porosity

Porosity (ε) is characterized by the ratio of pore volume to total soil volume. It provides a measurement of the material's storage capacity. The soil porosity was determined using equation 46:

$$\text{Porosity}(\varepsilon) = \frac{\text{Volume of pore}}{\text{Volume of soil}} \quad (46)$$

Soil Particle size Distribution

Soil and other unconsolidated earth materials' particle size distribution can influence physicochemical and biological processes. Why is radionuclide distribution in soil particle size fractions important? Physical movement of contaminated material is important in the absence of chemical remobilization (Hay and Ragsdale, 1978). Most natural transport systems move fine particles more efficiently. Second, actinides can reach humans through resuspension and breathing. Size affects resuscitation, air persistence, and inhalation outcome.

The relative proportions of sand, silt and clay are referred to as soil texture. The soil texture classes group soils with similar distributions of particle sizes as shown in Figure 12.

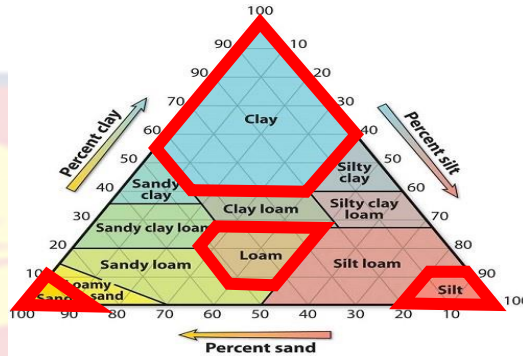


Figure 12: Diagram Showing Soil Classifications (USDA, 1999)

Lung Cancer Risk Associated with Radon

Radon is a proven human lung carcinogen, as established by experimental data from mutation studies in cell culture and lab animals, epidemiological controlled trials on uranium workers, and case analysis on the general public (IAEA, 2003). The earliest line of evidence regarding radon's propensity to cause lung cancer came from occupational studies on miners, notably uranium miners, who were exposed to high amounts of radon along with other radioactive compounds and dust particles (UNSCEAR, 2000).

Radon Entry into dwellings

Subsoil and geology beneath a building are the primary sources of radon (Otoo et al., 2020). However, only a very small proportion is believed to be associated with building materials (Pacheco-Torgal, 2012). Consequently, Radon penetration into a structure is a combination of contributions from soil exhalation and construction materials (Vasilyev & Zhukovsky, 2013). Another potential source of radon inside is the water supply; however, its contribution is

typically negligible (Thumvijit et al., 2020). Once it was believed that radon dispersion through soil and building materials governed radon entry into buildings (WHO, 2009).

Radon can enter a home via cracks in walls and floors, building joints, wall cavities, and spaces around service pipes and cables, among other entry points. Figure 13 displays the most prevalent radon entry sites. The ability of the soil to produce and transport radon gas is largely influenced by radium levels, emanation coefficient, soil permeability, porosity, and moisture content. Airtightness of the foundation and ventilation or air exchange rate affect indoor radon concentrations, as do tenant behaviour and environmental conditions. Because radon is heavier than air and originates from earth, it tends to collect in the lower levels of high-rise buildings (Yarahmadi et al., 2016)

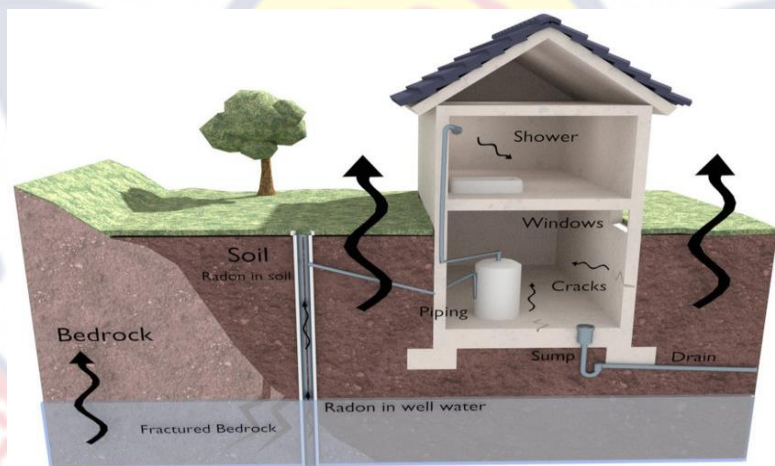


Figure 13: Diagram Showing the Radon Entry Points in a Building (Blanco-Nova et al., 2018)

Seasonal radon correction factor

When indoor radon data for a given season are known, seasonal adjustment factors can be used to determine annual mean radon levels (Park et al., 2018). Estimating annual mean radon concentrations by multiplying the

monthly j concentration by the adjustment factor $K_j^{(t)}$ according to equation 47 (Park et al., 2018):

$$Y^{(12)} = K_j^{(t)} \times B^{(t)} \quad (47)$$

where $Y^{(12)}$ represents 12 months of measurement results, $K_j^{(t)}$ = seasonal correction factors with $j = 1, 2, \dots, 12$, and $B^{(t)}$ = indoor radon levels measured during t months with $t = 1, 2, \dots, 12$.

The seasonal correction factor was determined using equation 48:

$$K_j^{(t)} = \frac{t \sum_{k=1}^{12} B_k}{12 \sum_{k=j}^{j+t-1} B_k} \quad (48)$$

where B_k = integrated radon concentration in months j .

With the convection that $B_k = B_{k+12}$ (Pine et al., 1995), B_k is geometric mean indoor radon level in month k for the population of dwellings (Pine et al., 1995).

Since in Ghana, there are only two seasonal datasets, letting $t = 2$ and $j = 6$ and

$12, \frac{\sum_{k=1}^{12} B_k}{12}$ = annual geometric mean radon concentration, and $\frac{\sum_{k=j}^{j+1} B_k}{2} =$

geometric mean radon concentration for each season in the study.

Chapter Summary

This chapter reviewed previous studies that are relevant to this study. A brief literature review on natural radioactivity in the environment was discussed, with an emphasis on radionuclides in soil. The main radionuclides found in soil were discussed: ^{226}Ra , ^{232}Th , and ^{40}K . Radioactive decay and growth, radioactive decay particles (alpha, gamma, and beta), decay series, and theoretical background to the decay series have all been investigated. The

interaction of gamma rays as they pass through matter was explained, as well as the three different processes involved (photoelectric and Compton effects, and pair production).

The linear, mass, and gamma ray attenuation coefficients were discussed. It was explained how natural radioactivity was detected using detectors such as HPGe detectors. A brief overview of the gamma ray spectrometer and NaI (TI) detectors and how they work was provided. Short literature on environmental radon monitoring that extensively discussed the properties, decay products, health hazards associated with radon, sources of radon exposure to humans, both meteorological parameters and geological factors that can affect the production and transport of ^{222}Rn into indoor and outdoor environment.

Consideration has been given to radon detection using both active and passive methods, with LR-115 type II and CR-39 as passive detectors and the AlphaGUARD and Sarad 7 radon monitoring active detectors. The biological effects of natural radioactive and radon were investigated using deterministic and stochastic effects. The absorbed, equivalent and effective doses were discussed to help people understand their radiation exposure. Finally, the production and transport of radon gas to the indoor and outdoor environments, radon exhalation rates, soil physicochemical properties, seasonal variation, and seasonal radon correction factors were discussed.

CHAPTER THREE

MATERIALS AND METHODS

Introduction

This chapter examines the various materials and methods employed in this study. The presentation includes an overview of the study area, sampling, and sample preparation, as well as brief descriptions of efficiency and energy calibration of the detector, data measurements and materials used for this study. The process of calculating different radiological risks indices due to radionuclides found in the soil as well as levels of radon found within buildings. In addition to this, the seasonal radon correction factor and the seasonal variation in the levels of radon found indoors will be discussed. The description of multivariate statistical analysis used in analyzing the data was presented. Sampling was carried out from 02/04/2021 to 02/04/2022.

Study Area

Tsakpa/Gabi, Torkor, and Agbenoxoe are the three study locations that were selected for the investigation. They are all situated in the Kpando Municipality of the Volta Region, Ghana and with coordinate, latitude $6^{\circ} 55' N$, $7^{\circ} 05' N$, and longitude $0^{\circ} 23' 35'' E$. The overall land area of the municipal is about 820 square kilometers, which accounts for 4.5% of the Volta Region, with the Volta Lake covering nearly 30% of the land area. The Volta Lake, which has a coastline that is more than 80 kilometers long, serves as the dividing line for the western territory (Figure 14). The municipal territory is bordered by Biakoye District to the north, Afadzato South District to the east, and North Dayi District to the south (Ansre et al., 2018).

Volta Region is the fourth largest of Ghana's sixteen administrative regions in terms of land area, covering 9,504 square kilometers and comprising 1.4% of Ghana's total land area. But is the seventh most populated region in Ghana, after the Greater Accra, Ashanti Region, Eastern Region, Central Region, Northern Region and Western Region, with a population of 1659040 and a population share of 5.4%. With 174.6 people living in per square kilometer, it is the fourth most densely inhabited location in Ghana (GSS, 2021).

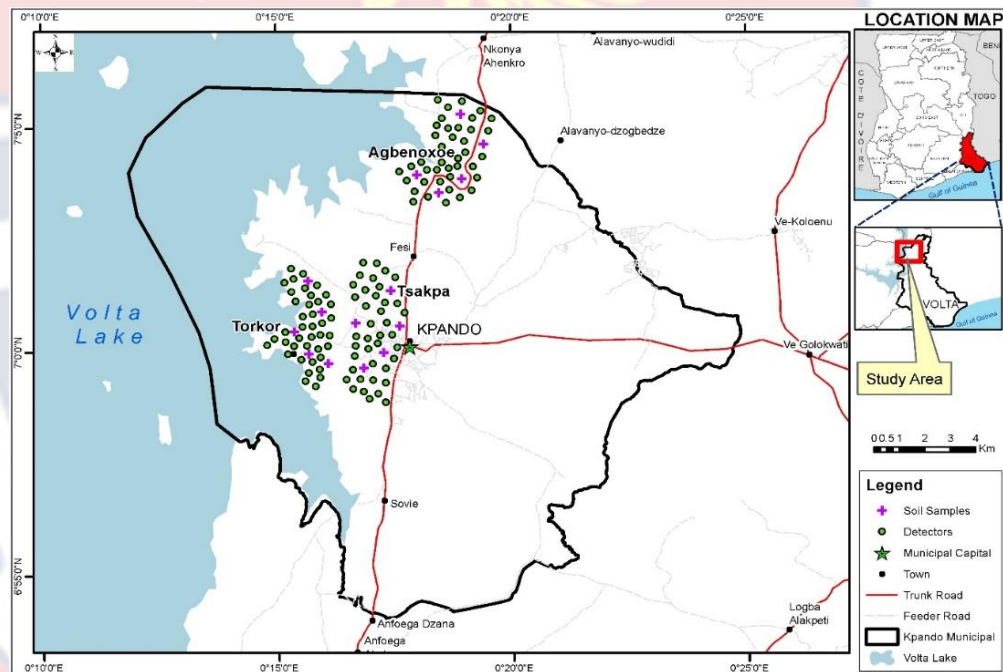


Figure 14: Map of Kpando Municipality Showing the Study Locations

Geology of the study Area

The geology of the research region consists of Buem volcanic rocks that can be found throughout the Jasikan and Kadjebi areas. The principal soil types derived from this parent rock are Savannah ochrosols (reddish, slightly acidic, and more fertile), "oxysol" (heavily drained; yellowish, and less fertile), and ground water laterites. These soils are distinguished by their sandy loamy

texture and local adaptation. The alluvial silt loam dominates along the Lake Volta and River Dayi. Large clay deposits exist in Tsakpa, Gbefi, and Kudzra, which are excellent for the development of the brick and tile, pottery, and ceramics industries.

Meteorology of the Study Area

There are two rainfall patterns within the region for all the climatic zones, but their intensity differs for the climatic zones. The principal rainy season runs from the middle of April to the beginning of July, whereas the minor rainy season runs from September to November (Dickson and Benneh, 1988). The yearly mean rainfall might vary anywhere from 900 to 1300 millimeters on average. The average annual temperature is approximately 27 degrees Celsius, whereas the average daily temperature ranges from 22 to 33 degrees Celsius. In general, the warmest months are February and March, while July and August are on the colder end of the temperature spectrum. The relative humidity is often about 80 percent (Dickson and Benneh, 1988).

Sample collection, preparation and analysis.

Sample Collection

The soil samples were sampled from the following locations within the Kpando Municipality, close to and far from the Volta Lake: Tsakpa (on the hill), Torkor and Agbenoxoe (along the Volta Lake). A preliminary survey was conducted in the municipality under investigation to choose suitable sampling locations. This was done so that the samples collected would be representative of the whole. The random sampling method was the one that was used for collecting soil samples.

The term "random sampling" refers to the process of collecting samples in an area of interest in an arbitrary manner and within predetermined parameters. For the purpose of randomly choosing sampling sites arbitrarily, each sampling point should be chosen independently of a location of all other locations. This ensures that any place within the area of interest has an equal opportunity to be considered as a sample location. Each area was divided into grids of 50 meters by 50 meters, and samples were collected at various spots before being combined to create a representative sample (IAEA, 2004). The soil samples were taken to a depth of between 5 and 10 cm using a coring tool.

At each of the places where samples were taken, soil was collected from at least three different parts of the surrounding area, and it was then put into plastic bags that were labelled. One kilogram (1kg) was the quantity of each sample that was extracted for the purpose of investigation. In order to get the natural soil for the indicated locations, unnecessary waste such as stones, wood, leaves, and bits of glass were removed. Within the research areas, a total of 51 soil samples (seventeen from each town) were collected, along with 17 soil samples taken using a steel ring. The samples were then sent to the Radiation Protection Institute (RPI) of the GAEC at Dome-Kwabenya and Soil Research Institute of the Council for Scientific and Industrial Research (CSIR) in Accra for processing and analysis.

Sample preparation

Each of the 51 soil samples was allowed to air-dry on trays for 7 days in the laboratory before being placed in an oven heated to 105 degrees Celsius for three to four hours, or until all traces of moisture content were gone. After that, the samples were put through a ball mill where they were reduced to a fine

powder. The powder was then filtered through a 5.0 μm mesh filter before being deposited inside the desired shapes and containers.

The dried samples of solid NORM waste from which radon emanation fraction was determined were transferred into a measuring container without any treatment and vacuum sealed.

Gamma Activity Measurement

Energy calibration of gamma-ray spectrometry system

Energy calibration allows qualitative assessments or radionuclide identification in a spectrum. To calibrate the HPGe detector (that is, to establish the channel number of the multichannel analyzer (MCA) in relation to gamma-ray energy), reference radionuclides with well-defined energies within the energy range of 60 - 2000 keV were counted (IAEA, 1989).

The calibration standard on the gamma detector was counted for ten (10) hours to get well-defined image peaks (36000 s). The channel number associated with the centroid of each complete energy event on the MCA was recorded and displayed, resulting in the formation of a linear curve associated with a second-order polynomial. The fact that the data points form a straight line suggests that the system is operationally sound, according to (IAEA, 1989).

Equation 49 is used to calculate energy and channel number:

$$E = A + A_i \times C \quad (49)$$

where E = energy, A and A_i are the calibration constants for a given geometry and C is the channel number for a radionuclide. Figure 15 shows an energy versus channel number graph.

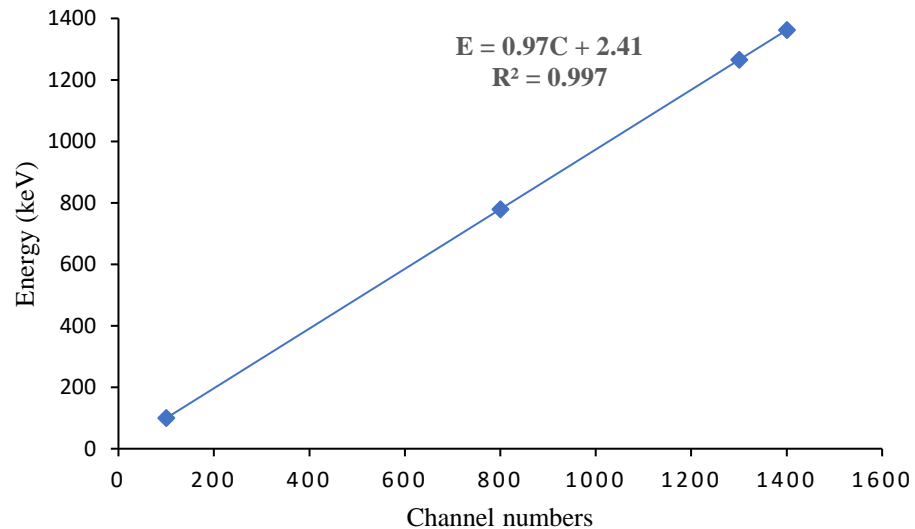


Figure 15: Graph Showing Energy Calibration of Gamma-ray Spectrometry System

When the trendline equation was compared to equation 49 in Figure 15, the following equation was obtained:

$$E = 2.41 + 0.97C \quad 50$$

Efficiency calibration of gamma-ray spectrometry system

The efficiency was calibrated with the same standard of mixed radionuclides used to calibrate the energy. The efficiency was calibrated using DEUTSCHER KALIBRIEDIENST's radioactive mixed nuclide 146A standard. Detector efficiency is the ratio of the number of actual events detected by the detector to the total number of events produced by the radiation source (IAEA, 1989). To quantify radionuclides contained in the sample, a precise calibration of the equipment's efficiency is needed. Ten hours were spent counting the standard on the detector (36000 s). Utilizing the net counts for each of the spectrum's full-energy events and their respective energies, the efficiencies were computed.

The standard was kept in the same sealed Marinelli beaker as the samples. Using equation 50 and the certificate's known concentration, counting efficiency for each photopeak was calculated on a Microsoft Excel spreadsheet, and the corresponding efficiency was plotted against energy to produce an efficiency curve. As a result, the calibration curve was used to determine the efficiency of all additional photopeaks. Different energy peaks encompassing a range of up to 2000 keV were used to create the efficiency calibration curve. Equation 51 was used to determine the efficiency:

$$n(E) = \frac{C_T - C_B}{P_E A_{STD} T_{STD}} \quad (51)$$

where:

P_E = Gamma emission probability

$\eta(E)$ = detector efficiency

C_T = total counts under a photo peak.

C_B = background counts

A_{STD} = Activity (Bq) of the radionuclide in the calibration standard at the time of calibration

T_{STD} = Counting time of the standard

The relation between efficiency and energy is given as:

$$\ln \varepsilon(E) = B_0 + B_1 \ln E + B_2 (\ln E)^2 \quad (52)$$

where:

B_0 , B_1 and B_2 are the calibration constants for a given geometry and the other symbols have their usual meanings. The efficiency calibration curve is shown in Figure 16.

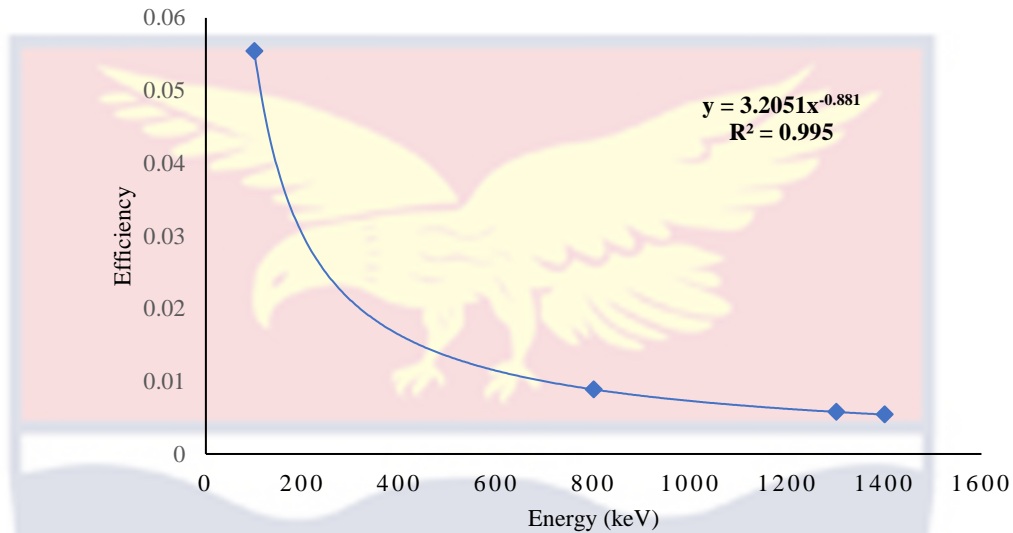


Figure 16: Graph Showing Efficiency Calibration of Gamma-ray Spectrometry System

By comparing the efficiency calibration curve equation ($y = 3.2051x^{-0.881}$) in Figure 16 to equation 52, equation 53 was obtained:

$$\ln \varepsilon = 1.16 - 0.881 \ln E_\gamma \quad \text{for } E_\gamma > 100 \text{ keV} \quad (53)$$

Activity concentration estimation

The concentration of a nuclide with multiple peaks in its spectrum was calculated as the weighted average concentration at each peak. Their activities were computed using the full energy gamma – ray peaks of ^{40}K and radionuclides in the ^{226}Ra and ^{232}Th decay series. The parents' activities were calculated using a weighted average of the daughter's activities, which were considered to be in secular equilibrium. The activity of ^{226}Ra was determined

using the emissions of ^{214}Bi (609.31, 1120.29, 1764.49 keV) and ^{214}Pb (295.22, 351.93 keV). The activity of ^{232}Th was estimated using the gamma emission lines of ^{212}Bi (727.33 keV), ^{228}Ac (209.25, 409.46, 463.0, 794.95, 911.20, 964.77, 968.97 keV), and ^{212}Pb (238.63, 300.09 keV). ^{40}K was evaluated using its only gamma – ray line of peak energy 1460.82 keV.

The environmental gamma – ray background was evaluated with an empty Marinelli beaker under similar measurement conditions as the samples prior to sample measurement. The total time spent counting was 72000 seconds. The Genie 2000 V3.3 (1) spectroscopic software from Canberra was used for data capture, presentation, and on-line spectrum analysis. Each radionuclide's activity concentration (C) (Bq/kg) in any particular sample was determined from the spectrum using the analytical equation 54:

$$C(^{226}\text{Ra}, ^{232}\text{Th} \& ^{40}\text{K}) = \frac{N_s}{\varepsilon_\gamma(E) \times P(E) \times T_c \times M_s} \quad (54)$$

where, M_s (kg) is the mass of sample, N_s (cps) is the net peak area for the sample in the peak range, $P(E)$ is the gamma emission probability, T_c is the counting time in seconds, and $\varepsilon_\gamma(E)$ is the photo peak efficiency which had been obtained from the standard solution.

Radiological hazards indices

By computing several radiological indices (such as internal and external hazard indices, activity utilization index, representative level index and radium equivalent index), the gamma radiation and alpha radiation dangers posed by the specific radionuclide in soil are calculated. Despite the fact that the overall activity concentration of radionuclides has been calculated, it does not give a

precise representation of the entire radiation dangers. These indices are also utilized to choose the best building materials.

Radium equivalent index

Naturally occurring radionuclides ^{40}K , ^{226}Ra and ^{232}Th are not equally distributed in soil, resulting in different exposure doses. A common index known as radium equivalent index (Ra_{eq}) in Bqkg^{-1} is used to calculate the weighted total of the activities of building materials having varied levels ^{40}K , ^{226}Ra and ^{232}Th . Hence, the main objective of calculating Ra_{eq} is to estimate the amount of radiation dose that will be emitted externally due to gamma radiation. This Ra_{eq} provides useful guidelines in regulating radiation safety standards for the general public since soil is the main building material of the locals in the study location.

This index is calculated by assuming that 1.0 Bq/kg of ^{226}Ra , 0.7 Bq/kg of ^{232}Th , and 13.0 Bq/kg of ^{40}K yield the same gamma-ray dosage (OECD, 1979; UNSCEAR, 2000):

$$\text{Ra}_{\text{eq}} = C_{\text{Ra}} + 0.077C_{\text{K}} + 1.430C_{\text{Th}} \quad (55)$$

where C_{Ra} , C_{K} and C_{Th} are concentrations (Bq/kg) of ^{226}Ra , ^{40}K and ^{232}Th . The maximal permissible Ra_{eq} activity is equal to 370 Bqkg^{-1} corresponding to an effective dose of 1.0 mSv per year (UNSCEAR, 2000) and to maintain the outdoor dose to 1.50 mSv/y (OECD, 1979).

Internal and external hazards indices

To assess the radiation dangers associated with the building materials, both internal and exterior hazard indices were computed. The equations 56 to 3.10 were utilized to determine the radiation dose expected to be delivered

externally and internally if a building is constructed using the soil sample. To maintain the radiation hazard level insignificant, ICRP (ICRP, 1991) proposed that the index value must be less than one.

$$H_{ex} = C_{Ra} + 1.43C_{Th} + 0.077C_K \leq 1 \quad (56)$$

Or

$$H_{ex} = \frac{Ra_{eq}}{370} \leq 1 \quad (57)$$

$$H_{in} = C_{Ra} + 0.71C_{Th} + 0.038C_K \leq 1 \quad (58)$$

Gamma index (I_γ)

The gamma radiation index was calculated using equation 59. The gamma radiation index should not exceed certain values depending on the dose criterion and, the way and amount of the material is used in a building. The European Commission (EC, 1999) suggests that if excess gamma radiation from building materials raises the annual effective dosage of a member of the public by no more than 0.30 mSv, they should be excluded from all regulations relating to their radioactivity. Contrarily, doses more than 1.00 mSv should only be tolerated in extremely rare circumstances, such as when materials are employed locally.

$$I_\gamma = C_{Ra} + 1.5C_{Th} + 0.1C_K \leq 1 \quad (59)$$

Alpha index (I_α)

The alpha radiation hazard (I_α) is one of the critical radiological indexes that have been established to confirm the protection of human dwellings from

uncontrolled exposure to radiation. The alpha index (I_α) for a building material shows the concentration of ^{226}Ra in the building material and when ^{226}Ra activity exceeds the value of 200 Bqkg^{-1} , the indoor radon levels may exceed 200 Bqm^{-3} due to excessive radon emanation from the building material. The alpha index was computed using equation 60:

$$I_\alpha = \frac{C_{Ra}}{200} \leq 1 \quad (60)$$

Absorbed and Effective Dose Rates

Absorbed Dose Rate

If the concentrations of natural radioactivity in soil are known, and are evenly distributed in the soil, the radiation exposure dose rate in air (UNSCEAR, 2000) can be calculated. The absorbed dose rate in air can be computed in units (nGy/h) based on guidelines (UNSCEAR, 2000). The absorbed dose rate was calculated from using equation 61 with the corresponding conversion factors of $0.462 \text{ nGy/h per Bq/kg}$ for ^{226}Ra , $0.604 \text{ nGy/h per Bq/kg}$ for ^{232}Th and $0.0417 \text{ nGy/h per Bq/kg}$ for ^{40}K (UNSCEAR, 2000):

$$D = 0.462 \times C_{Ra} + 0.604 \times C_{Th} + 0.042 \times C_K \quad (61)$$

Annual Effective Dose Equivalent (AED)

The AED in $\mu\text{Sv/y}$ received by the public was calculated from the absorbed dose rate using a dose conversion factor of 0.7 Sv/Gy , occupancy factor for outdoor and indoor 0.2 ($5/24$) and 0.8 ($19/24$) respectively

(UNSCEAR, 2000). The AED in the outdoor and indoor environment was determined using equations 62 and 63, respectively:

$$AED_{Outdoor} = D \times 0.7 \times 8760 \times 0.2 \times 10^{-3} \quad (62)$$

$$AED_{Indoor} = D \times 0.7 \times 8760 \times 0.8 \times 10^{-3} \quad (63)$$

Excess lifetime cancer risk (ELCR)

The possibility of developing cancer as a result of exposure to radiation from radioactive materials over a lifetime at a given exposure level is called ELCR (UNSCEAR, 2008) and was calculated using equation 64:

$$ELCR = AED \times D_k \times R_F \quad (64)$$

where, D_k = average duration of life (estimated to be 70 years) and R_F = risk factor i.e., fatal cancer risk per sievert. For stochastic effects, ICRP uses R_F as 0.05 for the public (UNSCEAR, 2000).

The Activity Utilization Index (AUI)

The AUI, measures the dosage rate in air from various combinations of the three original radionuclides observed in soil samples. The AUI was calculated using equation 65:

$$AUI = \left(\frac{C_{Ra}}{50} \right) f_{Ra} + \left(\frac{C_{Th}}{50} \right) f_{Th} + \left(\frac{C_K}{500} \right) f_K \leq 1 \quad (65)$$

where f_{Ra} (0.462), f_{Th} (0.0604) and f_K (0.041) are the fractional contributions to the total dose rate in air due to gamma radiation from the actual concentrations of ^{226}Ra , ^{232}Th and ^{40}K , respectively. The concentration per unit mass of ^{226}Ra , ^{232}Th and ^{40}K in building materials, C_{Ra} , C_{Th} and C_K are reported to be 50, 50 and 500 Bq/kg (OECD, 1979), respectively.

Annual gonadal equivalent dose (AGED)

The gonads, active bone marrow and bone surface cells are considered to be the organs of importance by UNSCEAR (UNSCEAR, 2000). Increase in AGED affects the bone marrow, causing red blood cells to be destroyed and replaced by white blood cells. Leukemia, a deadly blood malignancy, can develop as a result of this condition. The AGED was computed using equation 66:

$$AGED (\mu Sv / y) = 3.09C_{Ra} + 4.18C_{Th} + 0.314C_K \quad (66)$$

Representative level index (RLI)

To identify soil that may be hazardous to human health when used for construction of dwellings, the RLI was determined using equation 67 (NEA-OECD, 1979):

$$RLI = \frac{C_{Ra}}{150} + \frac{C_{Th}}{100} + \frac{C_K}{1500} \quad (67)$$

Physiochemical properties of Soil Samples

One of the most important soil characteristics that determines the formation and transport of radioactive gases through the soil is porosity. Other soil properties that affect the radionuclides in the soil are bulk density, soil moisture, and particle size distribution. These properties were determined at Soil Research Institute, Council for Scientific and Industrial Research, Ghana.

Soil composition

To determine the composition of the soil samples, modified Bouyoucos Hydrometer techniques (Day, 1965) were used. A plastic bottle was filled with

40.0 grams of the air-dried and sieved soil sample and 100 mL of a 5 % sodium hexametaphosphate ((NaPO₃)₆) solution. The contents of the bottle were then transferred to a 1.0 litre measuring cylinder and filled to the 1.0 litre mark with distilled water. The contents of the bottle were then shaken for two hours on a mechanical shaker. The mixture was then stirred with a plunger, and five minutes later, a hydrometer was used to measure the density of the suspension (which included clay and silt).

After five hours, a new hydrometer reading of the suspension was obtained. After the fifth-hour reading, the cylinder's contents were dumped onto a 47 µm sieve, and the effluent was then thrown away. After being removed from the sieve and placed in a moisture container, the sand was dried for 24 hours at 100 ± 5 °C, and its dry weight was then recorded (Day, 1965). The readings from the blank hydrometers were also noted. Equations 68 to 70 were then used to determine the particle size distribution:

$$\% \text{Clay} = \frac{\text{Hydrometer reading at 5hours}}{40\text{g}} \times 100 \quad (68)$$

$$\% \text{Silt} = \frac{\text{Hydrometer value at 5min} - \text{Hydrometer value at 5hours}}{40\text{g}} \times 100 \quad (69)$$

$$\% \text{Sand} = \frac{\text{Weight of oven dried sample}}{40\text{g}} \times 100 \quad (70)$$

where 40.0 g = weight of soil sample in grams

Bulk Density

The core rings method described by Yerima and Van Ranst (2005) was used to sampled a known volume of soil samples. Equation 71 was used to determine the bulk density:

$$\text{Bulk density} = \frac{M_d}{V_c} \quad (71)$$

where V_C = volume of the core ring (cm^3) and M_d = mass of oven dried soil (g)

Soil Porosity

Soil porosity is the ratio of air and water in soil pores to total soil volume (Salih et al., 2019). Increasing overall soil porosity obviously increases the likelihood of radon exiting the grain surface, resulting in increased soil radon concentrations. Total soil porosity does not express the volume ratio of air to water in soil pores, which effects both radon emission and transit in soil. The soil moisture saturation was developed to express the volume ratio of water to air in soil pores. The porosity was calculated from bulk density and assumed particle density of 2.65 g/cm^3 , using equation 72.

$$\% \text{ Porosity} = \frac{1 - \text{Bulk density}}{\text{Particle density} (2.65)} \times 100 \quad (72)$$

Soil moisture content

The soil moisture content is the increase in the mass due to water present in the pores of the soil (Otoo et al., 2021). The gravimetric method was used to determine the percentage soil moisture content of soil analyzed. The wet soil was first weighted and then, the soil sample was dried in an oven at a temperature of approximately $100 \pm 5 \text{ }^\circ\text{C}$ for a duration of about 24 hours. The soil sample was removed from the oven once the drying time has passed and reweighed after it has cooled down. The percentage soil moisture content (MC) was calculated using equation 73 (Otoo et al., 2021):

$$mc(\%) = \frac{m_m - m_d}{m_m} \times 100 \quad (73)$$

where m_m = mass of moist soil, m_d = mass of dry soil and MC = percentage moisture content.

Radon Measurements

Characterisation of the Buildings

The radon detectors were exposed in residential buildings, namely, the bedroom, hall and kitchen. Before the dosimeter was exposed in the rooms, questions such as type of building materials, age of the building and hours spent in the building were determined through oral interview. The construction materials for buildings were mostly sandcrete blocks and clay. The soil characteristics and properties of the residential areas of Tsakpa, Torkor and Agbenoxoe were noted using soil characterization chart.

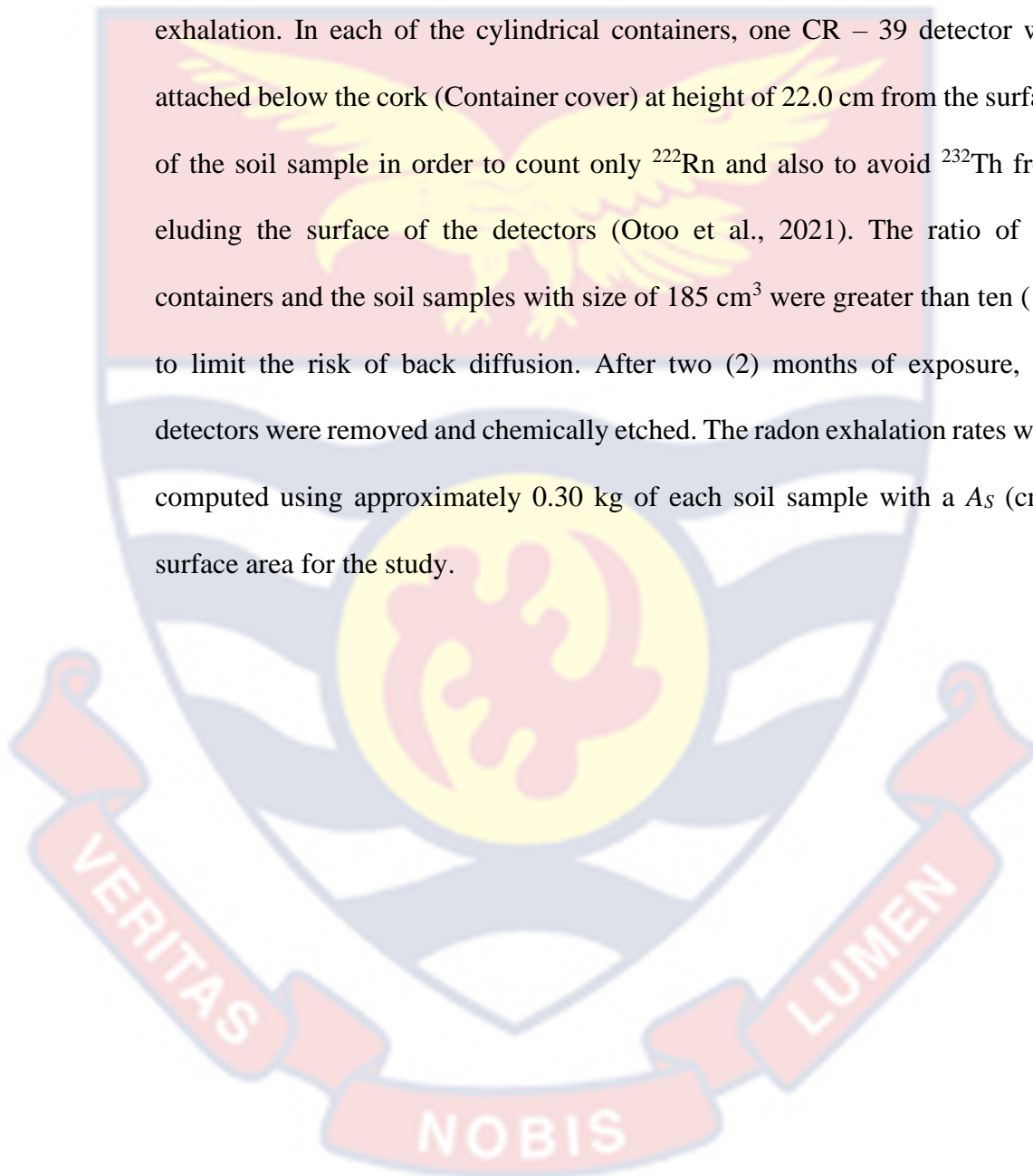
Distribution of the Radon Detectors in Buildings

In this study, passive radon CR-39 detectors (SSNTD) were used. The radon detectors were distributed in one hundred and twenty (120) (forty in each town) randomly selected houses within the Kpando municipality of the Volta Region for a period of six (6) months and twice in the year and a year from 2nd April, 2021 to 2nd April, 2022. The study areas were selected randomly among residences in Tsakpa, Torkor and Agbenoxoe. The detectors were exposure in bedrooms, sitting rooms and kitchen. In each room three (3) detectors were used, one for annual radon studies and two for seasonal radon studies.

^{222}Rn exhalation and concentration, ^{226}Ra effective contents

For ^{222}Rn concentration and ^{222}Rn exhalation measurements in the soil samples, this study used a tightly closed vessel method with a cylindrical glass container. The soil samples were carefully positioned at the bottom of

cylindrical glass containers and sealed, and stored for thirty (30) days so that the radon and its daughters attain an equilibrium concentration (Otoo et al., 2021). The cylindrical glass containers were designed having 10.0 cm diameter (D) and a height (H) of 25.0 cm as shown in Figure 17 for measurement of radon exhalation. In each of the cylindrical containers, one CR – 39 detector was attached below the cork (Container cover) at height of 22.0 cm from the surface of the soil sample in order to count only ^{222}Rn and also to avoid ^{232}Th from eluding the surface of the detectors (Otoo et al., 2021). The ratio of the containers and the soil samples with size of 185 cm^3 were greater than ten (10) to limit the risk of back diffusion. After two (2) months of exposure, the detectors were removed and chemically etched. The radon exhalation rates were computed using approximately 0.30 kg of each soil sample with a A_s (cm^2) surface area for the study.



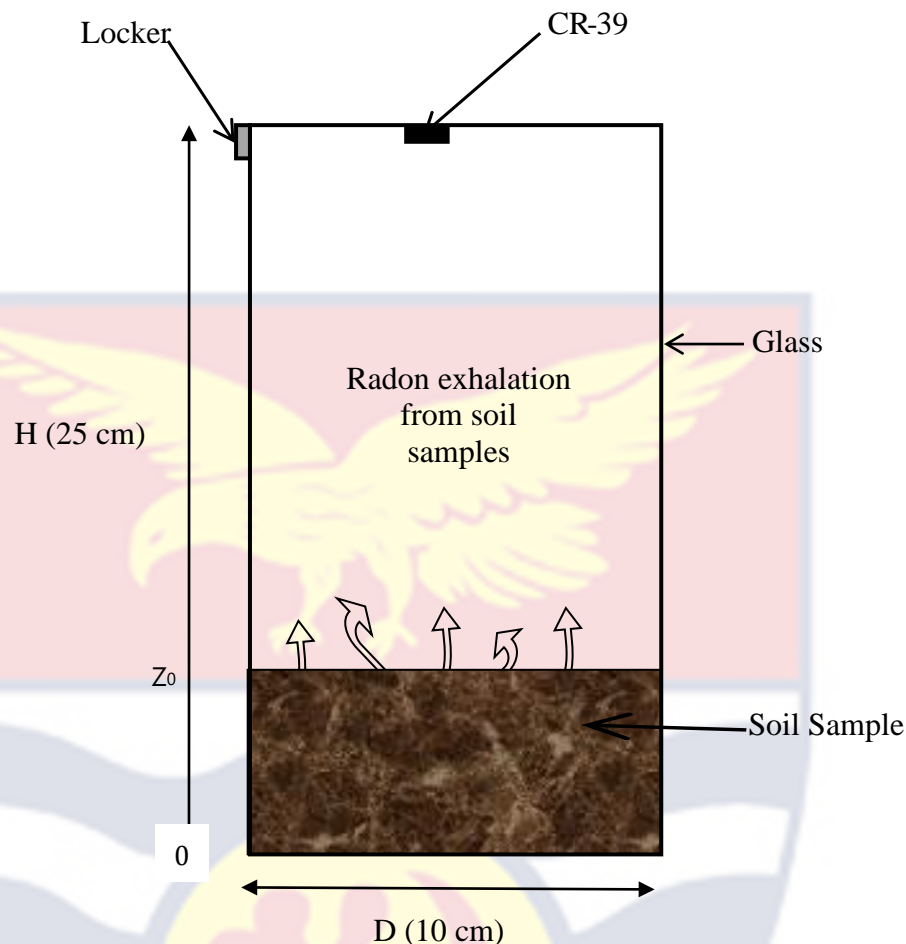


Figure 17: Experimental Setup for Radon Exhalation Measurement Using Closed Can Method.

Preparation, Collection and Chemical Etching of Radon Dosimeters

The radon sensitive plastic pieces inside the Radopot exposure canister were carried to Radiation Protection Institute Laboratory of GAEC for analysis after the radon dosimeters were exposed. To avoid contamination on the surface of the dosimeters, the plastic chips were removed from the exposure chamber with cotton gloves on and placed in the RadoSlide holder unit. For each RadoSlide, 12 chips were placed in a thermostatic bath with 4000 mL of distilled water and 1.0 kg of pellet Sodium Hydroxide. After that, the RadoSlide

containing chips were mounted on the etching carousel and etched for 4 hours and 15 minutes in a 90 °C solution.

Since any shorter or longer etching time could result in inaccurate alpha track size, the etching time was carefully monitored. Additionally, the condenser maintains the temperature of the solution, while the thermometer monitors the temperature of the solution throughout the etching process. The temperature-controlled bath solution was then drained. To clean the dosimeters, a new solution was produced out of 36 mL of 96 % diluted acetic acid and 4000 mL distilled water, which was placed into the thermostatic bath for fifteen (15) minutes. Finally, the detectors were rinsed for fifteen (15) minutes in 4000 mL of distilled water before draining into the laboratory wash basin. The etching carousel was removed from the thermostatic bath and placed in a rinse tray, where it was dried for four (4) days before the detector holder with the radon test plastic chips was taken for evaluation with the Radometer.

Detector Scanning and Counting Tracks

The RadoMeter 2000 system was used to scan and count the latent tracks created on the detectors. The setup comprises a desktop computer with Rado 6 software installed for latent track evaluation and a digital optical microscope with a 40 times optical magnification lens linked to it. With the lens, the digital optical microscope reads a 47 mm² detector divided into 144 fields. The recorded tracks are circled, and their geometries are typically circular or elliptical, depending on the angle of incidence of the particle with the detector. Only tracks with a diameter of 11 to 33 μm are counted by the RadoMeter, but over-etched tracks are not, as seen in Figure 18.

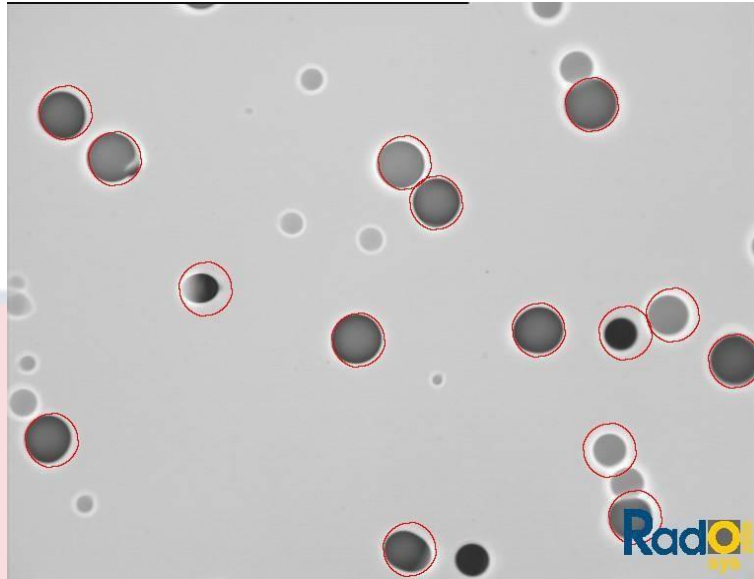


Figure 18: Latent Tracks Formed on the CR-39 Detector from one Location (Torkor)

Evaluation of Radon Parameters

The radon concentration, radium effective content, and radon exhalation rate values in the soil samples were then evaluated using the tracks density left on track films.

Activity of radon concentration was estimated using equation 74:

$$C_{Rn} \left(Bq / m^3 \right) = \frac{\rho}{\varepsilon \times t} \quad (74)$$

where, ε = calibration factor (track/cm²d/(Bq/m³), ρ = measured surface density of tracks (tracks/cm²) and t = exposure time.

Radon exhalation rate was determined using equation 75:

$$E_{Rn} \left(Bq / m^2 s \right) = \frac{\rho V_c \lambda_{Rn}}{\varepsilon A_s T_c} \quad (75)$$

where, V_c = volume of diffusion chamber (m³), A_s = surface area of the sample (m²), λ_{Rn} = decay constant of radon (1/s) and T_c = effective exposure in the diffusion chamber.

Radon Risk Assessment

Annual Effective Dose (AED)

The AED due to exposure to indoor radon gas was calculated using equation 76 (UNSCEAR, 2000):

$$AED = C_{Rn} \times O_f \times I_f \times T_y \times D_f \quad (76)$$

where C_{Rn} = ^{222}Rn concentration (Bq/m^3), I_f = equilibrium factor (0.4), O_f = indoor occupancy factor (0.8), T_y = hours per year (8766 h per year) and D_f = dose conversion factor ($6.7 \times 10^{-6} \text{ mSv}/\text{Bq}\cdot\text{m}^{-3}\cdot\text{h}$), which converts radon concentration into effective dose (ICRP, 2007).

Excess lifetime cancer risk (ELCR)

The ELCR linked to the annual effective dose to the residence was estimated using equation 77:

$$ELCR = AED \times d_L \times R_F \quad (77)$$

where AED = annual effective dose, d_L = mean lifetime (62.8 years) for Ghanaian public (WHO, 2015) and R_F = cancer risk per sievert ($5.5 \times 10^{-2} \text{ Sv}^{-1}$) (ICRP, 2007).

Effective Dose Equivalent

The effective equivalent dose to the residents due to radon was estimated using equation 78. The weighting factors for alpha particle for lung tissue were based on ICRP, 2007.

$$AEDE (mSv / y) = AED \times m_R \times m_T \quad (78)$$

where AED is the annual exposure dose (mSv), m_R is a weighting factor for alpha particle taken to be 20 and m_T is a weighting factor for lung tissue taking to be 0.12.

Seasonal variation of Radon

The radon levels not only depend upon the local geology, dwelling type, dwellers lifestyle and building materials but also depend on the seasons. The occurrence of atmospheric variations during different seasons of the year can also affect the variation of radon concentration. In order to know the variation in radon levels, the dosimeters were installed in the dwelling of the study area in the two different seasons of a year (rainy – April to September and dry – October to March, season). For each season, new CR-39 dosimeters were deployed and the old dosimeters used for the previous season were retrieved for data evaluation in the laboratory.

Seasonal Radon Correction Factors

The seasonal correction factor for indoor radon measurement in the three towns was calculated based on the geometric mean from six months values and the geometric mean from the annual radon values according to equation 79:

$$S_{CF} = \frac{(GM)_6}{(GM)_{12}} \quad (79)$$

Multivariate statistical analysis

Principal component analysis (PCA), Pearson correlation analysis, and cluster analysis are examples of multivariate statistical analyses that were used

in the studies. These techniques were utilized to highlight the relationship between the various factors, particularly the impact of the radiological characteristics of soil on the distribution of natural radionuclides. To assess the strength of the association between the variables under study, the Pearson correlation coefficient was determined. Cluster analysis is crucial because it enables the display of the degree of association between the variables under study. To summarize the collection of patterns between investigated variables in a set of data, PCA is typically employed as a standard tool.

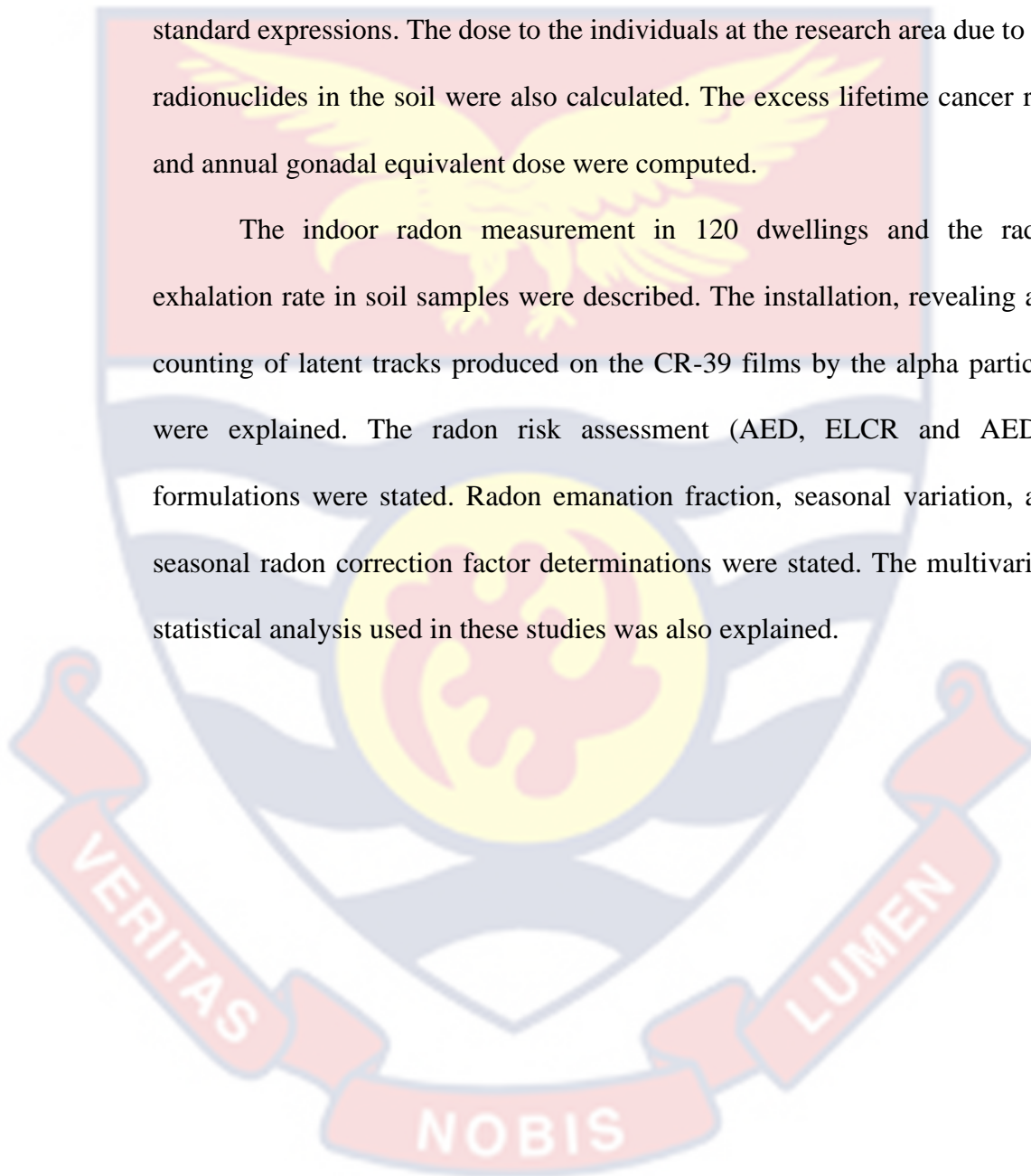
Data processing for PCA evaluation used the varimax normalized approach. Typically, the PCA is used as a technique to identify patterns in variables and represent data by emphasizing their differences and similarities. The benefit of PCA is its ability to compress data by lowering the number of dimensions and optimizing information loss to the lowest possible level. The related statistical analysis of the data was performed using OriginPro 2022. Data can be visualized, explored, analyzed, and interpreted using the sophisticated and dependable OriginPro 2022 scientific graphing and data analysis program.

Chapter Summary

Fifty-one (51) soil samples were collected from seventeen (17) different locations within the study location for gamma ray analysis at RPI of GAEC and also for physicochemical analysis at the soil research institute of CSIR, Accra. The ^{226}Ra , ^{232}Th , and ^{40}K were determined using an HPGe detector, and the porosity, bulk density, and particle size distribution were also determined. The energy and efficiency calibrations were done before the detectors were used.

The standard equations used to determine radiological hazard indices associated with soil samples were presented. To ascertain the level of soil safety for use as building materials, parameters such as the representative level index, activity utilization index, and activity concentration index were estimated using standard expressions. The dose to the individuals at the research area due to the radionuclides in the soil were also calculated. The excess lifetime cancer risk and annual gonadal equivalent dose were computed.

The indoor radon measurement in 120 dwellings and the radon exhalation rate in soil samples were described. The installation, revealing and counting of latent tracks produced on the CR-39 films by the alpha particles were explained. The radon risk assessment (AED, ELCR and AEDE) formulations were stated. Radon emanation fraction, seasonal variation, and seasonal radon correction factor determinations were stated. The multivariate statistical analysis used in these studies was also explained.



CHAPTER FOUR

RESULTS AND DISCUSSION

Introduction

The objective of this research was to measure the levels of natural radioactivity and radon in the soil and homes of three different towns located within the Kpando Municipal area, and then to analyse the results using both statistical and graphical techniques. Using HPGe and CR-39 detectors, the activity of radionuclides and radon levels in soils and dwellings were measured, and the following quantities were determined as a result: The absorbed dose rate and the annual effective dose rate; the radium equivalent activity index; the activity utilisation index; the representative level index; the seasonal radon correction factor; outdoor and indoor hazard indices; the gamma and alpha indices and the excess cancer lifetime risk. These values have been calculated, and the results are shown in tables and figures.

Activity Concentrations in Soil samples

The activity levels of radium-226, thorium-232 and potassium-40 in soils collected from seventeen (17) different locations each from Torkor, Agbenoxoe and Tsakpa communities of Kpando Municipal have been measured and tabulated in Figure 19 and Tables 1 to 3. From Table 1 and Figure 19, levels of ^{226}Ra , ^{232}Th and ^{40}K for Torkor community, ranged from 6.50 to 50.50 Bq/kg, 10.90 to 56.80 Bq/kg and 83.50 to 421.60 Bq/kg with the mean concentration of 27.42 ± 0.21 Bq/kg, 30.95 ± 0.88 Bq/kg and 241.03 ± 5.90 Bq/kg, respectively.

Table 2 and Figure 19 represents the activity concentration levels of ^{226}Ra , ^{232}Th and ^{40}K for Agbenoxoe community, which varied from 3.10 to

53.30 Bq/kg, 4.30 to 52.60 Bq/kg and 65.80 to 371.30 Bq/kg having a mean concentration of 27.63 ± 1.09 Bq/kg, 28.85 ± 0.96 Bq/kg and 232.60 ± 6.27 Bq/kg, respectively. Finally, Table 3 and Figure 19 represents the activity concentration levels of ^{226}Ra , ^{232}Th and ^{40}K for Tsakpa community, ranging from 2.80 to 40.10 Bq/kg, 3.40 to 58.80 Bq/kg and 62.70 to 402.10 Bq/kg with average concentration of 15.90 ± 0.60 Bq/kg, 26.89 ± 0.77 Bq/kg and 242.09 ± 7.42 Bqkg⁻¹, respectively.

The activity levels of ^{40}K in all the soils from the three towns were greater than the values of radium-226 and thorium-232. From Figure 19, the mean activity concentration of ^{226}Ra , ^{232}Th and ^{40}K in the soils followed the order $^{226}\text{Ra} < ^{232}\text{Th} < ^{40}\text{K}$ as observed by Akortia et al. (2021). It was observed that the activity levels varied greatly from town to town that were studied. The uneven and irregular distribution of radionuclides in the earth's crust could be responsible for these variations in radionuclides that were observed (Al-Khawlany et al., 2017; Otoo et al., 2018; Ademola, 2021). Other possible causes include geological formations, variations in terrain, and agricultural activities in the locations that were analysed (Akortia et al., 2021).

Table 1: Average Activity Levels (Bq kg⁻¹) of ²²⁶Ra, ⁴⁰K and ²³²Th in Soil from Torkor.

SC	NS	²²⁶ Ra	²³² Th	⁴⁰ K
SL1	3	6.73 ± 0.15	11.33 ± 0.18	86.87 ± 1.30
SL2	3	14.93 ± 0.20	21.53 ± 0.20	110.73 ± 0.49
SL3	3	11.03 ± 0.11	22.30 ± 0.16	170.03 ± 1.89
SL4	3	9.53 ± 0.10	29.07 ± 0.21	220.47 ± 0.60
SL5	3	30.70 ± 1.08	26.30 ± 0.20	131.13 ± 0.84
SL6	3	35.47 ± 0.57	28.53 ± 0.32	241.20 ± 1.21
SL7	3	46.40 ± 1.08	56.47 ± 0.35	420.57 ± 0.93
SL8	3	48.83 ± 1.46	46.37 ± 0.40	311.53 ± 1.00
SL9	3	39.67 ± 0.38	26.73 ± 0.55	300.33 ± 0.90
SL10	3	32.67 ± 0.50	48.63 ± 0.40	398.57 ± 1.75
SL11	3	41.83 ± 0.21	52.47 ± 0.65	363.07 ± 2.21
SL12	3	29.37 ± 0.25	22.50 ± 0.26	201.13 ± 2.18
SL13	3	45.47 ± 0.64	49.90 ± 0.30	356.10 ± 3.16
SL14	3	24.87 ± 0.40	24.80 ± 0.30	229.43 ± 2.10
SL15	3	8.80 ± 0.26	23.17 ± 1.02	220.67 ± 1.70
SL16	3	22.93 ± 0.35	24.40 ± 0.72	231.73 ± 2.01
SL17	3	16.87 ± 0.21	11.57 ± 0.21	103.93 ± 2.56
Range	51	6.50 – 50.50	10.90 – 56.80	83.50 – 421.60
Mean	51	27.42 ± 0.21	30.95 ± 0.88	241.03 ± 5.90

SC = Sample code, SL = sampling location and NS = number of soil samples

Source: Field work, 2021-2022

Table 2: Average Activity Levels (Bq Kg⁻¹) Of ²²⁶Ra, ⁴⁰K And ²³²Th in Soil from Agbenoxoe.

SC	NS	²²⁶ Ra	²³² Th	⁴⁰ K
SL1	3	18.67 ± 0.49	17.53 ± 0.55	99.63 ± 1.45
SL2	3	3.60 ± 0.50	4.47 ± 0.23	68.70 ± 0.54
SL3	3	38.10 ± 0.80	47.30 ± 1.31	304.23 ± 1.04
SL4	3	6.77 ± 0.42	13.27 ± 0.47	142.90 ± 0.26
SL5	3	4.63 ± 0.45	10.23 ± 0.51	134.07 ± 0.52
SL6	3	52.10 ± 1.59	49.40 ± 1.06	361.57 ± 1.17
SL7	3	46.00 ± 1.15	34.23 ± 0.42	323.77 ± 1.57
SL8	3	51.33 ± 1.20	48.57 ± 1.04	356.97 ± 2.45
SL9	3	20.67 ± 1.25	19.70 ± 0.72	282.37 ± 1.23
SL10	3	20.10 ± 0.92	15.37 ± 0.70	186.67 ± 0.97
SL11	3	46.10 ± 0.92	47.63 ± 1.32	242.40 ± 1.03
SL12	3	37.57 ± 0.67	51.57 ± 1.17	355.47 ± 2.85
SL13	3	24.97 ± 0.80	25.47 ± 0.71	245.70 ± 2.55
SL14	3	37.50 ± 0.56	38.73 ± 0.40	296.67 ± 1.79
SL15	3	21.30 ± 1.06	9.50 ± 0.72	114.90 ± 0.48
SL16	3	8.43 ± 0.35	20.77 ± 0.65	155.87 ± 0.11
SL17	3	31.93 ± 1.03	36.70 ± 0.56	282.27 ± 1.37
Range	51	3.10 – 53.30	4.20 – 52.60	65.80 – 371.30
Mean	51	27.63 ± 1.09	28.85 ± 0.96	232.60 ± 6.27

SC = Sample code, SL = sampling location and NS = number of soil samples

Source: Field work, 2021-2022

Table 3: Average Activity Levels (Bq kg^{-1}) of ^{226}Ra , ^{40}K and ^{232}Th in Soil from Tsakpa.

SC	NS	^{226}Ra	^{232}Th	^{40}K
SL1	3	3.37 ± 0.45	4.80 ± 0.05	67.40 ± 0.70
SL2	3	3.07 ± 0.25	4.60 ± 0.03	87.43 ± 1.85
SL3	3	11.13 ± 0.95	15.80 ± 0.81	102.57 ± 3.50
SL4	3	7.87 ± 0.31	9.40 ± 0.70	90.63 ± 1.91
SL5	3	24.50 ± 0.85	54.60 ± 1.30	399.57 ± 2.50
SL6	3	17.20 ± 0.90	24.70 ± 0.90	300.53 ± 5.65
SL7	3	22.70 ± 0.51	39.70 ± 0.90	240.47 ± 4.60
SL8	3	15.63 ± 0.55	54.60 ± 0.42	399.63 ± 1.25
SL9	3	11.63 ± 0.42	21.60 ± 0.18	298.87 ± 3.05
SL10	3	14.47 ± 0.50	36.80 ± 0.33	340.67 ± 5.85
SL11	3	18.63 ± 0.72	25.70 ± 0.44	300.57 ± 4.55
SL12	3	17.40 ± 0.66	25.40 ± 0.35	256.83 ± 1.95
SL13	3	19.37 ± 0.45	28.90 ± 0.30	299.63 ± 2.75
SL14	3	22.30 ± 0.10	24.60 ± 0.51	230.63 ± 3.75
SL15	3	15.83 ± 0.18	18.80 ± 0.30	189.50 ± 2.50
SL16	3	38.50 ± 0.65	51.30 ± 3.10	389.70 ± 4.30
SL17	3	6.70 ± 0.80	15.80 ± 0.40	120.87 ± 1.05
Range	51	2.80 – 40.10	3.40 – 58.80	62.70 – 402.10
Mean	51	15.90 ± 0.60	26.89 ± 0.77	242.09 ± 7.42

SC = Sample code, SL = sampling location and NS = number of soil samples

Source: Field work, 2021-2022

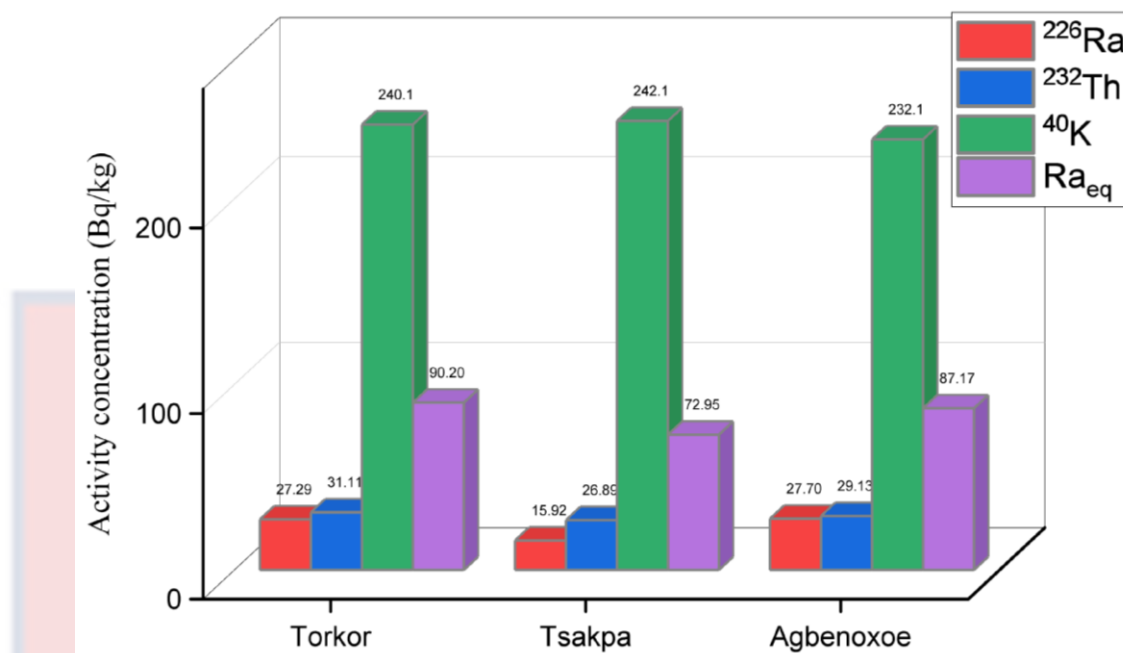


Figure 19: Average Activity Levels of ^{226}Ra , ^{40}K and ^{232}Th at Torkor, Tsakpa and Agbenoxoe.

Radon exhalation rates

The radon exhalation rate for 51 soil samples, seventeen (17) each from Torkor, Agbenoxoe and Tsakpa were determined using can techniques and the results tabulated in Table 4. From the Table 4, the radon exhalation rate varied from 3.00 to $13.10 \times 10^{-5} \text{ Bq/m}^2\text{h}$ with the overall mean value of $8.76 \pm 0.25 \times 10^{-5} \text{ Bq/m}^2\text{h}$ for Torkor, 1.10 to $15.00 \times 10^{-5} \text{ Bq/m}^2\text{h}$ with the overall mean value of $8.75 \pm 0.73 \times 10^{-5} \text{ Bq/m}^2\text{h}$ for Agbenoxoe and 1.00 to $12.40 \times 10^{-5} \text{ Bq/m}^2\text{h}$ with an overall average value of $6.84 \pm 0.48 \times 10^{-5} \text{ Bq/m}^2\text{h}$. The result obtained for radon exhalation rate for Torkor and Agbenoxoe in this study, had 11.8 % (for 2 soil samples) and 23.5 % (for 4 soil samples), respectively having values greater than the global average value of $1.25 \times 10^{-4} \text{ Bq/m}^2\text{h}$ (UNSCEAR, 1993). whereas all the values determined for Tsakpa were less than the global average value proposed by UNSCEAR (UNSCEAR, 1993).

Table 4: Radon Exhalation Rates of Torkor, Agbenoxoe and Tsakpa, Kpando

Municipality		Radon exhalation rate, $R_{n_{ex}}$ (Bq/m^2h) $\times 10^{-5}$		
SC	NS	Torkor	Agbenoxoe	Tsakpa
SL1	3	3.13 \pm 0.15	7.10 \pm 0.26	1.33 \pm 0.25
SL2	3	7.07 \pm 0.15	1.43 \pm 0.35	1.13 \pm 0.15
SL3	3	4.83 \pm 0.25	10.50 \pm 0.62	4.10 \pm 1.00
SL4	3	3.67 \pm 0.38	3.80 \pm 0.50	3.30 \pm 0.50
SL5	3	8.77 \pm 0.50	3.03 \pm 0.15	8.80 \pm 1.30
SL6	3	9.45 \pm 0.21	13.77 \pm 0.51	7.83 \pm 0.95
SL7	3	12.90 \pm 0.20	12.87 \pm 0.25	8.60 \pm 0.80
SL8	3	12.40 \pm 0.30	14.60 \pm 0.53	9.57 \pm 1.50
SL9	3	11.00 \pm 0.46	8.27 \pm 0.38	6.30 \pm 0.80
SL10	3	11.37 \pm 0.50	9.17 \pm 0.25	6.80 \pm 1.30
SL11	3	11.37 \pm 0.31	12.57 \pm 0.76	7.40 \pm 1.10
SL12	3	9.03 \pm 0.31	10.67 \pm 0.38	8.70 \pm 1.00
SL13	3	12.90 \pm 0.26	10.03 \pm 0.68	8.90 \pm 1.20
SL14	3	8.57 \pm 0.32	8.57 \pm 0.45	10.50 \pm 1.60
SL15	3	5.13 \pm 0.25	8.20 \pm 0.26	7.90 \pm 1.10
SL16	3	11.57 \pm 0.47	4.80 \pm 0.30	10.90 \pm 1.50
SL17	3	6.00 \pm 0.10	9.43 \pm 0.55	4.13 \pm 1.11
Range	51	3.00 - 13.10	1.10 - 15.00	1.00 - 12.40
Mean	51	8.76 \pm 3.25	8.75 \pm 3.73	6.84 \pm 3.08

SC = Sample code, SL = sampling location and NS = number of soil samples

Source: Field work, 2021-2022

Soil characteristics

The soil characteristics such as soil texture (% sand, % silt and % clay), soil moisture (MC), porosity (PT) and bulk density (BD) were analyzed from the seventeen (17) soil samples each taken from Torkor, Agbenoxoe and Tsakpa were tabulated in Tables 5 to 7, respectively. The soil texture is an estimate of the relative quantities of sand, silt and clay particles in the soil samples and are computed as a percentage for the study.

From the soil samples of Torkor indicated in Table 5, the percentage of sand ranges from 1.68 to 51.50 %, silt vary from 7.45 to 49.11 % and clay ranges from 6.50 to 50.00 % with the corresponding mean values of 19.83 ± 1.83 %, 42.87 ± 2.88 % and 37.30 ± 1.21 %, respectively. The dominant soil texture found in the Torkor studied area was silty clay (USDA, 1999). Bulk density (BD Mg/m^{-3}), porosity (PT) and soil moisture content (MC %) of the studied soil samples vary from 1.11 to 1.65 Mg/m^{-3} , 0.12 to 0.45 and 6.00 to 19.00 % with the corresponding mean values of $1.39 \pm 0.07 \text{ Mg/m}^{-3}$, 0.27 ± 0.02 and 10.47 ± 0.78 %, respectively. The sampling code SL1 with soil texture loamy, BD (1.11 Mg/m^{-3}), PT (0.21) and MC (9.00 %) in Table 5, recorded the least activity concentration of radium – 226, thorium – 232 and potassium – 40 (Table 1). The maximum activity concentration of radium – 226 recorded at the sampling location, SL8 and thorium – 232 and potassium - 40 corresponds to the soil texture, silty clay (Table 5).

From Table 6 (Agbenoxoe), the percentage of sand varies from 1.00 to 48.00 %, silt varies from 30.51 to 48.00 % and clay ranges from 11.89 to 55.00 % with the corresponding mean values of 18.26 ± 1.78 %, 42.25 ± 2.46 % and 39.50 ± 1.47 %, respectively. The dominant soil texture found in the Agbenoxoe

studied area was silty clay. The BD Mg/m^3 , PT and MC % of the studied soil samples varies from 1.11 to 1.64 Mg/m^3 , 0.10 to 0.45 and 3.00 to 19.00 % with the corresponding mean values of $1.39 \pm 0.04 \text{ Mg/m}^3$, 0.28 ± 0.01 and 10.53 ± 0.30 %, respectively. The sampling code SL2 with soil texture loamy, BD (1.23 Mg/m^3), PT (0.39) and MC (13.00 %) Table 5, recorded the minimum activity concentration of radium – 226, thorium – 232 and potassium – 40 (Table 2) whereas the maximum activity concentrations of radium – 226 and potassium – 40 were recorded at the sampling location, SL6 and thorium – 232 (SL12) corresponds to the soil texture, silty clay (Table 6).

From Table 7, the soil samples from Tsakpa have the percentage of sand ranging from 1.45 to 45.33 %, silt ranging from 30.21 to 51.21 % and clay ranging from 9.56 to 52.22 % with the corresponding mean values of 20.83 ± 1.768 %, 43.37 ± 2.93 % and 35.80 ± 1.56 %, respectively. The dominant soil texture found in the Tsakpa studied area was clay loam. The BD Mg/m^3 , PT and MC % of the studied soil samples varies from 1.21 to 1.66 Mg/m^3 , 0.12 to 0.65 and 5.00 to 19.00 % with the corresponding mean values of $1.37 \pm 0.04 \text{ Mg/m}^3$, 0.38 ± 0.01 and 11.71 ± 1.22 %, respectively. The sampling code SL1 with soil texture clay loamy, BD (1.21 Mg/m^3), PT (0.31) and MC (13.00 %) (Table 7), recorded the minimum activity concentration of potassium – 40 whereas soil texture (loamy), BD (1.58 Mg/m^3), PT (0.65) and MC (6.00 %) (Table 7) had radium – 226 and thorium – 232 minimal at the sampling location, SL8 (Table 3). The sampling locations, SL8 and SL16 with BD (1.39 Mg/m^3), PT (0.36) and MC (11.00 %), and BD (1.21 Mg/m^3), PT (0.12) and MC (5.00 %) with both having soil texture, silty clay (Table 7) recorded the maximum

activity concentrations of thorium – 232 and potassium – 40, and radium – 226

(Table 3), respectively.

Table 5: Properties of Soil Samples from Torkor

Sample ID	% (sand, silt and clay)			Soil texture	BD (Mg/m ⁻³)	PT	MC (%)
	Sand	Silt	Clay				
SL1	42.00	33.21	24.79	Loamy	1.11	0.21	9.00
SL2	47.22	7.45	45.33	Sandy clay	1.42	0.32	19.00
SL3	43.10	48.00	8.90	Loamy	1.11	0.42	12.00
SL4	40.11	45.21	14.68	Loamy	1.12	0.44	12.00
SL5	7.00	45.00	48.00	Silty clay	1.42	0.40	14.00
SL6	3.79	46.21	50.00	Silty clay	1.54	0.34	7.00
SL7	4.68	48.66	46.66	Silty clay	1.65	0.35	6.00
SL8	6.68	43.66	49.66	Silty clay	1.51	0.12	8.00
SL9	1.68	49.11	49.21	Silty clay	1.55	0.15	9.00
SL10	8.78	42.00	49.22	Silty clay	1.32	0.12	9.00
SL11	6.24	46.55	47.21	Silty clay	1.54	0.14	7.00
SL12	3.79	48.66	47.55	Silty clay	1.31	0.20	10.00
SL13	11.43	46.25	42.32	Silty clay	1.53	0.14	6.00
SL14	4.28	47.51	48.21	Silty clay	1.32	0.35	9.00
SL15	51.50	42.00	6.50	Sandy loam	1.21	0.28	12.00
SL16	8.89	43.11	48.00	Silty clay	1.43	0.19	11.00
SL17	46.00	46.22	7.78	Loamy	1.52	0.45	18.00
Min.	1.68	7.45	6.50		1.11	0.12	6.00
Max.	51.50	49.11	50.00		1.65	0.45	19.00
Mean	19.83	42.87	37.30	Silty clay loam	1.39	0.27	10.47
StDev	1.83	2.88	1.21		0.07	0.02	0.78

Source: Field work, 2021-2022

Table 6: Properties of Soil Samples from Agbenoxoe

Sample ID	% (sand, silt and clay)			Soil texture	BD (Mg/m ⁻³)	PT	MC (%)
	Sand	Silt	Clay				
SL1	44.66	42.00	13.34	Loamy	1.33	0.23	15.00
SL2	42.32	45.55	12.13	Loamy	1.23	0.39	13.00
SL3	11.45	44.00	44.55	Silty clay	1.51	0.22	12.00
SL4	48.00	40.11	11.89	Loamy	1.34	0.35	19.00
SL5	41.21	32.22	26.57	Loamy	1.24	0.45	12.00
SL6	6.66	43.34	50.00	Silty clay	1.54	0.12	9.00
SL7	4.14	45.65	50.21	Silty clay	1.64	0.13	12.00
SL8	19.50	30.51	49.99	Clay	1.53	0.10	5.00
SL9	3.00	48.00	49.00	Silty clay	1.41	0.34	5.00
SL10	6.90	42.66	50.44	Silty clay	1.57	0.30	13.00
SL11	1.00	44.00	55.00	Silty clay	1.41	0.30	9.00
SL12	7.79	45.21	47.00	Silty clay	1.42	0.21	5.00
SL13	10.00	40.00	50.00	Silty clay	1.11	0.21	15.00
SL14	5.44	44.56	50.00	Silty clay	1.31	0.34	8.00
SL15	8.15	41.85	50.00	Silty clay	1.22	0.38	11.00
SL16	45.00	42.00	13.00	Loamy	1.31	0.43	13.00
SL17	5.13	46.55	48.32	Silty clay	1.45	0.21	3.00
Min.	1.00	30.51	11.89		1.11	0.10	3.00
Max.	48.00	48.00	55.00		1.64	0.45	19.00
Mean	18.26	42.25	39.50	Silty clay loam	1.39	0.28	10.53
StDev	1.78	2.46	1.47		0.04	0.01	0.30

Source: Field work, 2021-2022

Table 7: Properties of Soil Samples from Tsakpa

Sample ID	% (sand, silt and clay)			Soil texture	BD (Mg/m ⁻³)	PT	MC (%)
	Sand	Silt	Clay				
SL1	35.00	30.21	34.79	Clay loam	1.21	0.31	13.00
SL2	40.46	42.55	16.99	Loamy	1.58	0.65	6.00
SL3	45.00	37.00	18.00	Loamy	1.22	0.23	11.00
SL4	45.33	44.00	10.67	Loamy	1.22	0.45	13.00
SL5	12.89	39.11	48.00	Clay	1.21	0.61	9.00
SL6	1.68	48.21	50.11	Silty clay	1.47	0.40	19.00
SL7	5.89	44.00	50.11	Silty clay	1.61	0.33	7.00
SL8	1.45	46.33	52.22	Silty clay	1.39	0.36	11.00
SL9	40.44	50.00	9.56	Loamy	1.35	0.43	19.00
SL10	45.00	41.00	14.00	Loamy	1.36	0.31	14.00
SL11	2.24	51.21	46.55	Silty clay	1.31	0.31	15.00
SL12	1.53	46.33	52.14	Silty clay	1.46	0.35	9.00
SL13	9.49	44.00	46.51	Silty clay	1.34	0.35	15.00
SL14	9.00	43.00	48.00	Silty clay	1.31	0.40	11.00
SL15	8.58	44.21	47.21	Silty clay	1.33	0.33	10.00
SL16	6.45	44.00	49.55	Silty clay	1.21	0.12	5.00
SL17	43.66	42.11	14.23	Loamy	1.66	0.47	12.00
Min.	1.45	30.21	9.56		1.21	0.12	5.00
Max.	45.33	51.21	52.22		1.66	0.65	19.00
Mean	20.83	43.37	35.80	Clay loam	1.37	0.38	11.71
StDev	1.76	2.93	1.56		0.04	0.01	1.22

Source: Field work, 2021-2022

Regression Analysis of the Radionuclides

T – Test and correlation between radionuclides in soil

In order to establish the relationship between the measured data for activity levels of ^{226}Ra , ^{232}Th , ^{40}K , and ^{222}Rn levels in soils and dwellings with some soil characteristics, a linear regression analysis of the measured values of the activity levels of ^{226}Ra , ^{232}Th , and ^{40}K , and ^{222}Rn in the soil and dwelling with some soil properties was carried out. A linear correlation coefficient was employed to find the correlation between any two radionuclides and also the influence of soil properties on radionuclide concentration level. On the other hand, it is important to point out that the linear correlation may be considered very dependable whenever the value of the correlation coefficient (R^2) is close to one. From Table 8, a linear association between ^{232}Th and ^{226}Ra , ^{40}K and ^{226}Ra and ^{232}Th and ^{40}K indicates a strong positive correlation coefficient of $R^2 = 0.78, 0.69$ and 0.79 , respectively. The statistical indicator of how closely the data matches the fitted regression line is identified as the R-squared value. In all cases, a strong positive linear correlation was observed. Indicating that the soil has the ability to hold on to these radionuclides even when the weather conditions (such as temperature, pressure) changes.

A comparison of the activity concentration levels of the radionuclides in soil in the three (3) towns of Kpando Municipality by t – test values at 95 % confidence interval is recorded in Table 9. From Table 9, it was observed that there was a statistically significant variation in indoor radon levels between the values of Torkor and Agbenoxoe ($t = 5.211, p = 0.000$ and $df = 39$), and that of Agbenoxoe and Tsakpa ($t = 6.139, p = 0.000$ and $df = 39$) while that of Torkor

and Agbenoxoe ($t = 0.157$, $p = 0.876$ and $df = 39$) shows no significant difference during the dry season.

For the rainy season, there was no significant variation in indoor radon concentrations in Torkor and Agbenoxoe ($t = 0.416$, $p = 0.680$ and $df = 39$) but significant variations were noted between the values obtained in Torkor and Tsakpa ($t = 5.202$, $p = 0.000$ and $df = 39$), and Agbenoxoe and Tsakpa ($t = 5.684$, $p = 0.000$ and $df = 39$). The variation in the indoor radon concentration levels between the three (3) towns may be attributed to the difference in geology, occupant lifestyle, building engineering and also the soil texture.

The different in geological formations, such as differences in the types of rocks and soils present in different towns can influence the presence and concentration of uranium and radium, which in turn affects the release of radon gas. Building materials, construction techniques, and the presence of cracks or gaps in the building foundation or walls can impact radon entry and accumulation in the dwellings. The dwellers behaviour such as ventilation practices (such as keeping windows open or using mechanical ventilation systems) greatly influence indoor radon concentrations. The different in soil textures, such as sandy or clayey soils, have varying permeabilities, affecting the ease with which radon gas can travel through them. Therefore, variation in soil texture, building engineering, geology and occupant lifestyle among the three towns can play a role in the differences in indoor radon levels.

Significant variations were observed between activity concentrations of ^{226}Ra from Torkor and Tsakpa ($t = 3.528$, $p = 0.003$ and $df = 16$), and Agbenoxoe and Tsakpa ($t = 2.670$, $p = 0.017$ and $df = 16$) whereas the variation

recorded from Torkor and Agbenoxoe were not significant ($t = -0.110$, $p = 0.914$ and $df = 16$).

From Table 9, activity concentrations of ^{232}Th in the soil samples from Torkor and Agbenoxoe ($t = 0.419$, $p = 0.681$ and $df = 16$), and Agbenoxoe and Tsakpa ($t = 0.419$, $p = 0.681$ and $df = 16$) show no significant difference but a significant variation was observed in Torkor and Tsakpa ($t = 1.141$, $p = 0.271$ and $df = 16$). Finally, there was no observed significant variation in the activity concentrations of ^{40}K in the soil samples from Torkor and Agbenoxoe ($t = 0.297$, $p = 0.770$, $df = 16$), Torkor and Tsakpa ($t = -0.077$, $p = 0.939$ and $df = 16$) and, Agbenoxoe and Tsakpa ($t = -0.326$, $p = 0.748$ and $df = 16$).

Table 8: Pearson Correlation Matrix of Radionuclides Concentration and Radon in Soil and Dwelling, and some Soil Properties.

	^{226}Ra	$^{222}\text{Rn}_{\text{ex}}$	^{232}Th	^{40}K	SD	ST	CY	BD	PT	MC
^{226}Ra	1.00									
$^{222}\text{Rn}_{\text{ex}}$	0.91	1.00								
^{232}Th	0.78	0.77	1.00							
^{40}K	0.69	0.75	0.89	1.00						
SD	0.48	0.64	0.42	0.46	1.00					
ST	0.36	0.40	0.30	0.41	0.48	1.00				
CY	-0.48	-0.58	-0.41	-0.50	-0.83	-0.89	1.00			
BD	0.51	0.49	0.36	0.34	0.23	0.37	-0.36	1.00		
PT	-0.70	-0.70	-0.56	-0.51	-0.25	-0.07	0.17	-0.16	1.00	
MC	-0.52	-0.40	-0.49	-0.41	-0.19	-0.14	0.19	-0.27	0.37	1.00

SD = sand, ST = silt, BD = bulk density, CY = clay, PT = porosity and MC = soil moisture

Source: Field work, 2021-2022

Table 9: T – test Comparison of the Activity Concentration Levels of Radionuclides in Torkor, Agbenoxoe and Tsakpa Soil Samples at 95 % Confidence Interval.

Towns	Radionuclides	t -value	p -value	df
Torkor/Agbenoxoe		0.157	0.876	39
Torkor/Tsakpa	²²² Rn (Dry season)	5.221	0.000	39
Agbenoxoe/Tsakpa		6.139	0.000	39
Torkor/Agbenoxoe		0.416	0.680	39
Torkor/Tsakpa	²²² Rn (Rainy season)	5.202	0.000	39
Agbenoxoe/Tsakpa		5.684	0.000	39
Torkor/Agbenoxoe		-0.110	0.914	16
Torkor/Tsakpa	²²⁶ Ra	3.528	0.003	16
Agbenoxoe/Tsakpa		2.670	0.017	16
Torkor/Agbenoxoe		0.419	0.681	16
Torkor/Tsakpa	²³² Th	1.141	0.271	16
Agbenoxoe/Tsakpa		0.436	0.669	16
Torkor/Agbenoxoe		0.297	0.770	16
Torkor/Tsakpa	⁴⁰ K	-0.077	0.939	16
Agbenoxoe/Tsakpa		-0.326	0.748	16

Source: Field work, 2021-2022

Radionuclide correlation with soil properties

Using Pearson linear correlations, the impact of soil physicochemical characteristics on the activity levels of radionuclides in soil of Kpando Municipal were studied. The findings are represented in Table 4.8. The radionuclides are either fixed within the lattice structure or absorbed onto clay surfaces with regard to soil particle size distribution. From the analysed soil samples, the majority of the soil falls into the silty loam, silty clay loam, or silty clay textural classes (USDA, 1999). In the analysed soil samples, sand and silt contents correlate positively with ²²⁶Ra, ²³²Th and ⁴⁰K activity concentrations, whereas clay was negatively correlated with the studied radionuclides. The soil particle surface area is higher in fine-grained soils than in coarse-grained soils.

There is a stronger tendency for radionuclide adsorption, as evidenced by this correlation analysis between radionuclide activity concentration and particle size distribution, as confirmed by Otoo et al. (2022). Soil bulk density correlated positively, whereas soil porosity correlated negatively with the activity levels of radium – 226, thorium – 232, and potassium – 40.

Effects of moisture, porosity and bulk density on radon exhalation rate in the soil.

The effect of the soil moisture content, porosity and bulk density on the radon exhalation are graphical represented in Figures 20 to 22. From the Figure 20, it can be observed that, the radon exhalation rate initially increases as the percentage moisture content of the soil increases, saturate and then decreases and increases with change in moisture content. This may be attributed to the capillary component of the soil water which enhances radon emanation from the grain containing radium by absorbing the recoil energy of the emanated gas. Back diffusion process is also an influencing factor for lower exhalation rate value at higher moisture content and vice versa (Pyngrope et al., 2022).

Figure 21 illustrates the effect of porosity on radon exhalation rate. From this figure, it has been noticed that there was no distinct or compelling pattern of variation of ^{222}Rn exhalation with soil porosity, in which it first increases, then saturates at specific values of porosity, and finally either increases or decreases. This pattern is in direct contradiction to the theoretical prediction, which states that exhalation rates are more likely to be favourable when there is a high porous volume. This may be due to the presence of a resisting agent, such as moisture, present in the pores, which prevents the smooth transport of radon

gas. In addition to this, the processes of absorption and adsorption that occur in the soil matrix also play a significant role as inhibitors (Pyngrope et al., 2022).

Figure 22 represents the variability of bulk density with radon exhalation rate. It was observed from the figure that, the radon exhalation rate initially decreases with increasing, then saturate at a certain values of soil bulk density, and finally either increases or decreases with change in soil bulk density. Again, there was no specific pattern noted and therefore the theoretical assumption that increase in soil bulk density will result in increase in radon exhalation rates was not observed (Otoo 2021).

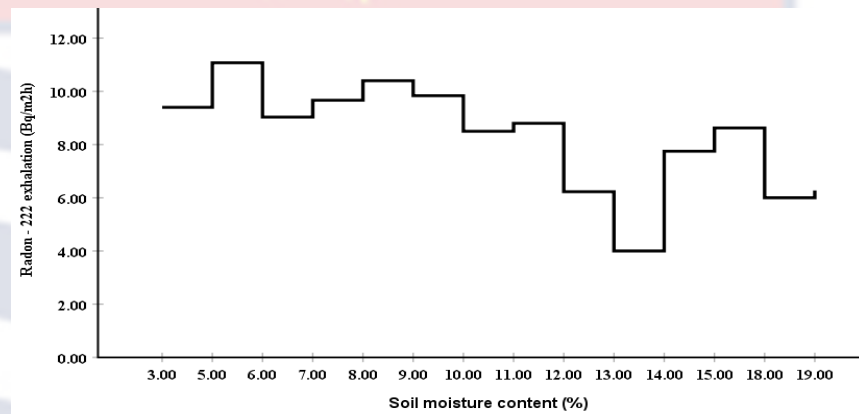


Figure 20: Variation of Soil Moisture Content with Radon Exhalation Rate

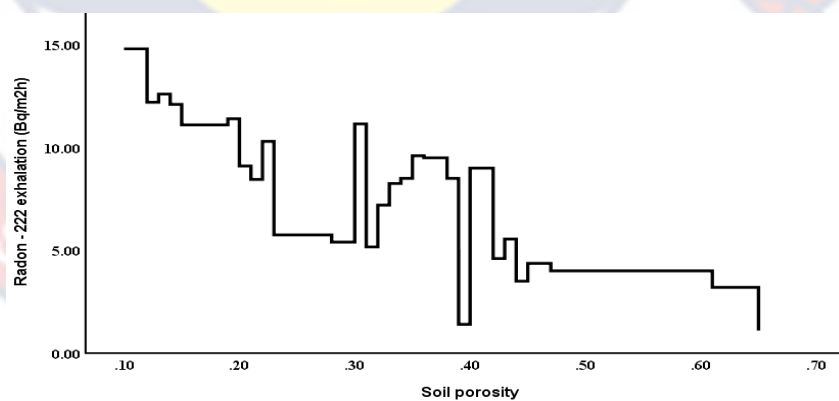


Figure 21: Variation of Soil Porosity with Radon Exhalation Rate

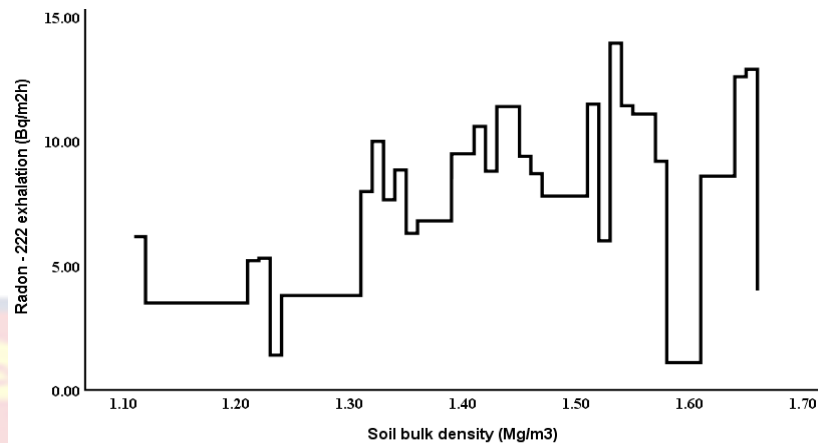


Figure 22: Variation of Soil Bulk Density with Radon Exhalation Rate

Effects of soil texture on radon exhalation rate in the soil.

The variation of radon exhalation rate in soil samples with respect to the soil composition (sand, silt and clay) is represented in Figure 23. This figure shows that the percentage clay content of the soil decreases as the radon exhalation rate increases, whereas the percentage sand and silt content of the soil increases as the radon exhalation rate also increases. This variation could be the result of an increase in the degree of pore space that occurs between the grains; as a consequence, there is now a greater amount of open space available for radon to permeate. The variation in soil texture with reference to the radon exhalation rate was not smooth as percentage sand or silt or clay increases, saturate and decrease as the radon exhalation rate changes. Generally, by line of best fit, the percentage sand and silt are directly proportional whiles clay is inversely proportional to radon exhalation rate.

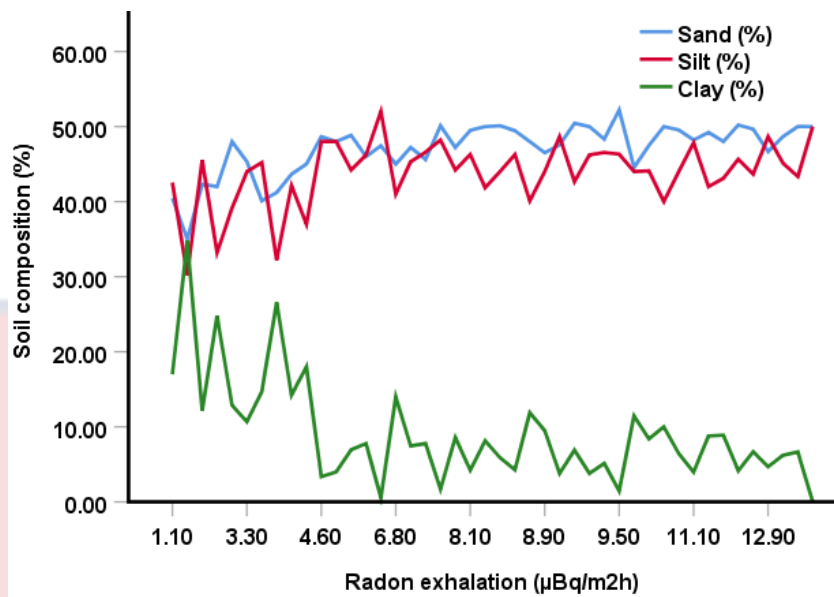


Figure 23: Variation of Soil Texture with Radon Exhalation Rate

Comparing current results to national and international data.

Table 10 shows the findings obtained in the current study for radionuclides in the soil compared with both the results of studies conducted in Ghana as well as those conducted in other parts of the world. From Table 10, the overall mean value of ^{226}Ra activity level ($23.64 \pm 0.46 \text{ Bqkg}^{-1}$) obtained for the current study was found approximately 1.2, 1.1, 1.1, 1.7 and 2.1 times greater than the values reported in Ghana by Faanu et al., 2010, Faanu et al., 2011, Amekudzie et al., 2011, Otoo et al., 2018 and Bekelesi et al., 2017, respectively. Whereas the values reported by Addo et al., 2020, Faanu et al., 2016 and Otoo et al., 2022 were 4.8, 2.8 and 1.1 times less than the values of this study, respectively.

The mean result of this study for ^{226}Ra was 1.1, 2.2, 1.1, 1.1, 1.2, 1.1, 2.6, 2.9 and 1.1 times higher than the values reported by Alharbi, 2020, Abd Elkader et al., 2021, Elsaman et al., 2018, Bui et al., 2020, Osman et al., 2022; Al – Khawlany et al., 2017, Al – Khawlany et al., 2018, Adziz & Khoo, 2018,

Al-Mutairi et al., 2020 and Kadiri et al., 2022, respectively. The ^{226}Ra mean values reported by Ademola, 2021, Lokesh et al., 2022, Dina et al., 2022, Abbasi et al., 2020, Yang & Sun, 2020, Kamalakar et al., 2022, Khan et al., 2020, Devi & Chauhan, 2020, Dieu Souffit et al., 2022, Sarki et al., 2020, Abate, 2022, Yachiso et al., 2022 and Kavasara et al., 2021 were 1.1, 1.2, 2.7, 5.4, 2.2, 1.5, 1.2, 3.6, 1.1, 2.0, 3.6, 3.2, 3.4 and 1.1 times greater than the result of this study, respectively.

Likewise, ^{232}Th overall mean activity concentration value (29.04 ± 0.66 Bq/kg), measured for the studied areas was approximately 2.0, 1.9 and 2.4 times higher than the values reported locally by Addo et al., 2020, Otoo et al., 2018 and Bekelesi et al., 2017, respectively. Whereas the values reported by Faanu et al., 2010, Otoo et al., 2022, Faanu et al., 2011, Amekudzie et al., 2011 and Faanu et al., 2016 were 1.4, 1.1, 1.7, 3.8, 2.5 and 1.8 times greater than the result of this study. With reference to the results reported internationally, the mean thorium activity concentration of this study was 1.4, 1.2, 2.3, 3.4, 1.5, 1.3, 1.4, 1.7 and 1.1 times greater than the reported values by Osman et al., 2022, Al – Khawlany et al., 2017, Al – Khawlany et al., 2018, Kadiri et al., 2022, Al-Mutairi et al., 2020, Kamalakar et al., 2022, Kavasara et al., 2021, Alharbi, 2020, Abd Elkader et al., 2021 and Elsaman et al., 2018, respectively. While the values reported by Abate, 2022, Sarki et al., 2020, Ademola, 2021, Adziz & Khoo, 2018, Yachiso et al., 2022, Bui et al., 2020, Devi & Chauhan, 2020, Dieu Souffit et al., 2022, Khan et al., 2020, Lokesh et al., 2022, Dina et al., 2022, Abbasi et al., 2020 and Yang & Sun, 2022 were 1.8, 2.4, 3.0, 1.1, 6.4, 1.5, 1.6, 2.1, 1.2, 2.2, 1.9, 3.5, 1.9 and 1.1 times greater than the values of this study.

The overall mean activity concentration of ^{40}K radioactivity (238.07 ± 3.70 Bq/kg) of this study was found to be 2.5, 1.8, 1.7, 2.4, 8.0, 2.1 and 2.1 times higher than those reported locally by Otoo et al., 2022, Faanu et al., 2010, Addo et al., 2020, Faanu et al., 2011, Amekudzie et al., 2011, Otoo et al., 2018 and Bekelesi et al., 2017, respectively. The values reported internationally by Kavasara et al., 2021, Abd Elkader et al., 2021, Sarki et al., 2020, Elsaman et al., 2018, Bui et al., 2020, Dieu Souffit et al., 2022, Al – Khawlany et al., 2018, Al – Khawlany et al., 2017, Kamalakar et al., 2022 and Adziz & Khoo, 2018 were 1.1, 1.3, 1.1, 1.5, 1.1, 1.1, 2.5, 2.5, 1.6 and 11.1 times less than the value of this study, respectively. The value of this study was found to be 4.9 times lower than the value reported by Faanu et al., 2016 and internationally reported values of Yachiso et al., 2022, Alharbi, 2020, Abate, 2022, Devi & Chauhan, 2020, Ademola, 2021, Osman et al., 2022, Khan et al., 2020, Lokesh et al., 2022, Dina et al., 2022, Abbasi et al., 2020, Yang & Sun, 2022, Kadiri et al., 2022 and Al-Mutairi & Kabir, 2020 were 1.6, 3.3, 1.4, 5.6, 2.0, 1.2, 1.8, 1.7, 3.2, 2.5, 2.3, 1.5 and 2.2 times greater than the value of this study, respectively.

Table 10: Comparing Current Results (^{226}Ra , ^{232}Th and ^{40}K Activity Levels) to

National and International data

Countries	^{226}Ra	^{232}Th	^{40}K	References
Ghana	23.64 ± 0.46	29.04 ± 0.66	238.07 ± 3.70	Present
Ghana	19.8	40.4	95.3	Faanu et al., 2010
Ghana	27	31	132	Otoo et al., 2022
Ghana	112.4	14.6	141.02	Addo et al., 2020
Ghana	22.3	49.8	99.6	Faanu et al., 2011
Ghana	22.04	108.60	29.78	Amekudzie et al., 2011
Ghana	65.1	71.8	1168.3	Faanu et al., 2016
Ghana	14.3	15.4	115.6	Otoo et al., 2018
Ghana	11.35	12.23	113.78	Bekelesi et al., 2017
Ethiopia	23.87 ± 0.70	52.50 ± 1.80	391.62 ± 11.35	Yachiso et al., 2022
India	28.07 ± 1.09	21.58 ± 0.90	237.68 ± 3.69	Kavasara et al., 2021
Saudi Arabia	23	24	790	Alharbi, 2020
Gaza Strip	11.00 ± 4.90	12.70 ± 6.30	184.00 ± 78.00	Abd Elkader et al., 2021
Ethiopia	64	70	330	Abate, 2022
Nigeria	128	86	237	Sarki et al., 2020
Egypt	22.32 ± 2.00	12.20 ± 0.60	158.24 ± 8.00	Elsaman et al., 2018
Laos	22.40 ± 2.10	30.80 ± 2.90	211.60 ± 16.50	Bui et al., 2020
India	52.00 ± 1.30	187.00 ± 6.80	1332.60 ± 92.30	Devi & Chauhan, 2020
Cameroon	35.00 ± 1.00	42.00 ± 1.00	215.00 ± 5.00	Dieu Souffit et al., 2022
Nigeria	28.69	45.86	481.22	Ademola, 2021
Egypt	19.98	19.39	277.16	Osman et al., 2022
Pakistan	86	62	427	Khan et al., 2020
India	26.47 ± 1.20	35.45 ± 1.20	403.11 ± 5.50	Lokesh et al., 2022
Bangladesh	47.00 ± 6.00	64.00 ± 5.00	762.00 ± 40.00	Dina et al., 2022
North Cyprus	84	54	594	Abbasi et al., 2020
China	75.10	101.00	535.80	Yang & Sun, 2022
Kosovo	22.32 ± 1.41	22.14 ± 1.31	358.16 ± 8.85	Kadiri et al., 2022
India	9.19	20.18	94.46	Al-Khawlany et al., 2018
India	8.18	17.41	96.50	Al-Khawlany et al., 2017
Malaysia	80	56	516	Al-Mutairi & Kabir, 2020
India	23.88	25.75	153.17	Kamalakar et al., 2022
Malaysia	20.83	32.87	21.50	Adziz & Khoo, 2018
World average	36	40	370	UNSCEAR, 2000

Source: Field work, 2021-2022

Radiological characterization

Radium equivalent activity index

The R_{eq} was used to ascertain the radiological hazard associated with the soil samples that contain ^{226}Ra , ^{232}Th and ^{40}K radionuclides (OECD, 1979), which was computed on the basis of the presumption that 370 Bq/kg of ^{226}Ra or 259 Bq/kg of ^{232}Th or 4810 Bq/kg of ^{40}K produced the same gamma radiation dose rate. To avoid radiation hazards, the use of building materials whose R_{eq} exceeds 370 Bq/kg which corresponds to an effective dose of 1.0 mSv/yr to inhabitants of dwellings is discouraged (UNSCEAR, 2000).

The radium equivalent activity index has been summarized in Table 11. The computed values of ^{226}Ra equivalent activity of this study for Torkor, Agbenoxoe and Tsakpa ranged from 29.50 to 160.74 Bq/kg, 14.16 to 152.19 Bq/kg and 13.30 to 147.00 Bq/kg, respectively. The overall mean values of R_{eq} observed in Torkor, Agbenoxoe and Tsakpa as shown in Table 11 were 90.17 ± 3.26 Bq/kg, 86.74 ± 0.71 Bq/kg and 72.93 ± 0.50 Bq/kg, respectively. The minimum mean radium equivalent activity was noted in Tsakpa whereas the maximum value was seen at Torkor. The radium equivalent activity index values from all the soil samples analyzed were less than the maximum permissible value of 370 Bq/kg (OECD, 1979; UNSCEAR, 2000). Therefore, it can be concluded that, the study soil samples would not pose any significant radiological hazard when used as a building material.

Table 11: R_{aeq} (Bq/kg) in the Soil Samples from Torkor, Agbenoxoe and Tsakpa

SC	NS	Torkor	Agbenoxoe	Tsakpa
SL1	3	29.61 ± 0.14	51.38 ± 1.10	15.41 ± 0.19
SL2	3	54.21 ± 0.82	15.27 ± 1.11	16.36 ± 0.32
SL3	3	55.97 ± 0.57	129.07 ± 2.83	41.59 ± 1.26
SL4	3	68.02 ± 0.71	36.71 ± 0.40	28.27 ± 0.11
SL5	3	78.36 ± 1.28	29.57 ± 0.88	133.24 ± 1.76
SL6	3	94.78 ± 0.75	150.48 ± 1.57	75.60 ± 0.43
SL7	3	159.42 ± 1.25	119.81 ± 0.71	97.91 ± 0.20
SL8	3	139.04 ± 1.10	148.17 ± 0.64	124.37 ± 1.35
SL9	3	100.96 ± 1.08	70.53 ± 0.42	65.48 ± 0.63
SL10	3	132.80 ± 0.29	56.41 ± 1.55	93.24 ± 1.11
SL11	3	144.71 ± 1.14	132.79 ± 2.73	78.47 ± 1.48
SL12	3	76.98 ± 0.28	138.58 ± 0.82	73.44 ± 1.03
SL13	3	144.14 ± 1.00	80.25 ± 0.25	83.70 ± 1.83
SL14	3	77.94 ± 0.20	115.65 ± 1.47	75.18 ± 1.86
SL15	3	58.87 ± 1.47	43.71 ± 1.42	57.27 ± 1.60
SL16	3	75.62 ± 1.35	50.09 ± 1.82	141.76 ± 1.29
SL17	3	41.39 ± 0.66	106.07 ± 1.90	38.57 ± 0.15
Range	51	29.50 – 160.74	14.16 – 152.19	13.30 – 147.00
Mean	51	90.17 ± 3.26	86.74 ± 0.71	72.93 ± 0.50

SC = Sample code, SL = sampling location and NS = number of soil samples

Source: Field work, 2021-2022

External and Internal Hazard Indices

Tables 12 to 14, summarize the hazard indices associated with soil samples from the three towns analyzed. The external hazards calculated for the studied towns in Kpando Municipals ranging from 0.04 to 0.43 with the mean values ranged from 0.20 to 0.24. The minimum values were recorded in both Agbenoxoe and Tsakpa whereas the maximum value was noted at Torkor. For internal hazard index calculated, the less mean value was recorded in Tsakpa

(0.24) and the maximum mean value seen in Torkor (0.32). All the hazard indices computed were generally less than the recommended limits, indicating that the hazards of these building materials are minimal.

Table 12: H_{ex} , H_{in} , I_{γ} , I_{α} , AUI and RLI for Soil Samples from Torkor.

SC	SN	H_{ex}	H_{in}	I_{γ}	I_{α}	AUI	RLI
SL1	3	0.08	0.10	0.11	0.03	0.11	0.22
SL2	3	0.15	0.19	0.19	0.07	0.23	0.39
SL3	3	0.15	0.18	0.20	0.06	0.18	0.41
SL4	3	0.18	0.21	0.25	0.05	0.18	0.50
SL5	3	0.21	0.29	0.28	0.15	0.44	0.56
SL6	3	0.26	0.35	0.34	0.18	0.51	0.68
SL7	3	0.43	0.56	0.58	0.23	0.70	1.15
SL8	3	0.38	0.51	0.50	0.24	0.71	1.00
SL9	3	0.27	0.38	0.37	0.20	0.57	0.73
SL10	3	0.36	0.45	0.48	0.16	0.51	0.97
SL11	3	0.39	0.50	0.52	0.21	0.63	1.05
SL12	3	0.21	0.29	0.28	0.15	0.42	0.55
SL13	3	0.39	0.51	0.52	0.23	0.67	1.04
SL14	3	0.21	0.28	0.28	0.12	0.37	0.57
SL15	3	0.16	0.18	0.22	0.04	0.16	0.44
SL16	3	0.20	0.27	0.28	0.11	0.34	0.55
SL17	3	0.11	0.16	0.15	0.08	0.24	0.30
Min.	51	0.08	0.10	0.11	0.03	0.11	0.22
Max.	51	0.43	0.56	0.58	0.24	0.71	1.15
Av.	51	0.24	0.32	0.33	0.14	0.41	0.65

SC = Sample code, SL = sampling location and NS = number of soil samples

Source: Field work, 2021-2022

Table 13: H_{ex} , H_{in} , I_{γ} , I_{α} , AUI and RLI for Soil Samples from Agbenoxoe.

SC	SN	H_{ex}	H_{in}	I_{γ}	I_{α}	AUI	RLI
SL1	3	0.14	0.19	0.18	0.09	0.27	0.37
SL2	3	0.04	0.05	0.06	0.02	0.06	0.11
SL3	3	0.35	0.45	0.46	0.19	0.57	0.93
SL4	3	0.10	0.12	0.14	0.03	0.11	0.27
SL5	3	0.08	0.09	0.11	0.02	0.08	0.22
SL6	3	0.41	0.55	0.54	0.26	0.76	1.08
SL7	3	0.32	0.45	0.43	0.23	0.66	0.86
SL8	3	0.40	0.54	0.53	0.26	0.75	1.07
SL9	3	0.19	0.25	0.26	0.10	0.31	0.52
SL10	3	0.15	0.21	0.21	0.10	0.29	0.41
SL11	3	0.36	0.48	0.47	0.23	0.67	0.95
SL12	3	0.37	0.48	0.50	0.19	0.57	1.00
SL13	3	0.22	0.28	0.29	0.12	0.37	0.58
SL14	3	0.31	0.41	0.42	0.19	0.55	0.84
SL15	3	0.12	0.18	0.16	0.11	0.29	0.31
SL16	3	0.14	0.16	0.18	0.04	0.15	0.37
SL17	3	0.29	0.37	0.38	0.16	0.48	0.77
Min.	51	0.04	0.05	0.06	0.02	0.06	0.11
Max.	51	0.41	0.55	0.54	0.26	0.76	1.08
Av.	51	0.23	0.31	0.31	0.14	0.41	0.63

SC = Sample code, SL = sampling location and NS = number of soil samples

Source: Field work, 2021-2022

Table 14: H_{ex} , H_{in} , I_{γ} , I_{α} , AUI and RLI for Soil Samples from Tsakpa.

SC	SN	H_{ex}	H_{in}	I_{γ}	I_{α}	AUI	RLI
SL1	3	0.04	0.05	0.06	0.02	0.05	0.12
SL2	3	0.04	0.05	0.06	0.02	0.05	0.12
SL3	3	0.11	0.14	0.15	0.06	0.17	0.30
SL4	3	0.08	0.10	0.10	0.04	0.12	0.21
SL5	3	0.36	0.43	0.49	0.12	0.41	0.98
SL6	3	0.20	0.25	0.28	0.09	0.28	0.56
SL7	3	0.26	0.33	0.35	0.11	0.36	0.71
SL8	3	0.34	0.38	0.46	0.08	0.30	0.92
SL9	3	0.18	0.21	0.25	0.06	0.20	0.49
SL10	3	0.25	0.29	0.35	0.07	0.26	0.69
SL11	3	0.21	0.26	0.29	0.09	0.29	0.58
SL12	3	0.20	0.25	0.27	0.09	0.28	0.54
SL13	3	0.23	0.28	0.31	0.10	0.31	0.62
SL14	3	0.20	0.26	0.27	0.11	0.33	0.55
SL15	3	0.15	0.20	0.21	0.08	0.24	0.42
SL16	3	0.38	0.49	0.51	0.19	0.59	1.03
SL17	3	0.10	0.12	0.14	0.03	0.12	0.28
Min.	51	0.04	0.05	0.06	0.02	0.05	0.12
Max.	51	0.38	0.49	0.51	0.19	0.59	1.03
Av.	51	0.20	0.24	0.27	0.08	0.26	0.54

SC = Sample code, SL = sampling location and NS = number of soil samples

Source: Field work, 2021-2022

Activity concentration indices (I_{γ} and I_{α})

The health risks associated with materials containing radionuclides rely on the concentrations of radionuclides present in them as a result of their use in daily life and building. The gamma and alpha activity indexes of the assessed radiological risk resulting from the use of soil in the construction of homes are summarized in Table 12 to 14. The gamma activity index values estimated for

the soil samples from Torkor, Agbenoxoe and Tsakpa ranged from 0.11 to 0.58, 0.06 to 0.54 and 0.06 to 0.51 with average value of 0.33, 0.31 and 0.27, respectively. The less gamma activity concentration index was seen in Tsakpa whereas the maximum value recorded in Torkor. The gamma activity concentration indexes computed for all the soil samples from the studied areas are within the recommended limits (EC, 1999; UNSCEAR, 2000).

The estimated alpha index values for the soil samples from Torkor, Agbenoxoe and Tsakpa ranged from 0.03 to 0.24, 0.02 to 0.26 and 0.02 to 0.19 having mean values of 0.14, 0.14 and 0.08, respectively. Both Torkor and Agbenoxoe recorded approximately the maximum mean values and Tsakpa, the least value. The calculated values for alpha activity index of all the soil samples under study were less than one (1) which is the recommended limit (UNSCEAR, 2000; EC, 1999).

Activity utilization index (AUI) and representative level index (RLI).

The values of AUI and RLI calculated for the studied soil samples are given in Table 12 to 14. From the results, the AUI values for Torkor, Agbenoxoe and Tsakpa ranged from 0.11 to 0.71, 0.06 to 0.76 and 0.05 to 0.59 having an average value of 0.41, 0.41 and 0.26, respectively. All the values for the AUI estimated are lower than 2 and corresponds to an AED less than 0.3 mSv/y (UNSCEAR, 2000), showing that soil as a building material from all the studied areas were safe.

From the results, the RLI estimated for soil samples from Torkor, Agbenoxoe and Tsakpa ranged from 0.22 to 1.15, 0.11 to 1.08 and 0.12 to 1.02 having mean values of 0.65, 0.68 and 0.54, respectively. From the results, approximately 18, 12 and 6 % of the values of RLI computed for Torkor,

Agbenoxoe and Tsakpa, respectively are greater than the dose criterion recommended by EC (EC, 1999), $RLI \leq 1$ correspond to dose rate ≤ 0.3 mSv/y whereas $RLI \leq 3$ correspond to dose rate ≤ 1.0 mSv/y.

Absorbed and effective dose rates

Absorbed dose rate (D)

The estimated outdoor and indoor absorbed gamma dose rates for Torkor, Agbenoxoe, and Tsakpa have been tabulated in Tables 15 to 17, respectively. From Tables 15 to 17, the outdoor dose rate calculated for the soil samples from Torkor, Agbenoxoe and Tsakpa ranged from 13.58 to 73.08 nGy⁻¹, 7.23 to 68.99 nGy/h and 7.27 to 65.02 nGy/h with the overall mean values of 41.41 ± 0.15 nGy/h, 39.89 ± 0.35 nGy/h and 33.68 ± 0.33 nGy/h, respectively. The world average outdoor dose rate value is 60 nGy⁻¹ (UNSCEAR, 2000), indicating that the overall mean dose rate of this study for Torkor, Agbenoxoe and Tsakpa was 1.4, 1.5 and 1.8 times respectively, less as compared to the world average value.

From Tables 15 to 17, the indoor dose rate calculated for the soil samples from Torkor, Agbenoxoe and Tsakpa varied from 25.61 to 138.45 nGy/h, 13.72 to 131.20 nGy/h and 13.77 to 123.03 nGy/h with an overall average value of 78.55 ± 0.29 nGy⁻¹, 75.76 ± 0.67 nGy/h and 63.57 ± 0.87 nGy⁻¹, respectively. The global mean indoor absorbed dose is 84 nGy⁻¹ (UNSCEAR, 2000), indicating that the overall indoor absorbed dose rate of all soil samples from Torkor, Agbenoxoe and Tsakpa was 1.1, 1.1 and 1.3 times respectively, less than the world average value. Approximately 29 %, 24 % and 12 % of the outdoor dose rate values of Torkor, Agbenoxoe and Tsakpa soil samples, respectively, were greater than that of the world outdoor average dose whereas

41 %, 47 % and 18 % of indoor dose rate were greater than the world average indoor dose rate of 84 nGy^{-1} proposed by UNSCEAR (UNSCEAR, 2000).

Table 15: External and Internal Absorbed Dose Rates and AED for Soil Samples

from Torkor.

SC	SN	D_{out}	D_{in}	AED_{out}	AED_{in}
SL1	3	13.58 ± 0.48	25.61 ± 0.91	16.70 ± 0.59	125.75 ± 0.47
SL2	3	24.52 ± 0.71	46.28 ± 0.35	30.16 ± 0.87	227.25 ± 0.62
SL3	3	25.66 ± 0.63	48.28 ± 0.21	31.56 ± 0.77	237.07 ± 0.94
SL4	3	31.15 ± 0.43	58.38 ± 0.83	38.32 ± 0.53	286.65 ± 1.08
SL5	3	35.54 ± 0.66	67.66 ± 0.28	43.71 ± 0.81	332.23 ± 1.29
SL6	3	43.68 ± 0.51	83.31 ± 0.97	53.72 ± 0.62	409.06 ± 1.78
SL7	3	73.08 ± 0.75	138.45 ± 0.46	89.89 ± 0.92	679.77 ± 3.14
SL8	3	63.56 ± 0.96	120.85 ± 0.87	78.18 ± 0.18	593.39 ± 2.15
SL9	3	47.00 ± 0.55	89.93 ± 0.13	57.81 ± 0.67	441.54 ± 1.03
SL10	3	61.09 ± 0.55	115.44 ± 1.05	75.14 ± 0.68	566.79 ± 1.14
SL11	3	66.16 ± 0.60	125.25 ± 1.12	81.37 ± 0.74	614.95 ± 2.47
SL12	3	35.54 ± 0.39	67.86 ± 0.74	43.72 ± 0.48	333.18 ± 1.61
SL13	3	65.99 ± 0.64	125.21 ± 1.22	81.17 ± 0.78	614.77 ± 2.00
SL14	3	36.03 ± 0.47	68.51 ± 0.89	44.32 ± 0.58	336.39 ± 1.39
SL15	3	27.26 ± 0.81	51.23 ± 0.50	33.53 ± 0.13	251.55 ± 1.38
SL16	3	35.00 ± 0.71	66.48 ± 0.32	43.05 ± 0.87	326.40 ± 1.50
SL17	3	19.11 ± 0.50	36.56 ± 0.95	23.51 ± 0.61	179.49 ± 0.64
Range	51	13.58 - 73.08	25.61 - 138.45	16.70 - 89.89	125.75 - 679.77
Av.	51	41.41 ± 0.15	78.55 ± 0.29	50.93 ± 0.18	385.66 ± 1.41

SC = Sample code, SL = sampling location and NS = number of soil samples

Source: Field work, 2021-2022

Table 16: External and Internal Absorbed Dose Rates and AED for Soil Samples

from Agbenoxoe.

SC	SN	D _{out}	D _{in}	AED _{out}	AED _{in}
SL1	3	23.37 ± 0.62	44.43 ± 0.18	28.74 ± 0.76	218.15 ± 1.77
SL2	3	7.23 ± 0.48	13.72 ± 0.92	8.89 ± 0.59	67.37 ± 0.50
SL3	3	58.86 ± 0.41	111.42 ± 0.66	72.40 ± 0.74	547.08 ± 3.04
SL4	3	17.10 ± 0.57	32.25 ± 0.38	21.03 ± 0.70	158.35 ± 1.32
SL5	3	13.91 ± 0.67	26.24 ± 0.26	17.11 ± 0.82	128.86 ± 1.19
SL6	3	68.99 ± 0.55	131.20 ± 1.96	84.85 ± 0.90	644.18 ± 4.51
SL7	3	55.43 ± 0.16	105.88 ± 1.04	68.18 ± 0.30	519.86 ± 3.03
SL8	3	67.94 ± 0.70	129.21 ± 1.25	83.56 ± 0.39	634.41 ± 5.92
SL9	3	33.22 ± 0.23	63.27 ± 0.36	40.86 ± 0.51	310.67 ± 2.59
SL10	3	26.35 ± 0.10	50.33 ± 0.39	32.41 ± 0.35	247.11 ± 3.27
SL11	3	60.18 ± 0.31	114.20 ± 1.46	74.02 ± 0.61	560.73 ± 2.06
SL12	3	63.33 ± 0.26	119.72 ± 1.37	77.89 ± 0.55	587.84 ± 3.60
SL13	3	37.16 ± 0.23	70.64 ± 0.96	45.71 ± 0.27	346.84 ± 1.63
SL14	3	53.09 ± 0.70	100.84 ± 0.34	65.30 ± 0.86	495.12 ± 2.57
SL15	3	20.37 ± 0.15	39.24 ± 0.21	25.06 ± 0.42	192.66 ± 0.82
SL16	3	22.94 ± 0.85	43.07 ± 0.61	28.21 ± 0.15	211.48 ± 0.89
SL17	3	48.69 ± 0.95	92.33 ± 0.83	59.89 ± 0.17	453.34 ± 1.96
Range	51	7.23 – 68.99	13.72 – 131.20	8.89 – 84.85	67.37 – 644.18
Av.	51	39.89 ± 0.35	75.76 ± 0.67	49.07 ± 0.44	372.00 ± 1.31

SC = Sample code, SL = sampling location and NS = number of soil samples

Source: Field work, 2021-2022

Table 17: External and Internal Absorbed Dose Rates and AED for Soil Samples
from Tsakpa.

SC	SN	D _{out}	D _{in}	AED _{out}	AED _{in}
SL1	3	7.27 ± 0.25	13.77 ± 0.33	8.94 ± 0.54	67.61 ± 0.44
SL2	3	7.84 ± 0.78	14.88 ± 0.45	9.64 ± 0.96	73.04 ± 0.51
SL3	3	18.96 ± 0.95	35.83 ± 0.66	23.33 ± 0.39	175.92 ± 1.98
SL4	3	13.09 ± 0.50	24.83 ± 0.79	16.10 ± 0.85	121.91 ± 1.69
SL5	3	60.96 ± 0.49	114.57 ± 1.62	74.98 ± 0.17	562.52 ± 2.65
SL6	3	35.40 ± 0.21	67.04 ± 0.77	43.54 ± 0.47	329.15 ± 1.50
SL7	3	44.49 ± 0.12	83.79 ± 0.76	54.73 ± 0.27	411.42 ± 2.09
SL8	3	56.87 ± 0.31	106.41 ± 1.15	69.94 ± 0.37	522.49 ± 3.15
SL9	3	30.88 ± 0.20	58.37 ± 0.17	37.99 ± 0.71	286.61 ± 2.46
SL10	3	43.12 ± 0.82	81.04 ± 0.21	53.03 ± 0.70	397.92 ± 3.36
SL11	3	36.67 ± 0.93	69.46 ± 0.34	45.10 ± 0.84	341.04 ± 2.02
SL12	3	34.09 ± 0.17	64.49 ± 0.89	41.93 ± 0.89	316.67 ± 2.89
SL13	3	38.90 ± 0.97	73.58 ± 0.57	47.84 ± 0.66	361.27 ± 2.35
SL14	3	34.78 ± 0.79	66.03 ± 0.11	42.78 ± 0.67	324.19 ± 3.89
SL15	3	26.57 ± 0.73	50.41 ± 0.18	32.68 ± 0.36	247.50 ± 2.39
SL16	3	65.02 ± 0.27	123.03 ± 1.75	79.98 ± 0.77	604.06 ± 2.23
SL17	3	17.68 ± 0.45	33.21 ± 0.42	21.74 ± 0.25	163.08 ± 1.50
Range	51	7.27 – 65.02	13.77 – 123.03	8.94 – 79.98	67.61 – 604.06
Av.	51	33.68 ± 0.33	63.57 ± 0.87	41.43 ± 0.23	312.14 ± 1.18

SC = Sample code, SL = sampling location and NS = number of soil samples

Source: Field work, 2021-2022

Annual Effective Dose Equivalent (AED)

The estimated indoor and outdoor AED values are tabulated in Tables 15 to 17. The outdoor AED computed for Torkor, Agbenoxoe and Tsakpa ranged from 16.70 to 89.89 $\mu\text{Sv/yr}$, 8.89 to 84.85 $\mu\text{Sv/yr}$ and 8.94 to 79.98 $\mu\text{Sv/yr}$ with the overall mean values of $50.93 \pm 0.18 \mu\text{Sv/yr}$, $49.07 \pm 0.44 \mu\text{Sv/yr}$ and $41.43 \pm 0.23 \mu\text{Sv/yr}$, respectively. The overall mean values of the outdoor

AED calculated for Torkor, Agbenoxoe and Tsakpa were 1.4, 1.4 and 1.7 times, respectively less than the global average value.

For indoor AED calculated using the soil samples from Torkor, Agbenoxoe and Tsakpa ranged from 125.75 to 679.77 $\mu\text{Sv/yr}$, 67.37 to 644.18 $\mu\text{Sv/yr}$ and 67.61 to 604.06 $\mu\text{Sv/yr}$ with average values of $385.66 \pm 1.41 \mu\text{Sv/yr}$, $372.00 \pm 1.31 \mu\text{Sv/yr}$ and $312.14 \pm 1.18 \mu\text{Sv/yr}$, respectively. The overall mean values of the indoor AED calculated for Torkor, Agbenoxoe and Tsakpa were 1.2, 1.2 and 1.4 times, respectively less than the global average value. The overall mean computed values for both indoor and outdoor AED are lower than that of the permissible dose equivalent limit of 70 $\mu\text{Sv/yr}$ and 450 $\mu\text{Sv/yr}$ recommended by ICRP, UNSCEAR and OCED (ICRP, 1991; UNSCEAR, 2008; OCED, 1979). Approximately 29 %, 29% and 12 % and, 29 %, 47 % and 35 % of soil samples from Torkor, Agbenoxoe and Tsakpa have the outdoor and indoor AED values greater than the world average value, respectively.

Excess lifetime cancer risk (ELCR)

The possibility of individuals developing lung cancer due to gamma radiation exposure from NORMs in soil samples for Torkor, Agbenoxoe and Tsakpa has been calculated and tabulated in Tables 18 to 20, respectively. The values obtained for ELCR, outdoor ranged from 0.06×10^{-3} to 0.31×10^{-3} having a mean value of 0.18×10^{-3} , 0.03×10^{-3} to 0.30×10^{-3} having a mean value of 0.17×10^{-3} and 0.03×10^{-3} to 0.28×10^{-3} having a mean value of 0.14×10^{-3} for Torkor, Agbenoxoe and Tsakpa, respectively. The ELCR values estimated for the soil samples were less than the permissible limit of 0.29×10^{-3} (UNSCEAR, 2000) except that of the sampling location, SS6 (Agbenoxoe) and SL7 (Torkor) which are greater than the proposed limit of 0.29×10^{-3} (UNSCEAR, 2000).

The values estimated for indoor ELCR ranged from 0.44×10^{-3} to 2.38×10^{-3} with a mean value of 1.35×10^{-3} , 0.24×10^{-3} to 2.25×10^{-3} with a mean value of 1.30×10^{-3} and 0.24×10^{-3} to 2.11×10^{-3} with a mean value of 1.09×10^{-3} for Torkor, Agbenoxoe and Tsakpa, respectively. Approximately 53, 53, and 41 % of the soil samples from Torkor, Agbenoxoe, and Tsakpa recorded indoor ELCR values that were higher than the global permissible limit of 1.16×10^{-3} , respectively (UNSCEAR, 2000).

Roughly, 29 %, 47 % and 41 % of the soil samples from Torkor, Agbenoxoe and Tsakpa, respectively had the total ELCR greater than the global recommended limit of 1.45×10^{-3} which is the sum of the indoor and outdoor ELCR values. The soil samples that recorded higher ELCR values were taken from farming and fishing areas and the farming and fishing practices might have contributed to the higher ELCR values. Building materials with substantially higher ELCR values should be avoided in construction because they may provide radiation hazards.

Table 18: ELCR and AGDE for Soil Samples from Torkor.

SC	SN	ELCR _{out} × 10 ⁻³	ELCR _{in} × 10 ⁻³	AGED (μSv/y)
SL1	3	0.06	0.44	95.46 ± 3.40
SL2	3	0.11	0.80	170.92 ± 4.84
SL3	3	0.11	0.83	180.70 ± 4.33
SL4	3	0.13	1.00	220.18 ± 2.92
SL5	3	0.15	1.16	245.97 ± 4.44
SL6	3	0.19	1.43	304.60 ± 3.48
SL7	3	0.31	2.38	511.46 ± 5.10
SL8	3	0.27	2.08	442.53 ± 6.51
SL9	3	0.20	1.55	328.62 ± 3.76
SL10	3	0.26	1.98	429.38 ± 3.79
SL11	3	0.28	2.15	462.58 ± 4.18
SL12	3	0.15	1.17	247.95 ± 2.72
SL13	3	0.28	2.15	460.89 ± 4.42
SL14	3	0.16	1.18	252.54 ± 3.26
SL15	3	0.12	0.88	193.32 ± 5.62
SL16	3	0.15	1.14	245.62 ± 4.92
SL17	3	0.08	0.63	133.10 ± 3.57
Range	51	0.06 – 0.31	0.44 – 2.38	95.49 - 511.46
Av.	51	0.18	1.35	289.75 ± 0.99

SC = Sample code, SL = sampling location and NS = number of soil samples

Source: Field work, 2021-2022

Table 19: ELCR and AGDE for Soil Samples from Agbenoxoe.

SC	SN	ELCR _{out} × 10 ⁻³	ELCR _{in} × 10 ⁻³	AGED (μS/y)
SL1	3	0.10	0.76	162.25 ± 4.28
SL2	3	0.03	0.24	51.37 ± 3.31
SL3	3	0.25	1.91	410.97 ± 9.83
SL4	3	0.07	0.55	121.23 ± 3.97
SL5	3	0.06	0.45	99.19 ± 4.65
SL6	3	0.30	2.25	481.01 ± 7.64
SL7	3	0.24	1.82	386.90 ± 7.37
SL8	3	0.29	2.22	473.72 ± 9.97
SL9	3	0.14	1.09	234.87 ± 8.52
SL10	3	0.11	0.86	184.96 ± 7.64
SL11	3	0.26	1.96	417.67 ± 8.99
SL12	3	0.27	2.06	443.25 ± 8.78
SL13	3	0.16	1.21	260.75 ± 7.19
SL14	3	0.23	1.73	370.93 ± 4.91
SL15	3	0.09	0.67	141.61 ± 8.01
SL16	3	0.10	0.74	161.81 ± 6.04
SL17	3	0.21	1.59	340.71 ± 6.56
Range	51	0.03 – 0.30	0.24 – 2.25	51.37 – 481.01
Av.	51	0.17	1.30	279.01 ± 2.47

SC = Sample code, SL = sampling location and NS = number of soil samples

Source: Field work, 2021-2022

Table 20: ELCR and AGDE for Soil Samples from Tsakpa.

SC	SN	ELCR _{out} × 10 ⁻³	ELCR _{in} × 10 ⁻³	AGED (μSv/y)
SL1	3	0.03	0.24	51.63 ± 1.72
SL2	3	0.03	0.26	56.16 ± 1.43
SL3	3	0.08	0.62	132.65 ± 1.65
SL4	3	0.06	0.43	92.06 ± 0.56
SL5	3	0.26	1.97	429.40 ± 7.22
SL6	3	0.15	1.15	250.76 ± 4.07
SL7	3	0.19	1.44	311.60 ± 2.63
SL8	3	0.24	1.83	402.02 ± 2.74
SL9	3	0.13	1.00	220.08 ± 1.38
SL10	3	0.19	1.39	305.50 ± 2.75
SL11	3	0.16	1.19	259.38 ± 2.32
SL12	3	0.15	1.11	240.58 ± 2.29
SL13	3	0.17	1.26	274.73 ± 2.71
SL14	3	0.15	1.13	244.15 ± 2.27
SL15	3	0.11	0.87	187.01 ± 1.93
SL16	3	0.28	2.11	455.76 ± 1.30
SL17	3	0.08	0.57	124.70 ± 2.23
Range	51	0.03 – 0.28	0.24 – 2.11	51.63 – 455.76
Av.	51	0.14	1.09	237.54 ± 3.92

SC = Sample code, SL = sampling location and NS = number of soil samples

Source: Field work, 2021-2022

Annual gonadal equivalent dose (AGED).

The AGED ($\mu\text{Sv/y}$) for people living in dwellings in Torkor, Agbenoxoe and Tsakpa due to activity levels of radium-226, thorium-232 and potassium-40 were estimated and tabulated in Tables 18 to 20, respectively. The obtained values of AGED in Torkor, Agbenoxoe and Tsakpa ranged from 95.49 to 511.46 $\mu\text{Sv/y}$, 51.37 to 481.01 $\mu\text{Sv/y}$ and 51.63 to 455.76 $\mu\text{Sv/y}^{-1}$ with an average value of $289.75 \pm 0.99 \mu\text{Sv/y}^{-1}$, $279.01 \pm 2.47 \mu\text{Sv/y}$ and $237.54 \pm 3.92 \mu\text{Sv/y}$, respectively. Approximately 41 % (7 soil samples), 47 % (8 soil samples) and 29 % (5 soil samples) of Torkor, Agbenoxoe and Tsakpa, respectively were greater than the world recommended safe limit of 300 $\mu\text{Sv/y}$ (UNSCEAR, 2000). This may be due to the higher activity concentrations of radionuclides of ^{40}K , ^{226}Ra and ^{232}Th found the soil within the studied areas.

Indoor Radon Concentration

Annual indoor radon concentrations were measured in one hundred and twenty (120) dwellings (forty (40) each in Torkor, Agbenoxoe and Tsakpa). The results were tabulated in Table 21 and 22. The annual indoor radon concentration measured ranged from 22.50 recorded at Agbenoxoe to 127.90 Bq/m^3 at Torkor as shown in Table 22. From Table 21, the annual mean values varied from $25.23 \pm 0.16 \text{Bq/m}^3$ to $110.00 \pm 1.09 \text{Bq/m}^3$ both noted at Torkor. The overall annual mean values range from $46.49 \pm 0.29 \text{Bq/m}^3$ (Tsakpa) to $76.94 \pm 0.89 \text{Bq/m}^3$ (Torkor). The minimum and maximum mean annual indoor radon concentrations observed in Torkor at sampling location, SL1 and SL8 (Table 21) corresponded to the activity concentration of radium – 222 (Table 1).

The minimum concentrations of annual mean indoor radon and radium were recorded at the same location (SL2) whereas the maximum values were recorded in different sampling locations at Tsakpa. This may be as a result of dwellers lifestyle (such as ventilation practices – keeping windows open or using mechanical ventilation systems), building material, dwelling ventilation and also soil properties such as moisture content and soil grain size. The overall annual mean values recorded in this study were less than the recommended global action level of 100 Bq/m^3 (WHO, 2009). Approximately, 23 % (for four dwellings at Torkor) and 12 % (for two dwellings each at Agbenoxoe and Tsakpa) recorded values greater than the world proposed limit of 100 Bq/m^3 (WHO, 2009).

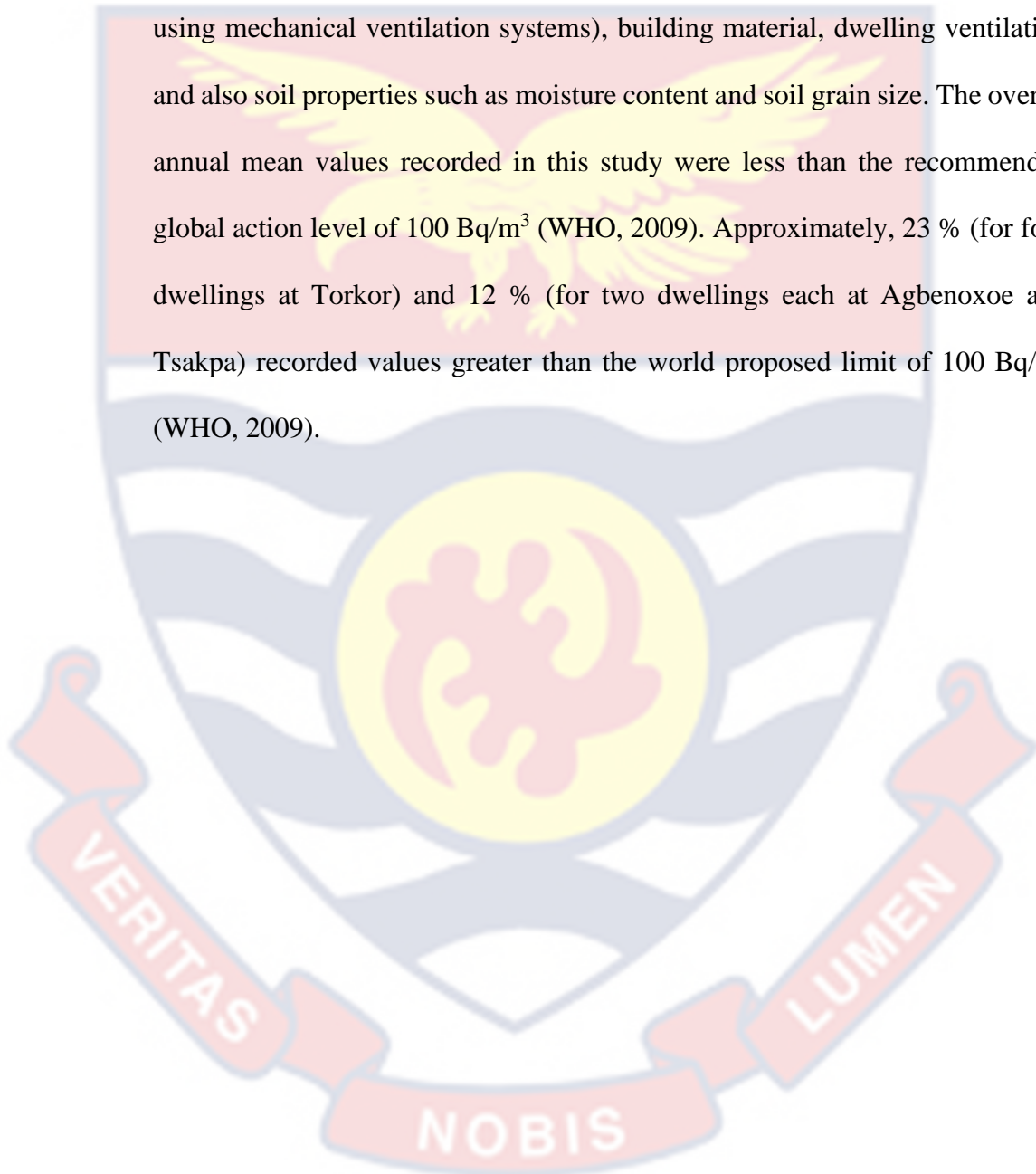


Table 21: Annual Mean indoor ^{222}Rn Levels in Torkor, Agbenoxoe and Tsakpa, Kpando Municipality

SC	ND	Indoor radon, ^{222}Rn (Bq/m ³)		
		Torkor	Agbenoxoe	Tsakpa
SL1	2	25.23 ± 0.16	27.33 ± 0.53	29.43 ± 0.07
SL2	2	36.20 ± 0.28	32.63 ± 0.28	28.30 ± 0.08
SL3	2	33.23 ± 0.70	33.55 ± 0.34	34.48 ± 0.92
SL4	2	54.85 ± 0.95	46.23 ± 0.38	31.58 ± 0.35
SL5	2	46.63 ± 0.29	50.40 ± 0.11	40.88 ± 0.71
SL6	2	53.63 ± 0.33	79.28 ± 0.18	90.85 ± 0.66
SL7	2	94.70 ± 0.69	104.40 ± 0.95	105.05 ± 1.05
SL8	2	110.17 ± 1.09	105.48 ± 1.02	94.88 ± 0.56
SL9	3	106.28 ± 1.07	96.92 ± 0.79	88.62 ± 0.13
SL10	3	62.45 ± 1.86	69.30 ± 0.17	59.55 ± 0.82
SL11	3	106.93 ± 1.03	94.42 ± 0.11	100.32 ± 1.66
SL12	2	85.30 ± 0.19	78.00 ± 0.79	82.57 ± 0.77
SL13	3	100.32 ± 0.22	83.70 ± 0.51	65.07 ± 0.90
SL14	3	59.20 ± 0.40	63.58 ± 0.80	89.03 ± 0.81
SL15	3	68.38 ± 0.23	87.08 ± 0.44	87.53 ± 0.92
SL16	2	56.60 ± 0.48	56.88 ± 0.73	56.68 ± 0.59
SL17	2	56.93 ± 0.36	62.68 ± 0.29	69.90 ± 0.31
Range	40	26.50 – 127.90	22.50 – 125.90	21.70 – 117.90
Mean	40	76.94 ± 0.89	70.15 ± 0.27	46.49 ± 0.29

SC = Sample code, SL = sampling location and NS = number of soil samples

Source: Field work, 2021-2022

Table 22: Minimum and Maximum Indoor Radon-222 Levels (Bq/m³) in Different Seasons and Annual Measurement.

Season	Torkor		Agbenoxoe		Tsakpa	
	Min	Max	Min	Max	Min	Max
Dry	24.50	120.50	23.50	124.70	23.70	110.80
Rainy	25.30	120.90	24.50	124.90	24.60	110.90
Annual	26.50	127.90	22.50	125.90	21.70	117.90

Source: Field work, 2021-2022

Relationship between ²²⁶Ra and ²²²Rn levels in soils and dwellings.

The activity concentration level of ²²⁶Ra and ²²²Rn exhalation rates in 51 soils (17 each from Torkor, Agbenoxoe and Tsakpa) were determined. The relationship between activity concentration levels of ²²⁶Ra and ²²²Rn exhalation rates in soil samples, and indoor ²²²Rn concentration were graphically represented in Figures 24 and 25. The correlation between the indoor ²²²Rn concentration and soil ²²⁶Ra concentration shows a good positive correlation with each other (Figure 24), indicating that the indoor radon concentration does not only depends on room parameters but also geological parameters.

Radon-222 exhalation rate and radium-226 activity levels in soil samples in this study showed a very good positive correlation with each other, as shown in Figure 25. The good positive correlation coefficient of 0.91 observed between ²²²Rn and ²²⁶Ra in soil affirms that ²²²Rn is a decay product of ²²⁶Ra. Hence, the higher the concentration of radionuclide ²²⁶Ra in soil the greater the radon-222 exhalation rates and vice versa. The findings presented here are consistent with other studies (Otoo et al., 2018; Nsiah – Akoto et al.,

2019; Abbas et al., 2020; Otoo et al., 2021) where they indicated that the concentration of radon depends on the level of radium in the soil.

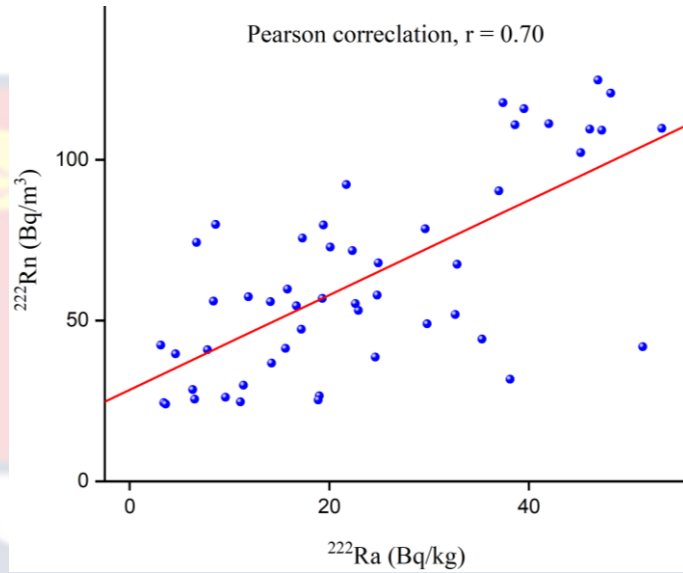


Figure 24: Radium-226 Levels in Soil and Corresponding Radon-222 Level in Dwellings.

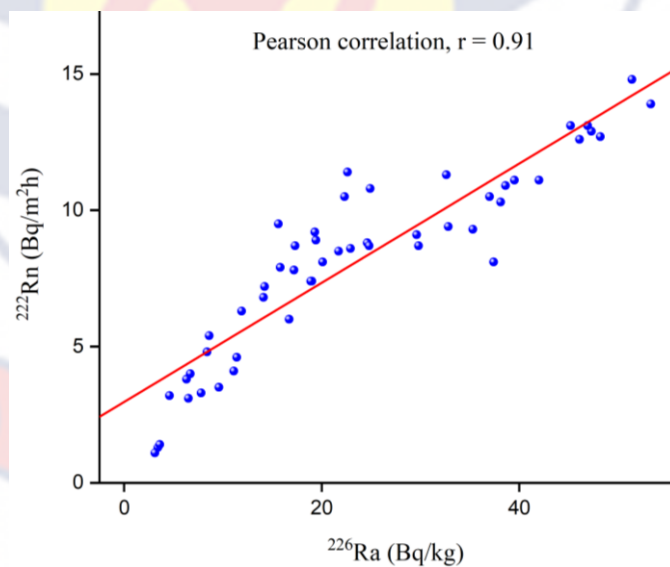


Figure 25: Correlation Between Radium-226 Levels and Radon-222 Exhalation Rates.

Seasonal variability in indoor radon concentrations

Indoor radon-222 concentration levels have been measured in 120 dwellings (40 dwellings per community) at three communities of Kpando Municipality, namely Torkor, Agbenoxoe and Tsakpa. For one entire year, measurements were taken separately throughout the dry and rainy seasons. The results of the measurements were represented in Figure 26 and, Tables 22 and 23. Table 22 represents the minimum and maximum indoor radon-222 levels recorded in each town in two major seasons of the year. From the table, indoor radon levels varied from 24.50 to 120.90 Bq/m³, 23.50 to 124.90 Bq/m³ and 23.70 to 110.90 Bq/m³ in Torkor, Agbenoxoe and Tsakpa, respectively. Both the minimum and maximum indoor radon concentration levels were noted in Agbenoxoe (23.50 Bq/m³ and 124.90 Bq/m³, respectively). The variations observed within indoor radon levels may be due to the type of building materials used for construction, ventilation conditions of the houses, the age of the dwellings, the geochemistry of the soil beneath the houses and the occupant life style. However, the results of this current study are far lower than the action levels recommended by the ICRP (ICRP, 1993), 200 to 600 Bq/m³ and European Commission for future and existing dwellings (EC, 1999), 200 to 400 Bq/m³.

The average indoor radon-222 concentration by communities and seasons for the three communities studied was tabulated in Table 23. Annual average indoor radon-222 levels in the studied three communities are 76.94 ± 3.47 Bq/m³, 70.15 ± 2.27 Bq/m³ and 46.49 ± 1.42 Bq/m³, respectively whereas seasonal average indoor radon-222 concentration levels were found to be 60.54

$\pm 2.49 \text{ Bq/m}^3$, $63.85 \pm 2.28 \text{ Bq/m}^3$ and $62.19 \pm 2.39 \text{ Bq/m}^3$ in Torkor, Agbenoxoe and Tsakpa, respectively.

The mean variations in the indoor radon measurements during the two major seasons in the studied areas were graphically represented in Figure 26.

From the Figure 26, the mean indoor radon levels varied from $40.71 \pm 1.67 \text{ Bq/m}^3$ (Tsakpa) to $70.95 \pm 3.73 \text{ Bq/m}^3$ (Torkor) during the dry season whilst for rainy season its ranged from $44.27 \pm 1.18 \text{ Bq/m}^3$ (Tsakpa) to $74.94 \pm 3.20 \text{ Bq/m}^3$ (Torkor). The minimum and the maximum mean indoor radon values are approximately 11 and 82 % larger than the world mean value of 40 Bq/m^3 (UNSCEAR, 2000), respectively.

The overall arithmetic average of the study was found to be $62.19 \pm 2.39 \text{ Bq/m}^3$. The annual mean indoor radon values in the studied locations varied from $42.49 \pm 1.42 \text{ Bq/m}^3$ (Tsakpa) to $72.94 \pm 3.47 \text{ Bq/m}^3$ (Torkor). These values are greater than that of the global mean value of 40 Bq/m^3 (UNSCEAR, 2000) by 1.1 to 1.8 times. This could be as a result of the soil and construction materials in the studied area having higher ^{226}Ra content concentrations.

From Table 23, the maximum overall mean value of radon concentration was observed during the rainy season ($63.85 \pm 2.28 \text{ Bq/m}^3$) and minimum was recorded during the dry season ($60.54 \pm 2.49 \text{ Bq/m}^3$). The variations in the mean radon-222 concentration levels in dwellings may be attributed to the fact that during the rainy season, occupants tend to close windows and doors more frequently as compared to the dry season. The current study was in agreement with research conducted in Accra (Otoo et al., 2018; Kpordzro et al., 2022). The studied communities have dusty environments and that account for the minimal variation between the rainy and dry season mean indoor radon concentrations,

since the dwellers sometimes closed the windows and doors to prevent dust particles from entering their rooms during the dry season.

Table 23: Mean Indoor Radon-222 Level (Bq/m³) in Different Seasons and Annual Average Indoor Radon-222 Concentration.

Locations	Dry season	Rainy season	Annual Av. ²²² Rn Conc.
Torkor	70.95 ± 3.73	74.94 ± 3.20	76.94 ± 3.47
Agbenoxoe	69.97 ± 2.08	72.33 ± 2.47	70.15 ± 2.27
Tsakpa	40.71 ± 1.67	44.27 ± 1.18	46.49 ± 1.42
Seasonal Av.	60.54 ± 2.49	63.85 ± 2.28	62.19 ± 2.39

Source: Field work, 2021-2022

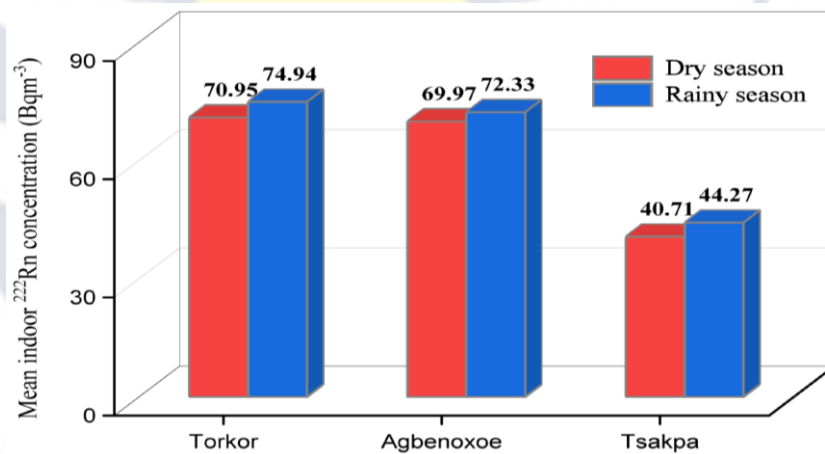


Figure 26: Mean Indoor ²²²Rn Concentration (Bq/m³) for Dry and Rainy Season.

The effects of building characteristics on the indoor radon levels

To assess the effects of the different building materials and ventilation on the radon concentration in dwellings, a box plot was used. The box plot of indoor radon concentration levels measured during the two major seasons (Dry

and Rainy) are shown in Figures 27 and 28, respectively. The indoor radon concentration ranged from 23.5 Bq/m³ (BM4) to 124.7 Bq/m³ (BM2) during the dry season shown in Figure 27 and 24.5 Bq/m³ (BM4) to 124.9 Bq/m³ (BM2) during the rainy season represented in Figure 28. The mean indoor radon values ranged from 28.87 ± 0.70 Bq/m³ (BM1) to 88.43 ± 2.37 Bq/m³ (BM2) and 30.99 ± 0.35 Bq/m³ (BM1) to 91.68 ± 2.37 Bq/m³ (BM2) for dry and rainy seasons, respectively.

The maximum radon levels that were recorded in dwelling with code BM2 (dwelling constructed with clay and having clay floor with small wooden windows) may be due to the fact that, the house contain more clay which may possess more radium content as compared to the other materials. The windows were also small and therefore the aeration was also reduced causing the accumulation of radon in those dwellings to increase. Since both the floor and the walls were all made of clay, which have cracks within the floor enabling more radon gas to emanate through into the indoor environment. The minimum indoor radon values were seen in dwellings constructed with sandcrete having cemented floor with a wooden window. There were no cracks in the sandcrete with cemented floors and therefore there was no pores for radon gas to travel into the indoor environment.

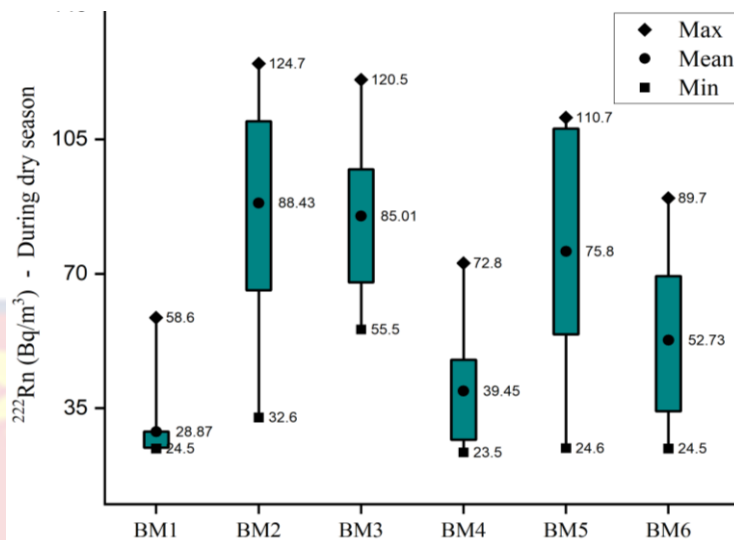


Figure 27: The Variability of Indoor Radon with Dwellings in Different Materials During Dry Season.

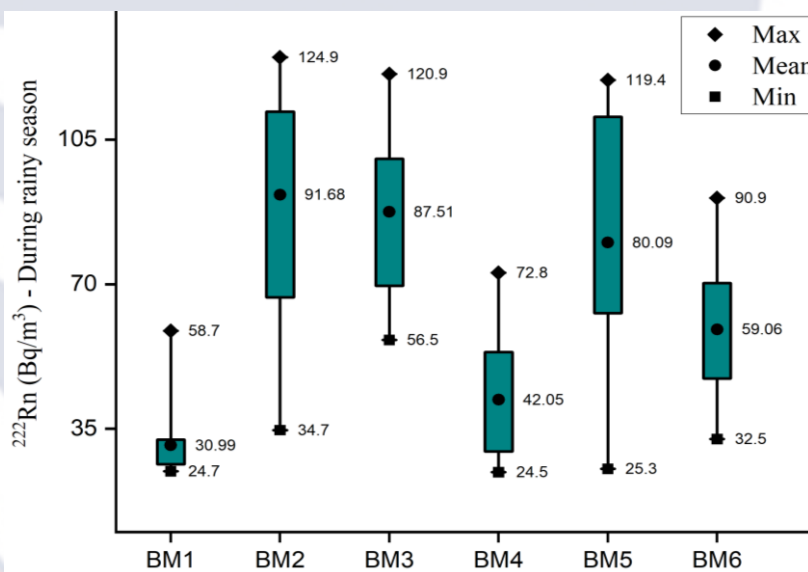


Figure 28: The Variability of Indoor Radon in Dwellings with Different Materials During Rainy Season.

Seasonal Correction Factor

The seasonal radon correction factors for towns, buildings with different building materials and different locations have been computed and tabulated in Tables 24 to 26 and Table 27 showing the different types of building materials.

The seasonal radon correction factor was calculated by dividing the geometric mean of the seasons by the radon concentration's annual geometric mean. From Table 24, the seasonal radon correction factor varies from 0.51 to 1.51 during dry season and 0.55 to 1.56 during rainy season. The least seasonal correction factors recorded during the dry season as compared to the rainy season, confirmed the variation observed between the indoor radon values during the dry and rainy season. The BM1 with the description in Table 27, registered the least correction factor for both seasons whereas the maximum correction factor for dry season was recorded by BM3 and, during the rainy season by BM2. This implies that, higher indoor radon concentrations were recorded in BM3 and BM2 during the dry and rainy seasons, respectively. The minimum indoor radon concentrations were registered at BM1 for both seasons.

From Table 25, the seasonal correction factors ranged from 1.02 to 1.05 during the rainy season and 0.95 to 0.98 during the dry season. Both minimum and maximum seasonal correction factors were noted in Tsakpa, 0.95 (during the dry season) and 1.05 (during rainy season), respectively. Table 26 represents the seasonal correction factors with respect to the exposure locations. The minimum seasonal correction factor was found in the sitting room (0.57 during dry season and 0.65 during rainy season) and maximum values were seen in Bedroom (1.26 during dry season and 1.31 during rainy season).

Table 24: ^{222}Rn Seasonal Correction Factors for Dwellings with Different Building Materials

BM	Dry season	Rainy season
BM1	0.51	0.55
BM2	1.49	1.56
BM3	1.51	1.55
BM4	0.68	0.73
BM5	1.25	1.32
BM6	0.89	1.04

Source: Field work, 2021-2022

Table 25: ^{222}Rn Seasonal Correction Factors Based on the Towns

Towns	Dry season	Rainy season
Torkor	0.96	1.03
Agbenoxoe	0.98	1.02
Tsakpa	0.95	1.05

Source: Field work, 2021-2022

Table 26: ^{222}Rn Seasonal Correction Factors Based on the Locations

Location	Dry season	Rainy season
Bed room	1.26	1.31
Sitting room	0.57	0.65
Kitchen	0.74	0.79

Source: Field work, 2021-2022

Table 27: Building Code (DC) and Description of Building Materials.

DC	Descriptions
BM1	Concrete blocks, tiles floor and glass louvre windows.
BM2	Clay, clay floor and small wooden windows
BM3	Clay, cemented walls, cemented floor and wooden windows
BM4	Sandcrete, cemented floor and wooden windows
BM5	Clay bricks, cemented floor and louvre blade windows
BM6	Block, cemented floor and wooden windows

Source: Field work, 2021-2022

From the determined indoor radon levels, seasonal radon correction factors for bedroom, sitting room and kitchen were computed by finding the ratio of the geometric mean for each season (dry and rainy season) to the annual geometric mean in the three studied communities. The results were tabulated in Table 28. The mean seasonal correction factors were found to be 0.96 ± 0.05 and 1.08 ± 0.08 for dry and rainy seasons, respectively.

The annual average values in bedrooms, sitting rooms and kitchens of the Torkor community were $89.75 \pm 2.10 \text{ Bq/m}^3$, $35.35 \pm 0.35 \text{ Bq/m}^3$ and $54.12 \pm 1.42 \text{ Bq/m}^3$, respectively. In Agbenoxoe and Tsakpa, the annual indoor radon average values were $85.74 \pm 2.09 \text{ Bq/m}^3$, $34.48 \pm 0.42 \text{ Bq/m}^3$ and $71.51 \pm 1.29 \text{ Bq/m}^3$ and, $47.62 \pm 0.95 \text{ Bq/m}^3$, $25.54 \pm 0.27 \text{ Bq/m}^3$ and $50.79 \pm 3.10 \text{ Bq/m}^3$ in bedrooms, sitting rooms and kitchens, respectively. The seasonal correction factors computed were seen to be higher during the rainy season as compared to dry season. Although, the average indoor radon levels and seasonal correction

factor values for bedrooms, sitting rooms, and kitchens differed, the differences were not statistically significant.

The variation in yearly indoor radon levels may be due to dwellers spending more time in sitting rooms, which are thus kept well-ventilated as opposed to kitchens and bedrooms. Therefore, the sitting rooms have relatively less indoor radon concentration levels.

Table 28: Ratio of the Seasonal to Annual Indoor Radon Concentration Levels of the Three Studied Locations.

Locations	Dwellings types	Annual av. ^{222}Rn conc.	Seasonal/Annual ratio	
			Dry/Annual	Rainy/Annual
Torkor	Bedroom	89.75 ± 2.10	0.98 ± 0.09	1.02 ± 0.02
	Sitting room	35.35 ± 0.35	0.90 ± 0.05	1.10 ± 0.03
	Kitchen	54.12 ± 1.42	0.97 ± 0.06	1.03 ± 0.06
Agbenoxoe	Bedroom	85.74 ± 2.09	0.99 ± 0.07	1.01 ± 0.03
	Sitting room	34.48 ± 0.42	0.95 ± 0.09	1.05 ± 0.07
	Kitchen	71.51 ± 1.29	0.99 ± 0.03	1.01 ± 0.07
Tsakpa	Bedroom	47.62 ± 0.95	0.96 ± 0.05	1.04 ± 0.04
	Sitting room	25.54 ± 0.27	0.97 ± 0.04	1.03 ± 0.06
	Kitchen	50.79 ± 3.10	0.95 ± 0.06	1.05 ± 0.03
	Overall mean	54.99 ± 1.07	0.96 ± 0.05	1.08 ± 0.08

Source: Field work, 2021-2022

Dose Estimation

Annual effective dose (AED)

From the measured indoor radon concentrations, the AED for each town in each season has been calculated and graphically represented in Figures 29 and 30. From Figure 29, the mean AED due to radon-222 ranged from 1.07 ± 0.09 mSv/y to 1.84 ± 0.07 mSv/y and the minimum annual effective dose occurred in Tsakpa (1.07 ± 0.09 mSv/y) whereas the maximum was recorded in Torkor (1.84 ± 0.07 mSv/y). Figure 30, shows the seasonal variability in AED computed for dry and rainy seasons. The figure shows that the annual mean effective dose in rainy season was maxima as compared to the values of dry season. The mean AED values due to the exposure to indoor radon concentrations estimated for Torkor and Agbenoxoe was found to be greater than those reported in other parts of the country (Otoo et al., 2018; Ansre et al., 2018; Kitson – Mills et al., 2019).

Comparing the current studies to that of Kpordzro et al. (2022) reveals that, the calculated values for AED during dry and rainy seasons were 1.8 and 1.7 times greater than current values. The AED to the individuals of the studied areas of Kpando Municipals were found to be far lower than the world average values ranging from 3 to 10 mSv/y (ICRP, 2010).

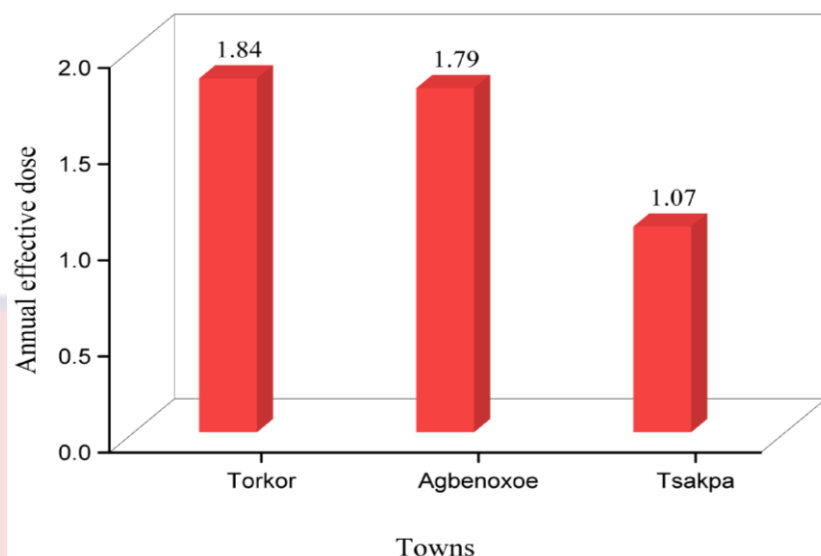


Figure 29: AED (mSv/y) Due to Radon-222 in Different Three Towns of the Kpando Municipal.

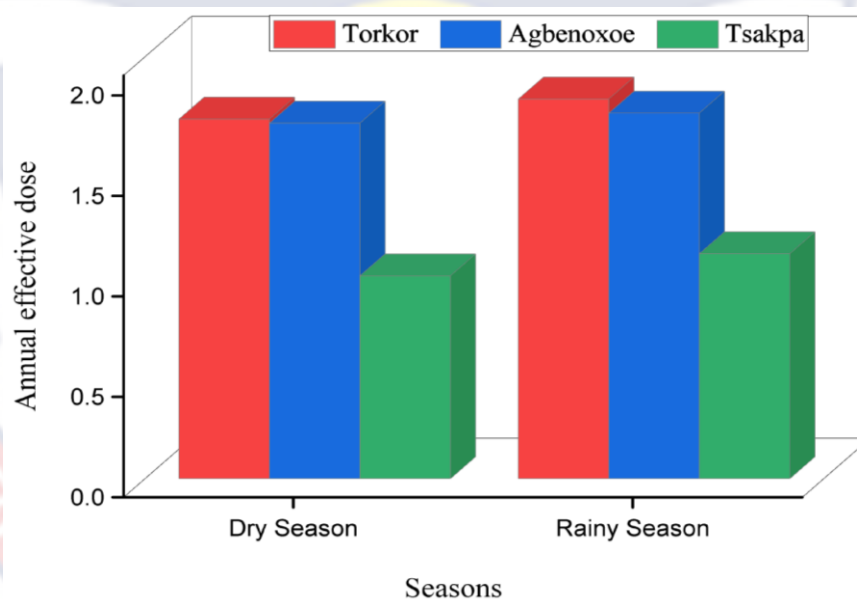


Figure 30: AED (mSv/y) Due to Radon-222 in Different Seasons for the Studied Towns.

Evaluation of Lung Cancer Risk from the measured indoor radon levels.

Lung cancer is mostly caused by prolonged human exposure to high radon concentrations, which is a well-established fact (Gogna et al., 2019). After

cigarette smoking, exposure to radon and its progenies is a significant risk factor for lung cancer. There was solid evidence from studies on miners who were occupationally exposed to radon and those who were exposed to radon inside their homes and places of employment that radon is the second most common human carcinogen (Kim et al., 2016; WHO, 2009). The target of this study was to assess the risk of lung cancer caused by radon exposure in homes in the study area. The estimated values of AED, AED_L and ELCR during the dry and rainy seasons were tabulated in Tables 29 and 30.

From Table 29, the AED, AED_L and ELCR during the dry season ranged from 0.44 (BM4) to 2.34 mSv/y (BM2), 1.06 (BM4) to 5.62 mSv/y (BM2) and 3.66 (BM4) to 37.42 mSv/y (BM5) with the mean values varying from 0.54 ± 0.06 (BM1) to 1.66 ± 0.06 mSv/y (BM2), 1.30 ± 0.39 (BM1) to 3.99 ± 0.34 mSv/y (BM2) and 4.50 ± 0.35 (BM1) to 24.73 ± 0.40 mSv/y (BM5), respectively. From Table 4.30, the AED, AED_L and ELCR during the rainy season ranged from 0.46 (BM1 and BM4) to 2.35 mSv/y (BM2), 1.10 (BM4) to 5.63 mSv/y (BM2) and 3.81 (BM4) to 19.45 mSv/y (BM2) with the mean values from 0.58 ± 0.06 (BM1) to 1.72 ± 0.05 mSv/y (BM2), 1.40 ± 0.08 (BM1) to 4.13 ± 0.02 mSv/y (BM2) and 4.82 ± 0.30 (BM1) to 14.27 ± 0.57 mSv/y (BM2), respectively.

Figure 31 represents the overall AED, AED_L and ELCR in Torkor, Agbenoxoe and Tsakpa. From the figure, both the minimum (0.45 mSv/y) and maximum (2.34 mSv/y) values of AED were recorded at Agbenoxoe whereas the overall mean values ranged from 0.80 ± 0.06 mSv/y (Tsakpa) to 1.37 ± 0.09 mSv/y (Torkor), respectively. The minimum and maximum values of AED_L (1.08 mSv/y and 5.62 mSv/y) and ELCR (3.74 mSv/y and 19.43 mSv/y) were

all observed at Agbenoxoe. The overall minimum mean values of AED_L (1.92 ± 0.07 mSv/y) and ELCR (6.62 ± 3.00 mSv/y) were all found in Tsakpa whilst the overall maximum average values of AED_L (3.29 ± 1.41 mSv/y) and ELCR (11.36 ± 4.88 mSv/y) were all observed at Torkor.

Figure 32 indicates the overall values of AED, AED_L and ELCR in Bedrooms, Sitting rooms and Kitchens. From Figure 32, the estimated values of AED, AED_L and ELCR ranged from 0.46 (Sitting room) to 2.08 mSv/y (Bedroom), 1.10 (Sitting room) to 5.00 mSv/y (Bedroom) and 3.80 (Sitting room) to 17.26 mSv/y (Bedroom) with the overall average values varying from 0.48 ± 0.02 (Sitting room) to 0.95 ± 0.06 mSv/y (Kitchen), 1.15 ± 0.04 (Sitting room) to 2.29 ± 0.14 mSv/y (Kitchen) and 3.98 ± 0.14 (Sitting room) to 7.91 ± 0.48 mSv/y (Kitchen), respectively.

The mean ELCR values determined for the studied areas were within the recommended limit of 2.3 for the total population from the lifetime exposure at 148 Bq/m^3 proposed by EPA (EPA, 2003). Therefore, the individuals in the studied areas have less probability of getting cancer as a result of inhaling radon gas.

Table 29: Estimated Values for AED, AED_L and ELCR Dry Season.

Codes	Dry season				
		Rn	AED	AED _L	ELCR
BM1	Mean	28.87 ± 0.70	0.54 ± 0.06	1.30 ± 0.39	4.50 ± 0.35
	Min.	24.50	0.46	1.10	3.81
	Max.	58.60	1.10	2.64	9.12
BM2	Mean	88.43 ± 2.69	1.66 ± 0.06	3.99 ± 1.34	13.77 ± 0.62
	Min.	32.60	0.61	1.47	5.08
	Max.	124.70	2.34	5.62	19.41
BM3	Mean	85.01 ± 1.63	1.60 ± 0.05	3.83 ± 0.84	13.24 ± 0.90
	Min.	55.50	1.04	2.50	8.64
	Max.	120.50	2.26	5.43	18.76
BM4	Mean	39.45 ± 0.51	0.74 ± 0.05	1.78 ± 0.61	6.14 ± 0.10
	Min.	23.50	0.44	1.06	3.66
	Max.	72.80	1.37	3.28	11.33
BM5	Mean	72.80 ± 3.53	1.42 ± 0.07	3.42 ± 1.38	24.73 ± 0.40
	Min.	24.60	0.46	1.11	8.32
	Max.	110.70	2.08	4.99	37.42
BM6	Mean	52.73 ± 1.53	0.99 ± 0.07	2.38 ± 0.88	8.21 ± 0.04
	Min.	24.50	0.46	1.10	3.81
	Max.	89.70	1.68	4.04	13.97

Source: Field work, 2021-2022

Table 30: Estimated Values for AED, AED_L and ELCR During Rainy Season.

Codes	Rainy season				
		²²² Rn	AED	AED _L	ELCR
BM1	Mean	30.99 ± 0.35	0.58 ± 0.06	1.40 ± 0.08	4.82 ± 0.30
	Min.	24.70	0.46	1.11	3.85
	Max.	58.70	1.10	2.65	9.14
BM2	Mean	91.68 ± 2.37	1.72 ± 0.05	4.13 ± 0.02	14.27 ± 0.57
	Min.	34.70	0.65	1.56	5.40
	Max.	124.90	2.35	5.63	19.45
BM3	Mean	87.51 ± 1.35	1.64 ± 0.06	3.94 ± 0.07	13.62 ± 0.31
	Min.	56.50	1.06	2.55	8.80
	Max.	120.90	2.27	5.45	18.82
BM4	Mean	42.05 ± 0.67	0.79 ± 0.06	1.90 ± 0.02	6.55 ± 0.13
	Min.	24.50	0.46	1.10	3.81
	Max.	72.80	1.37	3.28	11.33
BM5	Mean	80.09 ± 0.75	1.50 ± 0.06	3.61 ± 0.03	12.47 ± 0.94
	Min.	25.30	0.48	1.14	3.94
	Max.	119.40	2.24	5.38	18.59
BM6	Mean	59.06 ± 0.93	1.11 ± 0.08	2.66 ± 0.07	9.19 ± 0.33
	Min.	32.50	0.61	1.46	5.06
	Max.	90.90	1.71	4.10	14.15

Source: Field work, 2021-2022

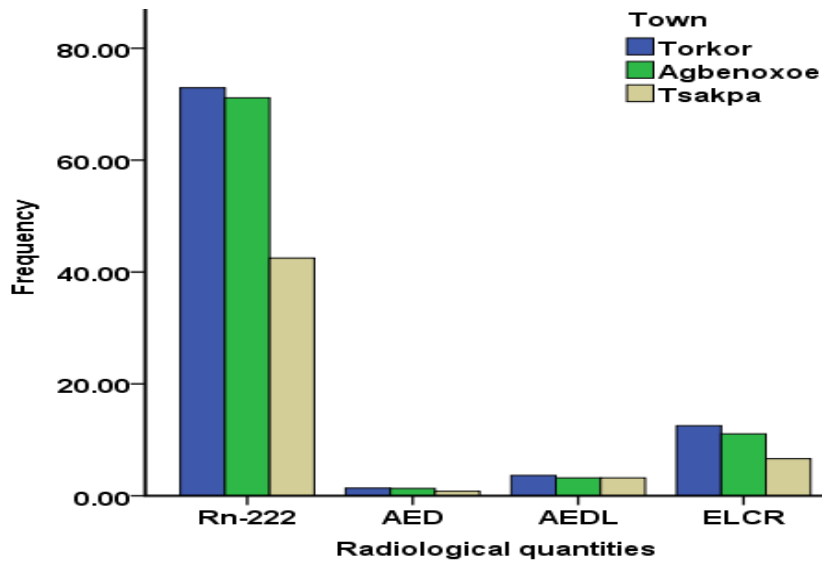


Figure 31: Bar Chart of Indoor Rn-222, AED, AED_L and ELCR of the Studied area.

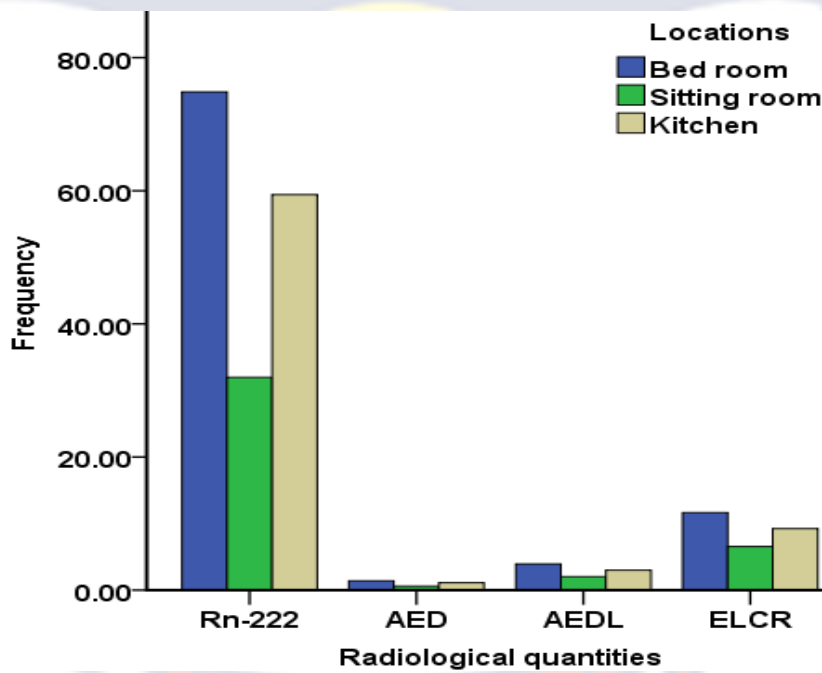


Figure 32: Bar Chart of Indoor Rn-222, AED, AED_L and ELCR of the Studied Locations.

Multivariate Statistical Analysis

The purpose of using multivariate analysis is to gain some information that will be helpful in the interpretation of the data as well as to compress the original data with a high degree of efficiency. This approach can also aid in the simplification and arrangement of sizable data sets in order to provide insightful information. Furthermore, this method can help identify the relationship between soil characteristics and natural radionuclides, highlighting similarities and differences (Otoo et al., 2021). Principal component analysis (PCA), cluster analysis, and other multivariate techniques were used to explain the correlation between many variables in terms of a small number of factors while retaining a significant amount of information.

Principal component analysis (PCA)

The data set (12 variables) is subjected to varimax rotation and Kaiser Normalization for factor analysis. The number of significant factors and, the percentage of variance explained by each of them were computed by taking the eigenvalues from the correlation table. The rotated factors 1, 2 and 3 values were shown in Table 31. The results indicate that, there were three principal components with eigenvalues larger than one as shown in the scree plot in Figure 33. These three factors account for 75.17 % of the overall variance, which leads to the conclusion that a three-factor explanation will likely be sufficient and give an acceptable description of the data. A good ordination result is typically one with a value of 75% or higher (Ghada et al., 2018).

From Table 31, the first component (PC1), which accounts for 56.60 % of the total variance and loaded heavily on ^{232}Th (0.78), PT (-0.80), SD (-0.73), CY (0.75), ^{40}K (0.74), $^{222}\text{Rn}_{\text{ex}}$ (0.77) and ^{226}Ra (0.75). The 2nd component

(PC2), correlated strongly with ^{222}Rnd and ^{222}Rnr with a high loading value of 0.87 and 0.89, respectively and accounts for about 10.09 % of the total variance. The third component (PC3) was loaded heavily on ST and moderately BD with a loading value 0.87 and 0.55, respectively, accounting for 8.49 % of the total variance.

Table 31: Rotated Component Matrix^a

Radiological/Soil parameters	Component		
	1	2	3
Rnd_222	0.30	0.87	0.22
Rnr_222	0.29	0.89	0.22
Ra_226	0.75	0.47	0.33
Rnex_222	0.77	0.37	0.38
Th_232	0.78	0.11	0.44
K_40	0.74	0.11	0.50
MC	-0.48	-0.39	-0.04
SD	-0.73	-0.45	-0.08
ST	0.05	0.11	0.87
CY	0.75	0.44	-0.12
BD	0.16	0.43	0.55
PT	-0.80	-0.15	0.28
Eigenvalue	6.79	1.21	1.02
%Total Variance	56.60	10.09	8.49
Cumulative %	56.60	66.69	75.17

^aRotation converged in 7 iterations

Source: Field work, 2021-2022

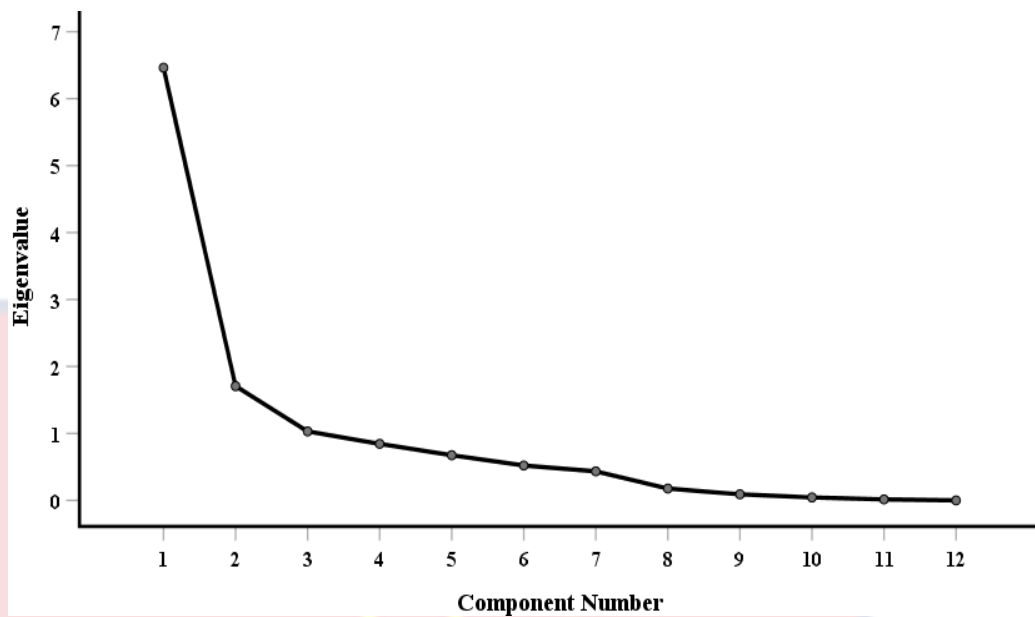


Figure 33: Scree Plot

Figure 34 shows the factor analysis plot for all the measured parameters. The relatively close proximity between the radium-226 and thorium-232 may be attributed to the fact that their decay series occurs together naturally whereas the ^{40}K may come from different sources with respect to sources of ^{226}Ra and ^{232}Th . (Otoo et al., 2021). The box plot also revealed the closeness between the percentage of SD, PT, MC, BD and ST as compared to that of CY of the soil. The occurrence of CY in a different quadrant may be linked to the different geological location and structural formation of the soil. The closeness of ^{226}Ra to $^{222}\text{Rn}_{\text{nd}}$, $^{222}\text{Rn}_{\text{nr}}$ and $^{222}\text{Rn}_{\text{ex}}$ reveals that, the radon-222 originates from the ^{226}Ra and the CY have direct effect on the radium-226 content of the soil.

Figure 35 represents the component plot for only radionuclides. The figure reveal that a strong positive correlation exists between the radionuclides. The closeness of $^{222}\text{Rn}_{\text{ex}}$ to ^{226}Ra indicates a direct relation and confirm that $^{222}\text{Rn}_{\text{ex}}$ is a direct decay product of ^{226}Ra . All the radionuclides fall within the

positive quadrant, showing that there is a positive correlation between them as observed in Figures 24 and 25.

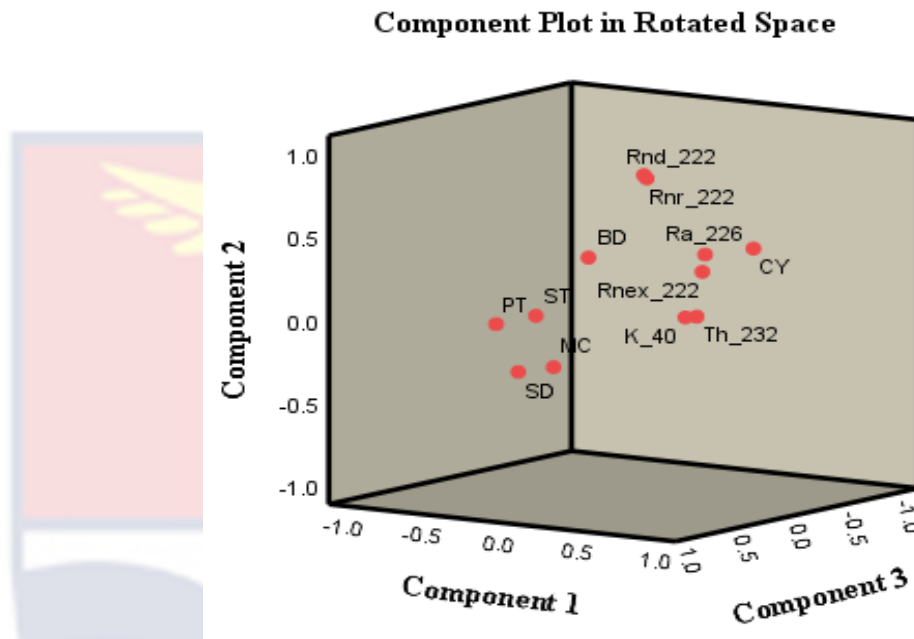


Figure 34: Box Plot for Radionuclides and Soil Properties.

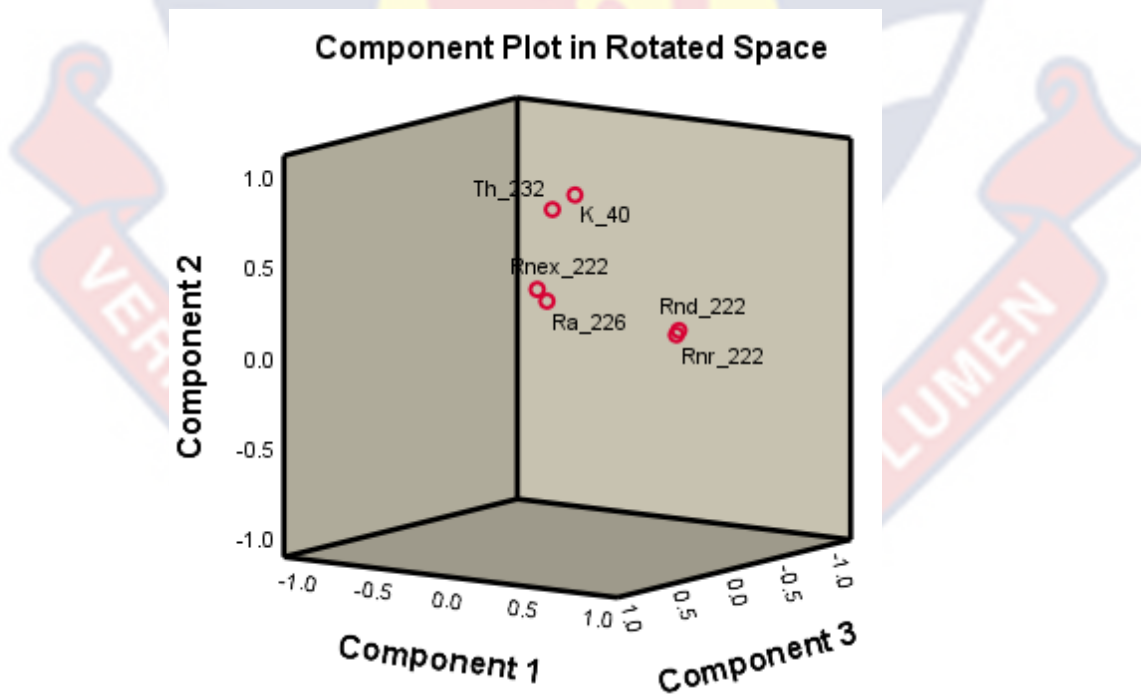


Figure 35: Box Plot for Only Radionuclides

Cluster analysis

Cluster analysis (CA) was employed to confirm the pre-existing correlation between the variables. For CA, the mean linkage technique along with the correlation coefficient distance was used and the outcome was represented by dendrogram as shown in Figure 36. In the figure, all the 12 parameters consisting of 4 radionuclides and soil properties were grouped into 3 clusters. Cluster I accounts for the BD, PT, MC, SD, CY, ST, ^{232}Th , $^{222}\text{Rn}_{\text{ex}}$ and ^{226}Ra . Cluster II consisting of $^{222}\text{Rn}_{\text{d}}$ and $^{222}\text{Rn}_{\text{r}}$ and cluster III comprises of only ^{40}K concentration. From this cluster analysis, indoor ^{222}Rn during the dry season was strongly correlated with that of the rainy season as shown in cluster II. The closeness of $^{222}\text{Rn}_{\text{d}}$ to $^{222}\text{Rn}_{\text{r}}$ may be due to the same source of origin. Cluster I confirmed that the ^{222}Rn exhalation rate depends on the activity concentration of ^{226}Ra since they are close to each other and also the radionuclides ^{226}Ra and ^{232}Th originate from a similar source. The effect of the soil properties was also confirmed as the radionuclides and the soil properties considered in this study fall in the same cluster. The cluster III is made up of only ^{40}K indicating that its source may not be the same as that of ^{226}Ra and ^{232}Th .

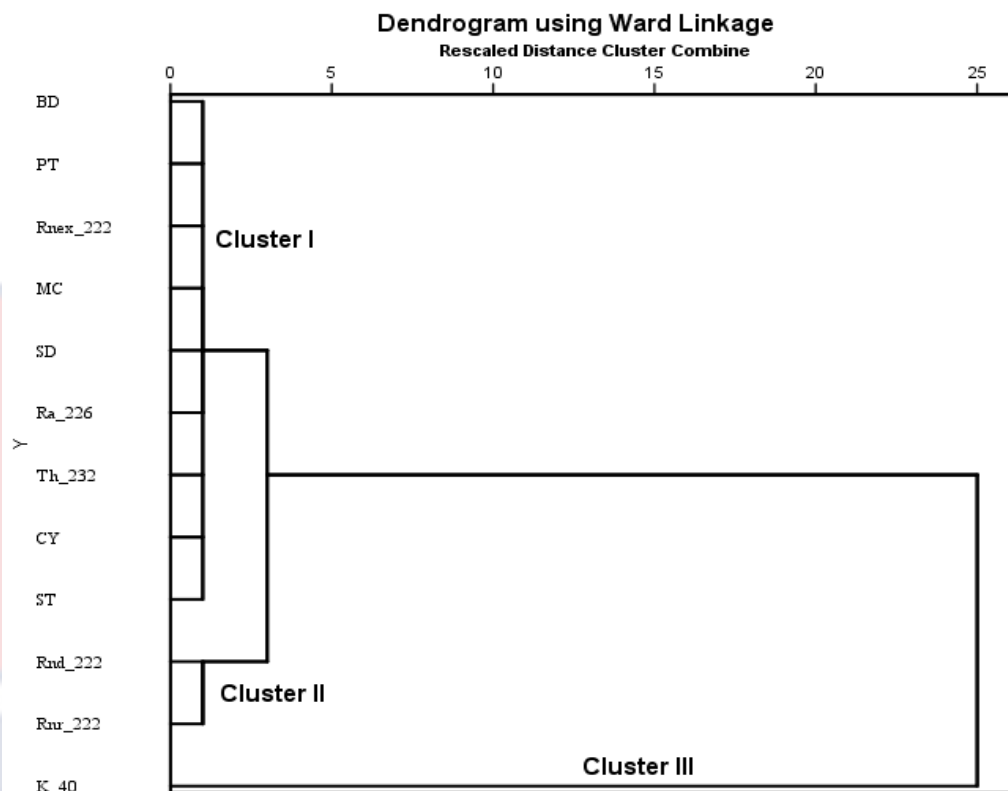


Figure 36: Dendrogram (Euclidean distance) using Ward linkage of hierarchical cluster analysis for 11 variables.

Chapter Summary

The activity concentrations of radium-226, thorium-232 and potassium-40 in 51 soil samples sampled from across the 3 towns of Kpando Municipality were determined using gamma spectroscopy. The activity concentrations varied from 2.80 (Tsakpa) to 53.30 Bqkg⁻¹ (Agbenoxoe) with a minimum and maximum average values of 15.90 ± 0.60 Bq/kg (Tsakpa) and 27.63 ± 1.09 Bq/kg (Agbenoxoe) for ²²⁶Ra while that of ²³²Th is 3.40 (Tsakpa) to 58.80 Bqkg⁻¹ (Tsakpa) with a mean ranging from 26.89 ± 0.77 Bqkg⁻¹ (Tsakpa) to 30.95 ± 0.88 Bqkg⁻¹ (Tsakpa), and for ⁴⁰K is 62.70 (Tsakpa) to 421.60 Bqkg⁻¹ (Torkor) with mean ranging from 232.60 ± 6.27 Bqkg⁻¹ (Agbenoxoe) to 242.09 ± 7.42 Bqkg⁻¹ (Tsakpa).

The radium equivalent activity values calculated using the concentrations of ^{226}Ra , ^{232}Th and ^{40}K ranged from 13.30 (Tsakpa) to 160.74 Bqkg^{-1} (Torkor) with the mean ranging from $72.93 \pm 0.50 \text{ Bq/kg}$ (Tsakpa) to $90.17 \pm 39.26 \text{ Bq/kg}$ (Torkor). These values are far less than the maximum permissible limit of 370 Bqkg^{-1} proposed by UNSCEAR (UNSCEAR, 2000). The radon exhalation rates determined for the studied locations ranged from 1.00×10^{-5} (Tsakpa) to $15.00 \times 10^{-5} \text{ Bq/m}^2/\text{h}$ (Agbenoxoe) with the mean value ranging from $(6.84 \pm 0.08) \times 10^{-5} \text{ Bq/m}^2/\text{h}$ (Tsakpa) to $(8.76 \pm 0.25) \times 10^{-5} \text{ Bq/m}^2/\text{h}$ (Torkor). It was observed that the radon exhalation rates from this study was 1.2 times greater as compared to the world average value of $1.25 \times 10^{-4} \text{ Bqm}^{-2}\text{h}^{-1}$ (UNSCEAR, 1993).

The physicochemical properties (soil particle size [SD, ST and CY], moisture content [MC], bulk density [BD] and porosity [PT]) of the soil samples were studied for the three towns. The percentage minimum and maximum of SD, ST, CY and MC occurred at Agbenoxoe ($18.26 \pm 1.78 \%$), Agbenoxoe ($42.25 \pm 2.46 \%$), Tsakpa ($35.80 \pm 1.56 \%$) and Torkor ($10.47 \pm 0.78 \%$), and Tsakpa ($20.83 \pm 1.76 \%$), Tsakpa ($43.37 \pm 2.93 \%$), Agbenoxoe ($39.50 \pm 1.47 \%$) and Tsakpa ($11.71 \pm 1.22 \%$), respectively. The PT and BD of the studied soil samples varied from 0.27 ± 0.02 (Torkor) to 0.38 ± 0.01 (Tsakpa) and $1.37 \pm 0.04 \text{ Mg/m}^3$ (Tsakpa) to $1.39 \pm 0.07 \text{ Mg/m}^3$ (Torkor), respectively. The soil texture is predominantly silty clay in all the three towns.

The radiological hazard indices were also seen to vary from 0.04 (Agbenoxoe and Tsakpa) to 0.43 (Torkor) for outdoor and 0.05 (Agbenoxoe and Tsakpa) to 0.56 (Torkor) for internal hazards. Activity concentration index for gamma and alpha was found to range from 0.06 (Agbenoxoe and Tsakpa) to

0.58 (Torkor) and 0.02 (Agbenoxoe and Tsakpa) to 0.26 (Agbenoxoe), respectively which is lower than the world acceptable value of 1.5 proposed by OECD. The minimum and maximum values of representative level index and activity utilization index was found to be 0.11 (Agbenoxoe) and 1.15 (Torkor), and 0.05 (Tsakpa) and 0.76 (Agbenoxoe), respectively. Both the representative level index and activity utilization index computed for the studied areas were less than the world average permissible limit proposed by UNSCEAR (UNSCEAR, 2000), showing that the soil from these areas is radiologically unarmful and can be used for construction.

The absorbed dose rate in air was estimated for both indoor and the outdoor environment and it ranged from 7.23 (Agbenoxoe) to 73.08 nGy/h (Torkor) with a minimum and maximum mean values of 33.68 ± 1.00 nGy/h (Tsakpa) and 41.41 ± 0.15 nGy/h (Torkor) for outdoor environment while the indoor absorbed dose rate varied from 13.72 (Agbenoxoe) to 138.45 nGy/h (Torkor) with a mean variation of 63.57 ± 1.87 nGy/h (Tsakpa) to 78.55 ± 0.29 nGy/h (Torkor). The mean concentration values for indoor and outdoor absorbed dose rates are lower than the world recommended limit except the maximum values that are higher than the 59.0 nGy/h for outdoor and 84.0 nGy/h for indoor (UNSCEAR, 2000) by 1.24 and 1.65 times, respectively.

The AED calculated for outdoor and indoor environment ranged from 8.89 (Agbenoxoe) to 89.89 μ Sv/y (Torkor) with the minimum and maximum mean value of 41.43 ± 0.23 (Tsakpa) to 50.93 ± 0.18 μ Sv/y (Torkor) for outdoor while for indoor, it ranged from 67.37 (Agbenoxoe) to 679.77 μ Sv/y (Torkor) with mean values ranging from 312.14 ± 1.18 (Tsakpa) to 385.66 ± 1.41 μ Sv/y (Torkor). The mean concentration levels for indoor and outdoor effective dose

rates were both less than the recommended limits except the upper limits of the computed values which are greater than the proposed limit of 70.00 $\mu\text{Sv/y}$ for outdoor and 450.00 $\mu\text{Sv/y}$ for indoor (ICRP, 1991; UNSCEAR, 2000; OCED, 1999) by 1.28 and 1.51 times, respectively.

The annual gonadal dose equivalent was found to range from 51.37 (Agbenoxoe) to 511.46 μSvy^{-1} (Torkor) with mean varied from 237.54 ± 3.92 (Tsakpa) to $289.75 \pm 0.99 \mu\text{Svy}^{-1}$ (Torkor).

The excess lung cancer risk associated with radionuclides in the soil of the studied area was found to range from 0.24 ((Agbenoxoe and Tsakpa) to 2.38×10^{-3} (Torkor) with mean value varying from 1.09 (Tsakpa) to 1.35×10^{-3} (Torkor) for indoor while for outdoor ranging from 0.03 (Agbenoxoe and Tsakpa) to 0.31×10^{-3} (Torkor) with average values varying from 0.14 (Tsakpa) to 0.18×10^{-3} (Torkor). The excess lung cancer risk values computed in this study for outdoor and indoor is 1.16 times greater and 1.61 times less than the global recommended mean values of 0.29×10^{-3} and 1.16×10^{-3} (UNSCEAR, 2000), respectively.

The seasonal radon concentration measured in 120 dwellings for two (dry and rainy) major seasons in the studied area. The indoor radon concentration during the dry season varied from 23.50 (Agbenoxoe) to 124.70 Bq/m^3 (Agbenoxoe) with a mean value ranging from $40.71 \pm 1.67 \text{Bq/m}^3$ (Tsakpa) to $70.95 \pm 3.73 \text{Bq/m}^3$ (Torkor) while the rainy range from 24.50 (Agbenoxoe) to 124.90 Bq/m^3 (Agbenoxoe) with the mean values varying from $44.27 \pm 1.18 \text{Bq/m}^3$ (Tsakpa) to $74.94 \pm 3.20 \text{Bq/m}^3$ (Torkor). The minimum and maximum yearly indoor radon levels was found to be $42.49 \pm 1.42 \text{Bq/m}^3$ (Tsakpa) and $72.94 \pm 3.47 \text{Bq/m}^3$ (Torkor). The mean indoor radon levels

measured were less than the global proposed limit of 100 Bq/m^3 (WHO, 2009) and 300 Bq/m^3 (ICRP, 2010).

Seasonal correction factor for indoor radon concentration was computed using the geometric mean for the seasons and annual radon values. The estimated values for correction factor ranged from 0.51 to 1.51 for the dry season and 0.55 to 1.56 for the rainy. The seasonal correction factors computed clearly indicates dwelling radon concentration level seasonal variations. All the correction factors determined for the rainy season were higher than that of the dry season. Hence, when an annual indoor radon is computed using the calculated correction factors when actual monthly radon concentration is known, the radon concentration during the rainy season will be higher as compared to that of the dry season.

The AEDE computed due to indoor radon concentration was identified to varied from 0.44 to 2.34 mSvy^{-1} with mean values ranging from $0.54 \pm 0.06 \text{ mSvy}^{-1}$ to $1.66 \pm 0.06 \text{ mSvy}^{-1}$ during the dry season and during the rainy season, it ranges from 0.46 to 2.35 mSvy^{-1} with mean values ranging from $0.58 \pm 0.06 \text{ mSvy}^{-1}$ to $1.72 \pm 0.05 \text{ mSvy}^{-1}$ during the dry season. These estimated AEDE values due to radon are far less than the allowable limit of 3 to 10 mSv per year recommended by ICRP (1993). The AEDE to the lungs was found to range from 1.06 to 5.62 mSv/y with average ranging from $1.30 \pm 0.09 \text{ mSvy}^{-1}$ to $3.99 \pm 0.04 \text{ mSvy}^{-1}$ whereas the values range from 1.10 to 5.63 mSvy^{-1} with mean values varying from $1.40 \pm 0.08 \text{ mSvy}^{-1}$ to $4.13 \pm 0.02 \text{ mSvy}^{-1}$ for the rainy season.

The estimated ELCR which is the possibility that an individual can develop cancer during his lifetime as a result of continuous exposure to indoor radon concentration during the dry season range from 3.66 to 37.42 mSv^{-1} with

the ranging from $4.50 \pm 0.05 \text{ mSv}^{-1}$ to $24.73 \pm 0.40 \text{ mSv}^{-1}$ during the dry season and 3.81 to 19.45 mSv^{-1} with mean varying from 4.82 ± 0.30 to $14.27 \pm 0.57 \text{ mSv}^{-1}$ for rainy season.



CHAPTER FIVE

SUMMARY, CONCLUSIONS AND RECOMMENDATIONS

Overview

This chapter presents the findings and recommendations from an assessment of radiation risks associated with naturally occurring radioactive substances in soil samples and radon in both soil and dwellings, and the dependence of radionuclides and radon levels on the soil properties.

Chapter Summary

The natural radioactivity in soil, soil properties, radon levels in soil and dwellings within Kpando Municipality have been studied using gamma and solid states nuclear tracks techniques. Gamma spectroscopy was used to evaluate the activity levels of ^{226}Ra , ^{232}Th , and ^{40}K in the soil samples taken from the study site. Radium-226, thorium-232, and potassium-40 activity concentrations in the research varied from place to place. The mean activity concentration of ^{226}Ra (23.64 ± 0.46 Bq/kg), ^{232}Th (29.04 ± 0.66 Bq/kg) and ^{40}K (238.07 ± 3.70 Bq/kg) were below the permissible limit set by UNSCEAR (UNSCEAR, 2000) as 35, 40 and 400 Bq/kg, respectively.

The activity concentration of ^{40}K in all the samples were higher than the concentrations of ^{226}Ra and ^{232}Th . Using the activity levels of radium-226, thorium-232, and potassium-40, as well as UNSCEAR and IAEA standard formulae, the radiological impact of these radionuclides were assessed: D, AED, AGDE, Raeq, Hin, and Hex, as well as RLI, I_α , I_γ , AUI, and ELCR values, were computed. The mean values of all the calculated hazard indices are within the permissible limit, with the exception of the ELCRin, which is 1.2 times

greater than the limit proposed by UNSCEAR (UNSCEAR, 2000). Hence, the soil from the studied areas were radiologically safe for use as a building material.

The seasonal variation of indoor radon levels during two major weather seasons (dry and rainy seasons) was measured in 120 dwellings in the studied location. The maximum radon concentration was recorded in Torkor (in bedroom) and the minimum value occurred at Agbenoxoe (in sitting room). All the mean values were less than 100 Bq/m^3 proposed WHO (WHO, 2009), and there was a clear variation between the indoor radon levels during the dry and rainy seasons. The seasonal correction factor for radon was also estimated to help determine an annual indoor radon concentration easily when the actual seasonal radon concentrations are known. The mean radon exhalation rates were found to be less than the average value of $1.25 \times 10^{-4} \text{ Bq/m}^3\text{h}$ proposed by UNSCEAR (UNSCEAR, 2000). The radiological risk from indoor radon levels were also assessed. The average values of AED, AED_L and ELCR were all less than the global recommended limits ICRP (ICRP, 1993).

The soil characteristics such as soil texture (% sand, % silt and % clay), soil moisture (MC), porosity (PT) and bulk density (BD) were determined. The values of MC, PT and BD ranged from 3.00 to 19.00 %, 0.10 to 0.65 % and 1.11 to 1.66 Mg/m^3 , respectively. The percentage sand, silt and clay component varied from 1.00 to 51.50 %, 7.45 to 51.21 % and 6.50 to 52.22 %, respectively. Generally, the soil texture found in the studied areas was silty clay loam (USDA, 1999).

The radionuclides, indoor ^{222}Rn levels and radon exhalation rate correlate well with soil characteristics showing that the soil properties have

great influence on these radiological parameters. Statistical analysis of radon exhalation rates with the soil composition of percentage sand, silt and clay revealed that, the percentage of sand is directly proportional to radon emanation rate. However, as the percentage of clay in the soil increases the radon exhalation rate decreases.

In addition, a multivariate statistical analysis was carried out on each and every one of the data obtained for this investigation. The principal component analysis was able to explain 80.53% of the variability in the data with just 3 factors. As a consequence of this, the fundamental variation information included in the data was given not by 11 soil parameters but rather by 3 combined variables.

Conclusions

The study focused on investigating the natural radioactivity levels in soil, radon levels in both soil and dwellings, and soil properties. The radiological impact of activity concentrations of ^{226}Ra , ^{232}Th and ^{40}K , and radon concentrations in both soil and dwellings were assessed as well as their dependence on soil properties. The radiological assessment of the soil revealed that the soils in the studied areas are radiologically safe.

The results of seasonal indoor radon concentration measurements conducted for two major weather seasons (rain and dry seasons) show higher indoor radon concentrations during the rainy season and less concentrations in dry season. This was due to the fact that, during rainy season dwellers frequently closed the doors and windows resulting in poor ventilation. High values of indoor radon concentrations recorded in some dwellings could be due to poor ventilation observed in those dwellings.

The principal component and cluster analysis confirms the dependence of natural radioactivity, indoor radon and radon exhalation rates on the soil moisture, soil texture, porosity and bulk density.

Recommendations

Research institutions/Academia

1. Further research should be conducted to estimate the levels of radionuclides in ground water, marine ecosystems and plants in Kpando Municipal coastal towns.
2. Other minor seasons should also be studied to estimate the doses due to ^{222}Rn gas and its decay products.
3. Studies on how building materials affect radiation exposure can be done in Kpando, and these studies can be expanded to other towns in the Kpando Municipality.
4. To determine accurately the seasonal radon correction factor, the radon measurement should be done on the monthly bases and also the annual measurement to verified the validity of the correction factor estimated.
5. It is recommended that a similar study concerning the measurement of indoor radon and natural radioactivity should be conducted in the remaining parts of the region.
6. The measurements should also be taken using both active and passive detectors in order to determine the short-term fluctuations in the indoor radon levels.
7. It is suggested that natural radioactivity should also be studied in food, water and vegetation samples in the current study area.

Regulatory Authorities

The data of this study could be added to the existing data base on radon levels in both soil and dwelling, and the radionuclides to aid in decision-making processes as setting standards and guidelines in order to control radiation exposure in the study areas.

Building Industries in Ghana

To minimize the amount of radon gas and cancer risk associated with NORMs, dwellers from Kpando Municipality are encouraged to use building materials with more percentage sand and also increase the size of the windows and doors to allow for a better exchange of air.

Residents/Dwellers

In the dwellings where indoor radon concentrations are higher than the 100 Bq/m³ proposed by WHO (WHO, 2009), the dwellers are encouraged to improve on the natural ventilation by regularly opening of doors and windows. The sizes of the doors and windows should also be increased. Any suspected cracks within the floor or the walls of the dwellings should be sealed as soon as possible. The residents in the Kpando Municipality should be educated on the possible consequences of radiation exposure and inhalation of indoor radon gas.

REFERENCES

- Abate, T. (2022). The activity concentrations of radionuclides ^{226}Ra , ^{232}Th and ^{40}K of soil samples in the case of Metekel Zone, Ethiopia. *EPJ Nuclear Sciences & Technologies*, 8, 14.
- Abbas, Y. M., Hegazy, T. M., Nassif, M. S., Shoeib, M. Y., & Abd-Elraheem, A. F. (2020). Measurement of ^{226}Ra concentration and radon exhalation rate in rock samples from Al-Qusair area using CR-39. *Journal of radiation research and applied sciences*, 13(1), 102-110.
- Abbasi, A. (2013). Calculation of gamma radiation dose rate and radon concentration due to granites used as building materials in Iran. *Radiation protection dosimetry*, 155(3), 335-342.
- Abbasi, A. (2017). *Levels of Radon and Granite Building Materials. Radon*.
- Abbasi, A., Kurnaz, A., Turhan, Ş., & Mirekhtiary, F. (2020). Radiation hazards and natural radioactivity levels in surface soil samples from dwelling areas of North Cyprus. *Journal of Radioanalytical and Nuclear Chemistry*, 324(1), 203-210.
- Abd Elkader, M. M., Shinonaga, T., & Sherif, M. M. (2021). Radiological hazard assessments of radionuclides in building materials, soils and sands from the Gaza Strip and the north of Sinai Peninsula. *Scientific Reports*, 11(1), 1-13.
- Addo, M. A., Lomotey, J. S., Osei, B., & Appiah, K. (2020). Measurement of natural radioactivity in soil dust samples along roadways in high commercial areas of the Ketu South district of the Volta Region, Ghana. *Radiation Protection and Environment*, 43(1), 6.

- Ademola, A. K. (2021). Radiological Risks from Natural Radionuclides in Surface Soil of Agbara Industrial Area, Ogun State, Nigeria. *Journal of Applied Sciences and Environmental Management*, 25(5), 733-739.
- Adziz, M. A., & Khoo, K. S. (2018). An assessment of absorbed dose and radiation hazard index from soil around repository facility at Bukit Kledang, Perak, Malaysia. In *IOP Conference Series: Materials Science and Engineering* (Vol. 298, No. 1, p. 012001). IOP Publishing.
- Ahad, A., (2004). Measurement of Natural Radioactivity in the Soil, Indoor Radon Level and Excess Cancer Risks in Bahawalpur Division, Pakistan. Ph. D Dissertation, Islamia University Bahawalpur, Pakistan.
- Akortia, E., Glover, E. T., Nyarku, M., Dawood, A., Essel, P., Sarfo, E. O., ... & Gbeddy, G. (2021). Geological interactions and radio-chemical risks of primordial radionuclides ^{40}K , ^{226}Ra , and ^{232}Th in soil and groundwater from potential radioactive waste disposal site in Ghana. *Journal of Radioanalytical and Nuclear Chemistry*, 328(2), 577-589.
- Akortia, E., Oppon, O. C., & Serfor-Armah, Y. (2010). Indoor radon gas levels in selected homes in the Greater Accra region of Ghana. *Research Journal of Applied Sciences, Engineering and Technology*, 2(8), 734-742.
- Al Mutairi, A. M. M., & Kabir, N. A. (2020). Natural radionuclides in soil and root vegetables in Malaysia: transfer factors and dose estimates. *Radiation protection dosimetry*, 188(1), 47-55.

Al Zabadi, H., Musmar, S., Issa, S., Dwaikat, N., & Saffarini, G. (2012). Exposure assessment of radon in the drinking water supplies: a descriptive study in Palestine. *BMC research notes*, 5(1), 1-8.

Alharbi, T. (2020). Establishment of natural radioactivity baseline, mapping, and radiological hazard assessment in soils of Al-Qassim, Al-Ghat, Al-Zulfi, and Al-Majmaah. *Arabian Journal of Geosciences*, 13(11), 1-11.

Al-khawlany, A. H., Khan, A. R. and Pathan, J. M. (2018). Determination of Natural Radioactivity Levels and Radiation Hazards for Soil Samples from Aurangabad Maharashtra-India. *Journal of multifaceted and multilingual studies*, v (2), 78–88.

Al-Khawlany, A. H., Khan, A. R., Pawar, P. P., & Pathan, J. M. (2017). Measurement of activity concentration levels of radionuclides and associated hazard indices in soil samples collected from Aurangabad, Maharashtra-India. *Int J Sci Eng Res*, 8(7), 1586-1593.

Andam, A. A. (1993). The contribution of radon to population dose from natural radiation in Ghana. *Journal of Science and Technology (Ghana)*, 13(2), 99-104.

Almayahi, B., Tajuddin, A., & Jaafar, M. (2011). In-Situ radon level measurement for a tropical country. In *Proceedings of International Conference on Chemical, Biological and Environment Sciences (ICCEBS'2011) in Thailand* (pp. 415-7).

Amekudzie, A. Emi-Reynolds, G., Faanu, A., Darko, E. O., Awudu, A. R., Adukpo, O., Ibrahim, A. (2011). Natural radioactivity concentrations

and dose assessment in shore sediments along the coast of Greater Accra, Ghana. *World Applied Sciences Journal*, 13(11), 2338-2343.

Amin, R. M. (2015). A study of radon emitted from building materials using solid state nuclear track detectors. *Journal of Radiation Research and Applied Sciences*, 8(4), 516-522.

Ansre, C. Y., Miyittah, M. K., Andam, A. B., & Dodor, D. E. (2018). Risk assessment of radon in the South Dayi District of the Volta Region, Ghana. *Journal of radiation research and applied sciences*, 11(1), 10-17.

Baskaran, M. (2016). *Radon: A tracer for geological, geophysical and geochemical studies* (Vol. 367). Basel: Springer.

Bekelesi, W. C., Darko, E. O., & Andam, A. B. (2017). Activity concentrations and dose assessment of ^{226}Ra , ^{228}Ra , ^{232}Th , ^{40}K , ^{222}Rn and ^{220}Rn in soil samples from Newmont-Akyem gold mine using gamma-ray spectrometry. *African Journal of Environmental Science and Technology*, 11(5), 237-247.

Blanco-Novoa, O., Fernández-Caramés, T. M., Fraga-Lamas, P., & Castedo, L. (2018). A cost-effective IoT system for monitoring indoor radon gas concentration. *Sensors*, 18(7), 2198.

Bui, V. L., Leuangtakoun, S., Bui, T. H., Vu, T. K. D., Le, T. N., Duong, T. D., ... & Tran, H. N. (2020). Natural radioactivity and radiological hazards in soil samples in Savannakhet province, Laos. *Journal of Radioanalytical and Nuclear Chemistry*, 323(1), 303-315.

- Cetnar, J., Stanisz, P., & Oettingen, M. (2021). Linear Chain Method for Numerical Modelling of Burnup Systems. *Energies* 2021, 14, 1520.
- Cheng, E. S., Egger, S., Hughes, S., Weber, M., Steinberg, J., Rahman, B., ... & Yu, X. Q. (2021). Systematic review and meta-analysis of residential radon and lung cancer in never-smokers. *European Respiratory Review*, 30(159).
- Chowdhury, M. I., Kamal, M., Alam, M. N., Aftabuddin, S., & Zafar, M. (2004). Environmental radioactivity of the St. Martin's Island of Bangladesh. *Radioprotection*, 39(1), 13-21.
- Corrales, L., Rosell, R., Cardona, A. F., Martin, C., Zatarain-Barrón, Z. L., & Arrieta, O. (2020). Lung cancer in never smokers: The role of different risk factors other than tobacco smoking. *Critical reviews in oncology/hematology*, 148, 102895.
- Darby, S., Hill, D., Auvinen, A., Barros-Dios, J. M., Baysson, H., & Bochicchio, F. & Heid, I. (2005). Radon in homes and risk of lung cancer: collaborative analysis of individual data from 13 European case-control studies. *Bmj*, 330(7485), 223.
- Darko, E. O., Tetteh, G. K., & Akaho, E. H. K. (2005). Occupational radiation exposure to norms in a gold mine. *Radiation Protection Dosimetry*, 114(4), 538-545.
- Day, P. R. (1965). Particle fractionation and particle-size analysis. *Methods of Soil Analysis: Part 1 Physical and Mineralogical Properties, Including Statistics of Measurement and Sampling*, 9, 545-567.

- Degu Belete, G., & Alemu Anteneh, Y. (2021). General Overview of Radon Studies in Health Hazard Perspectives. *Journal of Oncology*, 2021.
- Devi, V. & Chauhan, R. P. (2020). Estimation of natural radionuclide and exhalation rates of environmental radioactive pollutants from the soil of northern India. *Nuclear Engineering and Technology*, 52(6), 1289-1296.
- Dickson, K. B., & Benneh, G. (1988). *A geography of Ghana*. London: Longman.
- Dieu Souffit, G., Bobbo Modibo, O., Lepoire, D., & Tokonami, S. (2022). Risk Assessment of Exposure to Natural Radiation in Soil Using RESRAD-ONSITE and RESRAD-BIOTA in the Cobalt-Nickel Bearing Areas of Lomié in Eastern Cameroon. *Radiation*, 2(2), 177-192.
- Dina, N. T., Das, S. C., Kabir, M. Z., Rasul, M., Deebea, F., Rajib, M., ... & Ali, M. (2022). Natural radioactivity and its radiological implications from soils and rocks in Jaintiapur area, North-east Bangladesh. *Journal of Radioanalytical and Nuclear Chemistry*, 1-12.
- Duppen, P. V. & Andreyev, A. N. (2018). Alpha decay and beta-delayed fission: Tools for nuclear physics studies. In *The Euroschool on Exotic Beams-Vol. 5* (pp. 65-116). Springer, Cham.
- Durrani, S.A. & Ilic, R., (1997). Radon Measurements by Etch Track Detectors. World Scientific Publishing, Singapore.
- European commission. (1999). Radiological protection principles concerning the natural radioactivity of building materials, Radiation Protection 112.

Directorate General Environment, Nuclear Safety and Civil Protection,
EC, Geneva.

Elsaman, R., Omer, M. A. A., Seleem, E. M. M., & El-Taher, A. (2018). Natural radioactivity levels and radiological hazards in soil samples around Abu Karqas Sugar Factory. *Journal of Environmental Science and Technology*, *11*(1), 28-38.

El-Shanshoury, G. I., & Arafat, A. A. (2018). Statistical Analysis of Natural Radioactivity Measurements for the Soil of Marsa Alam-Shalateen Red-Sea Coast Area, Egypt. *International Journal of Advanced Scientific and Technical Research*, *1*(8), 71-85.

EPA. (2003). Environmental Protection Agency assessment of risks from radon in homes. U. S., Washington, 402-R-03-003.

Esan, D. T., Sridhar, M. K. C., Obed, R., Ajiboye, Y., Afolabi, O., Olubodun, B., & Oni, O. M. (2020). Determination of residential soil gas radon risk indices over the lithological units of a Southwestern Nigeria University. *Scientific Reports*, *10*(1), 1-10.

Faanu, A., Adukpo, O. K., Tettey-Larbi, L., Lawlivi, H., Kpeglo, D. O., Darko, E. O., ... & Agyeman, L. (2016). Natural radioactivity levels in soils, rocks and water at a mining concession of Perseus gold mine and surrounding towns in Central Region of Ghana. *SpringerPlus*, *5*(1), 1-16.

Faanu, A., Awudu, A. R., Darko, E. O., Emi-Reynolds, G., Inkoom, S., Adukpo, O., ... & Glover, E. T. (2010). Artificial and natural radioactivity

measurements in the vicinity of Ghana nuclear research reactor (GHARR-1).

Faanu, A., Darko, E. O., & Ephraim, J. H. (2011). Determination of natural radioactivity and hazard in soil and rock samples in a mining area in Ghana. *West African Journal of Applied Ecology*, 19(1).

Gilmore, G. (2008). *Practical gamma-ray spectroscopy*. John Wiley & Sons.

Gogna, P., Narain, T. A., O'Sullivan, D. E., Villeneuve, P. J., Demers, P. A., Hystad, P., ComPARE Study Team. (2019). Estimates of the current and future burden of lung cancer attributable to residential radon exposure in Canada. *Preventive Medicine*, 122, 100-108.

Gulan, L., Stajic, J. M., Spasic, D., & Forkapic, S. (2022). Radon levels and indoor air quality after application of thermal retrofit measures—a case study. *Air Quality, Atmosphere & Health*, 1-11.

Hendry, J. H., Simon, S. L., Wojcik, A., Sohrabi, M., Burkart, W., Cardis, E., ... & Hayata, I. (2009). Human exposure to high natural background radiation: what can it teach us about radiation risks? *Journal of Radiological Protection*, 29(2A), A29.

Hussein, Z. A., Jaafar, M. S., & Ismail, A. H. (2013). Measurement of radium content and radon exhalation rates in building material samples using passive and active detecting techniques. *International Journal of Scientific and Engineering Research*, 4(9), 1827-1831.

International Atomic Energy Agency (2003). Collection and preparation of bottom sediment samples for analysis of radionuclides and trace elements. IAEA-TECDOC-1360.

International Atomic Energy Agency (2010). Radiation Biology: A Handbook for Teachers and Students, Vienna: Vienna International Centre, 2010.

International Atomic Energy Agency (2011). Radioactive particles in the environment: sources, particle characterization and analytical techniques Vienna, IAEA-TECDOC-1663.

International Commission on Radiological Protection (1993). Radon-222 at Home and Work ICRP Publication 65, vol. 23.

International Commission on Radiological Protection (2007) 2006 recommendations of the International Commission on Radiological Protection. ICRP publication no.103, Pergamon Press, Oxford.

International Commission on Radiological Protection (1991). *ICRP publication 60: 1990 recommendations of the International Commission on Radiological Protection* (No. 60). Elsevier Health Sciences.

Ishimori, Y., Lange, K., Martin, P., Mayya, Y. S., & Phaneuf, M. (2013). *Measurement and calculation of radon releases from NORM residues*. Iaea.

Jasaitis, D. & Pečiulienė, M. (2021). Natural Radioactivity and Radon Exhalation from Building Materials in Underground Parking Lots. *Applied Sciences*, 11(16), 7475.

Jibiri, N. N. & Bankole, O. S. (2006). Soil radioactivity and radiation absorbed dose rates at roadsides in high-traffic density areas in Ibadan metropolis, southwestern Nigeria. *Radiation protection dosimetry*, 118(4), 453-458.

Kadiri, S., Dizman, S., Yeşilkanat, C. M., Aliu, H., & Hodolli, G. (2022). Radioactivity in Soils of Kosovo and Radiological Implications. *Applied Sciences*, 12(19), 9520.

Kamalakar V. D., Vinutha P. R., Kaliprasa C. S., & Yerol, N. (2022). Radiation level, radionuclide distribution and mineralogy of soils in Belagavi region of Karnataka, India. *International Journal of Environmental Analytical Chemistry*, 1-18.

Kavasara, M., Vinutha, P. R., Kaliprasad, C. S., & Narayana, Y. (2021). Studies on the dependence of natural radioactivity on clay minerals of soils in Davanagere district of Karnataka, India. *Journal of Radioanalytical and Nuclear Chemistry*, 330(3), 1461-1471.

Khalil, Y. T., & Al-Jubbori, M. A. (2020). Track parameters investigate of oblique incident of alpha particles irradiated CR-39 detector. In *IOP Conference Series: Materials Science and Engineering* (Vol. 928, No. 7, p. 072132). IOP Publishing.

Khan, I. U., Sun, W., & Lewis, E. (2020). Estimation of various radiological parameters associated with radioactive contents emanating with fly ash from Sahiwal coal-fueled power plant, Pakistan. *Environmental Monitoring and Assessment*, 192(11), 1-11.

Khan, S. M., Gomes, J., & Krewski, D. R. (2019). Radon interventions around the globe: A systematic review. *Heliyon*, 5(5), e01737.

Khan, S. M., Pearson, D. D., Rönnqvist, T., Nielsen, M. E., Taron, J. M., & Goodarzi, A. A. (2021). Rising Canadian and falling Swedish radon gas exposure as a consequence of 20th to 21st century residential build practices. *Scientific Reports*, *11*(1), 1-15.

Kim, S. H., Hwang, W. J., Cho, J. S., & Kang, D. R. (2016). Attributable risk of lung cancer deaths due to indoor radon exposure. *Annals of occupational and environmental medicine*, *28*(1), 8.

Kitson-Mills, D., Sovoe, S., Opoku-Ntim, I., Kyei, K. A., Marnotey, S., Anim-Sampong, S., ... & Baiden, F. (2019). An assessment of indoor radon level in a suburb of Ghana. *Environmental Research Communications*, *1*(6), 061002.

Knoll, G. F. (2010). *Radiation detection and measurement*. John Wiley & Sons.

Kpordzro, R. (2018). Assessment of Factors Affecting Indoor Radon -222 Concentration in Dome and its Environs - Greater Accra Region of Ghana (MPhil. Thesis, University of Ghana, Legon Accra).

Kpordzro, R., Gbadago, J. K., Andam, A. B., Adukpo, O. K., Otoo, F., Opoku-Ntim, I., ... & Amoatey, E. (2022). Assessment of Seasonal Radon Concentration in Dwellings and Soils in Selected Areas in Ga East, Greater Accra Region of Ghana. *Journal of Environmental and Public Health*, 2022.

Krebs, R. E. (2006). *The history and use of our earth's chemical elements: a reference guide*. Greenwood Publishing Group.

Kumar, A., Varadarajan, C., & Kadiyala, A. (2011). Management of radon data in the state of Ohio, USA. *The Open Environmental & Biological Monitoring Journal*, 4, 57-71.

L'Annunziata, M. F. (2020). The atomic nucleus, nuclear radiation, and the interaction of radiation with matter. In *Handbook of Radioactivity Analysis* (pp. 1-243). Academic Press.

Langanke, K., Martínez-Pinedo, G., & Zegers, R. G. T. (2021). Electron capture in stars. *Reports on Progress in Physics*, 84(6), 066301.

Le, V. S., Do, Z. P. H., Le, M. K., Le, V., & Le, N. N. T. (2014). Methods of increasing the performance of radionuclide generators used in nuclear medicine: daughter nuclide build-up optimisation, elution-purification-concentration integration, and effective control of radionuclidic purity. *Molecules*, 19(6), 7714-7756.

Lewis, R., Bleiler, D., Coons, M., Ruminski, J., DEP, R. F. P., & Turk, B. (2021). Radon Re-entrainment Study—An Initial Investigation.

Lokesh, N., Vinutha, P. R., Kamalakar, V. D., & Yerol, N. (2022). Assessment of natural radioactivity and its dependence on clay minerals of the soil of Dakshina Kannada district, South India. *International Journal Of Environmental Analytical Chemistry*.

Lorenzo-González, M., Ruano-Ravina, A., Torres-Durán, M., Kelsey, K. T., Provencio, M., Parente-Lamelas, I., ... & Barros-Dios, J. M. (2019). Lung cancer and residential radon in never-smokers: A pooling study in the Northwest of Spain. *Environmental research*, 172, 713-718.

Mishra, P., Rawat, R. B. S., Sharma, V. K., & Saxena, A. (2014). Concentration of Radon and its Progeny levels in air in the Dwelling of Moradabad of western UP. *India. (IJSR)*, 5(2).

Mostafa, A. M. A., Yamazawa, H., Uosif, M. A. M., & Moriizumi, J. (2015). Seasonal behavior of radon decay products in indoor air and resulting radiation dose to human respiratory tract. *Journal of Radiation Research and Applied Sciences*, 8(1), 142-147. Namibia-Windhoek, Namibia.

Muñoz, E., Frutos, B., Olaya, M., & Sánchez, J. (2017). A finite element model development for simulation of the impact of slab thickness, joints, and membranes on indoor radon concentration. *Journal of Environmental Radioactivity*, 177, 280-289.

Nguelem, E. J. M., Ndontchueng, M. M, & Motapon, O. (2016). Determination of ^{226}Ra , ^{232}Th , ^{40}K , ^{235}U and ^{238}U activity concentration and public dose assessment in soil samples from bauxite core deposits in Western Cameroon. *SpringerPlus*, 5(1), 1-12.

Nisti, M. B., Saueia, C. R., Malheiro, L. H., Groppo, G. H., & Mazzilli, B. P. (2015). Lixiviation of natural radionuclides and heavy metals in tropical soils amended with phosphogypsum. *Journal of Environmental Radioactivity*, 144, 120-126.

Nsiah-Akoto, I., Andam, A. B., Akiti, T. T., & Fletcher, J. J. (2019). Study of radium and radon exhalation rate in soil samples, Offinso municipality. In *AIP Conference Proceedings* (Vol. 2109, No. 1, p. 100003). AIP Publishing LLC.

Organization for Economic Cooperation and Development (1979). Exposure to radiation from the natural radioactivity in building materials. Report by a group of experts of the OECD, Nuclear Energy Agency, Paris, France.

Ojovan, M. I., Lee, W. E., & Kalmykov, S. N. (2019). *An introduction to nuclear waste immobilisation*. Elsevier.

Olszewski, G., Boryło, A., & Skwarzec, B. (2016). The radiological impact of phosphogypsum stockpile in Wiślinka (northern Poland) on the Martwa Wisła river water. *Journal of Radioanalytical and Nuclear Chemistry*, 307(1), 653-660.

Opoku-Ntim, I., Andam, A. B., Roca, V., Fletcher, J. J., & Akiti, T. T. (2020). Indoor radon concentration and risk assessment in some dwellings of Obuasi, mining town. *Radiation Protection Dosimetry*, 188(1), 30-37.

Osman, R., Dawood, Y. H., Melegy, A., El-Bady, M. S., Saleh, A., & Gad, A. (2022). Distributions and risk assessment of the natural radionuclides in the soil of Shoubra El Kheima, South Nile Delta, Egypt. *Atmosphere*, 13(1), 98.

Otoo F, Darko E.O., Emi-Reynolds G, Andam A.B. and Adukpo O.K. (2013). Radiological impact of soil as a source of Building material. *Radiat. Prot. Environ.* 35: 22-28.

Otoo, F., Arhin, I., & Darko, E. O. (2020). Studies of Radon Levels, Radium Concentration, and Estimated Effective Dose in Dwellings and Soils in Gold Mining Towns in Abirem of Eastern Region of Ghana. *Radiation Protection Dosimetry*, 191(3), 296-309.

Otoo, F., Darko, E. O., & Garavaglia, M. (2022). Correlation Analysis of Natural Radionuclides, Radon Exposure, Soil Particles, and Moisture from Quarry Towns in Greater Accra Region, Ghana. *Water, Air, & Soil Pollution*, 233(8), 1-16.

Otoo, F., Darko, E. O., Garavaglia, M., Adukpo, O. K., Amoako, J. K., Tandoh, J. B., ... & Adu, S. (2021). Assessment of natural radioactivity and radon exhalation rate associated with rock properties used for construction in greater Accra region, Ghana. *Journal of Radioanalytical and Nuclear Chemistry*, 328(3), 911-923.

Otoo, F., Darko, E. O., Garavaglia, M., Giovani, C., Pividore, S., Andam, A. B., J. K. Amoako, O. K. Adukpo, S. Inkoom & Adu, S. (2018). Public exposure to natural radioactivity and radon exhalation rate in construction materials used within Greater Accra Region of Ghana. *Scientific African*, 1, e00009.

Pacheco-Torgal, F. (2012). Indoor radon: an overview on a perennial problem. *Building and environment*, 58, 270-277.

Park, J. H., Lee, C. M., Lee, H. Y., & Kang, D. R. (2018). Estimation of seasonal correction factors for indoor radon concentrations in Korea. *International Journal of Environmental Research and Public Health*, 15(10).

Pinel, J., Fearn, T., Darby, S. C., & Miles, J. C. H. (1995). Seasonal correction factors for indoor radon measurements in the United Kingdom. *Radiation Protection Dosimetry*, 58(2), 127-132.

- Pyngrope, A., Saxena, A., Khardewsaw, A., Sharma, Y., & Sahoo, B. K. (2022). Effect of soil's porosity and moisture content on radon and thoron exhalation rates. *Journal of Radioanalytical and Nuclear Chemistry*, 331(4), 1975-1984.
- Rybalkin, A. (2012). *Numerical and analytical assessment of radon diffusion in various media and potential of charcoal as radon detector*. The University of Utah.
- Sabbarese, C., Ambrosino, F., & Roca, V. (2020). Analysis by scanner of tracks produced by radon alpha particles in CR-39 detectors. *Radiation Protection Dosimetry*, 191(2), 154-159.
- Sahu, P., Panigrahi, D. C., & Mishra, D. P. (2014). Sources of radon and its measurement techniques in underground uranium mines—an overview. *Journal of Sustainable Mining*, 13(3), 11-18.
- Sarki, S. H., Musa, G. P., Kassimu, A. A., Daniel, I. H., & Kure, N. (2020). Determination of activity concentration level of ²²⁶Ra, ⁴⁰K and ²³²Th in soil within Igabi Local Government Area of Kaduna State, Nigeria. *Science World Journal*, 15(1), 113-118.
- Sathyapriya, R., Nair, S., Kamesh, V., Prabhath, R., Nair, M., Acharya, R., & Rao, D. (2012). Estimation of thorium intake due to consumption of vegetables by inhabitants of high background radiation area by INAA. *Journal of Radioanalytical and Nuclear Chemistry*, 294(3), 387-390.
- Senitkova, I. & Kraus, M. (2019). Seasonal and Floor Variations of Indoor Radon Concentration. In *IOP Conference Series: Earth and Environmental Science* (Vol. 221, No. 1, p. 012127).

Soil Survey Staff. (1999). *Soil taxonomy: A basic system of soil classification for making and interpreting soil surveys*. USDA, Natural Resources Conservation Service.

Taapopi, E. E., Faanu, A., & Dampare, S. B. (2017). Assessment of background radiation in playgrounds of selected basic schools in the GA east municipal district, Accra, Ghana.

Theunis, J. V. R. (2017). Radiation Protection and Health Physics.

Thumvijit, T., Chanyotha, S., Sriburee, S., Hongriti, P., Tapanya, M., Kranrod, C., & Tokonami, S. (2020). Identifying indoor radon sources in pa Miang, Chiang Mai, Thailand. *Scientific reports*, 10(1), 1-14.

Tokonami, S. (2020). Characteristics of thoron (^{220}Rn) and its progeny in the indoor environment. *International Journal of Environmental Research and Public Health*, 17(23), 8769.

UNSCEAR (1993). *Sources and effects of ionizing radiation, united nations scientific committee on the effects of atomic radiation (UNSCEAR) 1993 report: report to the general assembly, with scientific annexes*. United Nations.

UNSCEAR (2000). Report of the United Nations Scientific Committee on the Effects of Atomic Radiation to the General Assembly.

UNSCEAR (2008). Exposures of the public and workers from various sources of radiation. *United Nations Scientific Committee on the effects of atomic radiation, Report to the general assembly, Annex B*.

UNSCEAR (2010). United Nations Scientific Committee on the Effects of Atomic Radiation. Sources and Effects of Ionizing Radiation. New York: United Nations; 20 p.

UNSCEAR (2017). *Sources, Effects and Risks of Ionizing Radiation, United Nations Scientific Committee on the Effects of Atomic Radiation (UNSCEAR) 2016 Report: Report to the General Assembly, with Scientific Annexes*. United Nations.

UNSCEAR. (2014). United Nations Scientific Committee on the Effects of Atomic Radiation Sources and Effects of Ionizing Radiation. Report to Assembly with Scientific Annexes. UNSCEAR, New York.

Uosif, M. A. M., Issa, S. A., & Abd El-Salam, L. M. (2015). Measurement of natural radioactivity in granites and its quartz-bearing gold at El-Fawakhir area (Central Eastern Desert), Egypt. *Journal of Radiation Research and Applied Sciences*, 8(3), 393-398.

Usikalu, M. R., Enemuwe, C. A., Morakinyo, R. O., Orosun, M. M., Adagunodo, T. A., & Achuka, J. A. (2020). Background Radiation from ²³⁸U, ²³²Th, and ⁴⁰K in Bells Area and Canaan City, Ota, Nigeria. *Open Access Macedonian Journal of Medical Sciences*, 8(E), 678-684.

Van Wijngaarden, M., Venema, L. B., De Meijer, R. J., Zwolsman, J. J. G., Van Os, B., & Gieske, J. M. J. (2002). Radiometric sand–mud characterisation in the Rhine–Meuse estuary: Part A. Fingerprinting. *Geomorphology*, 43(1-2), 87-101.

- Vasilyev, A. V. & Zhukovsky, M. V. (2013). Determination of mechanisms and parameters which affect radon entry into a room. *Journal of environmental radioactivity*, 124, 185-190.
- Wasikiewicz, J. M., Daraktchieva, Z., & Howarth, C. B. (2019). Passive etched track detectors application in outdoor radon monitoring. *Perspectives in Science*, 12, 100416.
- World Health Organization. (2009). *WHO handbook on indoor radon: a public health perspective*. World Health Organization.
- World Health Organization. (2010). *WHO guidelines for indoor air quality: selected pollutants*. World Health Organization. Regional Office for Europe.
- Yachiso, G., Chaubey, A. K., & Turi, B. (2022). Measurements of Natural Radioactivity Levels in Soil Samples and Hazards in Lega Dembi Gold Mining, East Guji, Oromia, Ethiopia.
- Yang, J. & Sun, Y. (2022). Natural radioactivity and dose assessment in surface soil from Guangdong, a high background radiation province in China. *Journal of Radiation Research and Applied Sciences*, 15(1), 145-151.
- Yang, S. Pernot, J. G., Jörin, C. H., Niculita-Hirzel, H., Perret, V., & Licina, D. (2020). Energy, indoor air quality, occupant behavior, self-reported symptoms and satisfaction in energy-efficient dwellings in Switzerland. *Building and Environment*, 171, 106618.
- Yarahmadi, M., Shahsavani, A., Mahmoudian, M. H., Shamsedini, N., Rastkari, N., & Kermani, M. (2016). Estimation of the residential radon levels and

the annual effective dose in dwellings of Shiraz, Iran, in 2015.

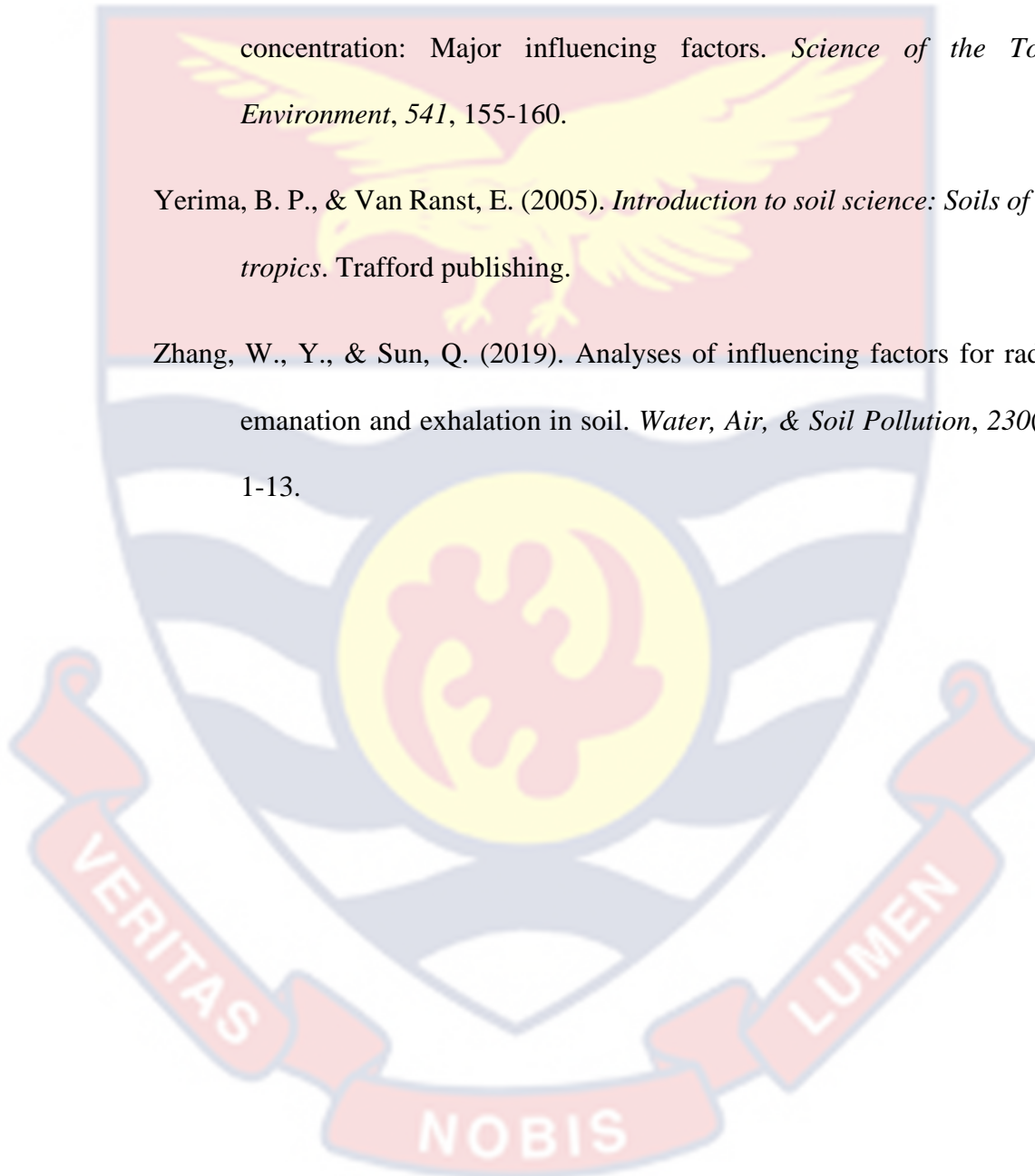
Electronic physician, 8(6), 2497.

Yarmoshenko, I., Vasilyev, A., Malinovsky, G., Bossew, P., Žunić, Z. S.,

Onischenko, A., & Zhukovsky, M. (2016). Variance of indoor radon concentration: Major influencing factors. *Science of the Total Environment*, 541, 155-160.

Yerima, B. P., & Van Ranst, E. (2005). *Introduction to soil science: Soils of the tropics*. Trafford publishing.

Zhang, W., Y., & Sun, Q. (2019). Analyses of influencing factors for radon emanation and exhalation in soil. *Water, Air, & Soil Pollution*, 230(1), 1-13.



APPENDICES

Appendix A: TABLE OF RADIONUCLIDES LEVELS AND RADON

EXHALATION RATES IN SOIL OF TORKOR

SC	²²⁶ Ra			Rn Exhalation rates $\times 10^{-5}$			²³² Th			⁴⁰ K		
	Ra ₁	Ra ₂	Ra ₃	Rnex ₁	Rnex ₂	Rnex ₃	Th ₁	Th ₂	Th ₃	K ₁	K ₂	K ₃
SL1	6.5	7	6.7	3.1	3.3	3	11.6	10.9	11.5	87	90.1	83.5
SL2	14.2	15	15.6	7.2	7.1	6.9	21.6	22.1	20.9	110.4	111.3	110.5
SL3	11.4	11.5	10.2	4.6	4.8	5.1	22.4	21.9	22.6	170.9	171.3	167.9
SL4	9.6	10.1	8.9	3.5	4.1	3.4	29.3	29	28.9	220.4	219.9	221.1
SL5	29.8	30.4	31.9	8.7	9.3	8.3	26.3	26.1	26.5	130.6	132.1	130.7
SL6	35.3	35	36.1	9.3	9.6	8.9	28.9	28.3	28.4	240.5	240.5	242.6
SL7	47.3	46.7	45.2	12.9	13.1	12.7	56.8	56.1	56.5	419.8	421.6	420.3
SL8	48.2	47.8	50.5	12.7	12.1	12.4	46.8	46.3	46	310.5	312.5	311.6
SL9	39.5	39.4	40.1	11.1	10.5	11.4	26.7	26.2	27.3	300.4	301.2	299.4
SL10	32.6	32.2	33.2	11.3	11.9	10.9	49	48.7	48.2	396.8	400.3	398.6
SL11	42	41.6	41.9	11.1	11.3	11.7	52.5	51.8	53.1	360.2	363.7	365.3
SL12	29.6	29.4	29.1	9.1	9.3	8.7	22.6	22.2	22.7	200.4	204.1	198.9
SL13	45.2	45	46.2	13.1	13	12.6	49.6	50.2	49.9	352.8	355.3	360.2
SL14	24.8	24.5	25.3	8.7	8.8	8.2	24.8	25.1	24.5	230.4	231.2	226.7
SL15	8.6	8.7	9.1	5.4	5.1	4.9	23.6	22	23.9	220.8	222.3	218.9
SL16	22.6	22.9	23.3	11.4	11.2	12.1	24.6	23.6	25	229.5	231.1	234.6
SL17	16.7	16.8	17.1	6	6.1	5.9	11.8	11.4	11.5	99.8	100.5	111.5

**Appendix B: TABLE OF RADIONUCLIDES LEVELS AND RADON
EXHALATION RATES IN SOIL OF AGBENOXOE**

SC	²²⁶ Ra			²²² Rn exhalation rates × 10 ⁻⁵			²³² Th			²³² K		
	Ra ₁	Ra ₂	Ra ₃	Rnex ₁	Rnex ₂	Rnex ₃	Th ₁	Th ₂	Th ₃	K ₁	K ₂	K ₃
SL1	19	18.1	18.9	7.4	7	6.9	17.5	17	18.1	99.6	101.1	98.2
SL2	3.6	3.1	4.1	1.4	1.1	1.8	4.6	4.2	4.6	69.8	65.8	70.5
SL3	38.1	38.9	37.3	10.3	11.2	10	48.2	47.9	45.8	300.5	311.2	301
SL4	6.3	6.9	7.1	3.8	4.3	3.3	13.8	13.1	12.9	145	140.5	143.2
SL5	4.6	5.1	4.2	3.2	3	2.9	10.8	9.8	10.1	134.9	137.1	130.2
SL6	53.3	50.3	52.7	13.9	14.2	13.2	49.8	50.2	48.2	360.7	366.1	357.9
SL7	46.1	44.8	47.1	12.6	13.1	12.9	34.7	34.1	33.9	320.8	331.3	319.2
SL8	51.4	50.1	52.5	14.8	14	15	48.9	49.4	47.4	350.7	348.9	371.3
SL9	20.1	19.8	22.1	8.1	8.7	8	19.9	20.3	18.9	280.8	288.2	278.1
SL10	19.3	19.9	21.1	9.2	9.4	8.9	14.7	15.3	16.1	188.9	191.2	179.9
SL11	46.9	45.1	46.3	13.1	12.9	11.7	48.8	46.2	47.9	242.8	244.2	240.2
SL12	37	38.3	37.4	10.5	11.1	10.4	52.6	50.3	51.8	355.7	361.2	349.5
SL13	24.9	25.8	24.2	10.8	9.8	9.5	25.6	24.7	26.1	245.8	251.2	240.1
SL14	37.4	38.1	37	8.1	8.6	9	38.8	39.1	38.3	298.7	300.1	291.2
SL15	21.7	20.1	22.1	8.5	8	8.1	8.9	9.3	10.3	112.9	121.1	110.7
SL16	8.4	8.8	8.1	4.8	5.1	4.5	20.8	21.4	20.1	156.9	162.4	148.3
SL17	32.8	32.2	30.8	9.4	10	8.9	36.8	37.2	36.1	280.9	286.1	279.8

**Appendix C: TABLE OF RADIONUCLIDES LEVELS AND ²²²Rn
EXHALATION RATES IN SOIL OF TSAKPA**

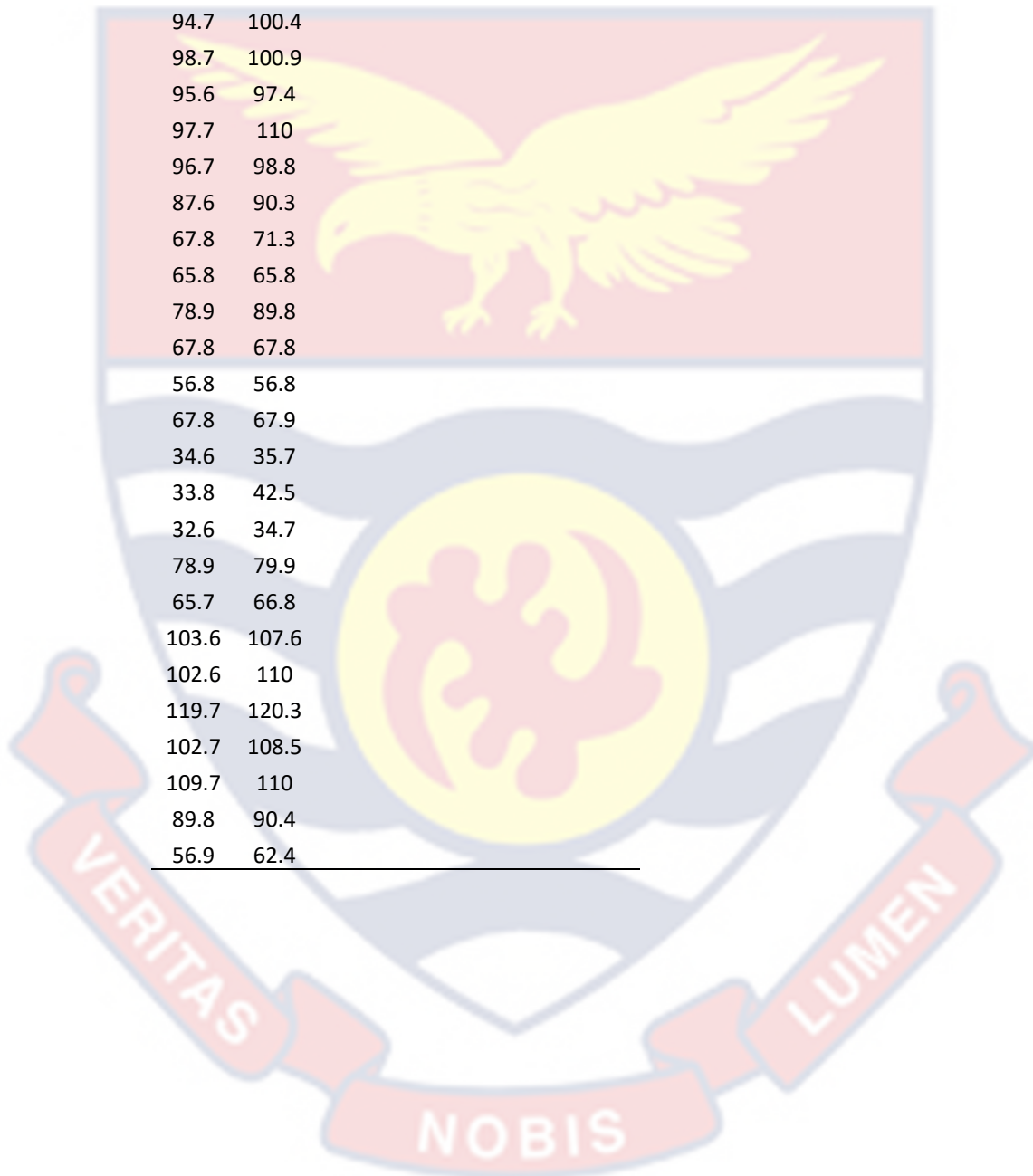
SC	²²⁶ Ra			²²² Rn exhalation rates × 10 ⁻⁵			²³² Th			⁴⁰ K		
	Ra ₁	Ra ₂	Ra ₃	Rnex ₁	Rnex ₂	Rnex ₃	Th ₁	Th ₂	Th ₃	K ₁	K ₂	K ₃
SL1	3.4	3.8	2.9	1.3	1.6	1.1	4.8	6.2	3.4	67.4	62.7	72.1
SL2	3.1	2.8	3.3	1.1	1.3	1	4.6	3.7	5.5	87.4	90.3	84.6
SL3	11.1	12.1	10.2	4.1	5.1	3.1	15.8	17.5	14.1	102.5	114.1	91.1
SL4	7.8	8.2	7.6	3.3	2.8	3.8	9.4	11.1	7.7	90.5	82.7	98.7
SL5	24.6	25.3	23.6	8.8	7.5	10.1	54.6	57.9	51.3	399.5	402.1	397.1
SL6	17.2	16.3	18.1	7.8	8.8	6.9	24.7	22.8	26.6	300.5	289.9	311.2
SL7	22.9	20.1	25.1	8.6	9.4	7.8	39.7	35.8	43.6	240.4	225.9	255.1
SL8	15.6	17.2	14.1	9.5	11.1	8.1	54.6	50.4	58.8	399.6	400.9	398.4
SL9	11.9	12.9	10.1	6.3	5.5	7.1	21.6	19.8	23.4	298.9	287.8	309.9
SL10	14.1	12.6	16.7	6.8	8.1	5.5	36.8	40.1	33.5	340.5	319.9	361.6
SL11	18.9	20.2	16.8	7.4	8.5	6.3	25.7	21.3	30.1	300.4	289.1	312.2
SL12	17.3	16.8	18.1	8.7	7.7	9.7	25.4	21.9	28.9	256.8	238.9	274.8
SL13	19.4	17.9	20.8	8.9	10.1	7.7	28.9	25.9	31.9	299.6	311.4	287.9
SL14	22.3	24.4	20.2	10.5	8.9	12.1	24.6	20.6	28.6	230.6	240.4	220.9
SL15	15.8	13.8	17.9	7.9	9	6.8	18.8	16.5	21.1	189.7	198.9	179.9
SL16	38.6	36.8	40.1	10.9	12.4	9.4	51.3	48.2	54.4	389.7	400	379.4
SL17	6.7	7.5	5.9	4	5.3	3.1	15.8	11.8	19.8	120.9	104.8	136.9

Appendix D: TABLE OF INDOOR RADON CONCENTRATION (Bq/m³)

Torkor		Agbenoxoe		Tsakpa	
Dry	Rainy	Dry	Rainy	Dry	Rainy
24.5	26.5	28.6	24.5	24.2	24.6
36.0	37.5	23.5	24.5	39.3	45.4
28.1	31.7	31.1	32.3	23.7	25.6
26.1	26.2	24.5	32.5	25.5	56.3
34.5	63.4	34.0	45.2	31.7	45.6
33.9	54.5	104.8	114.7	45.7	48.8
107.8	110.6	108.6	110.5	52.6	53.7
120.5	120.9	41.8	41.9	40.8	41.8
115.8	115.9	72.8	72.8	55.8	58.9
51.8	52.0	56.8	56.9	55.8	55.9
110.7	111.8	124.7	124.9	24.9	25.7
78.4	78.6	89.7	90.9	75.6	75.7
101.6	102.8	67.9	68.0	79.6	79.8
57.9	57.9	117.6	117.9	70.9	72.6
79.8	79.9	91.7	92.8	59.5	60.1
54.8	55.8	55.5	56.5	110.8	110.9
54.2	54.9	67.0	67.9	73.7	74.9
54.2	63.4	88.9	93.8	34.7	36.3
35.6	35.7	99.7	100.4	26.7	29.7
55.6	63.0	92.3	98.4	33.7	36.0
67.5	71.3	94.7	100.4	34.7	42.0
78.9	79.0	98.7	100.9	25.7	27.9
100.9	110.0	95.6	97.4	45.9	54.0
24.6	25.3	97.7	110.0	46.8	53.6
110.7	119.4	96.7	98.8	47.6	53.6
89.4	92.8	87.6	90.3	45.8	48.9
89.5	93.0	67.8	71.3	46.8	49.4
34.3	43.4	65.8	65.8	34.8	37.5
56.5	59.3	78.9	78.8	26.8	29.5
34.8	36.3	67.8	67.8	25.8	27.6
35.7	38.8	56.8	56.8	34.7	36.5
102.5	110.0	67.8	67.9	26.9	32.4
65.7	66.8	56.9	57.8	24.5	26.6
103.6	107.6	76.9	78.9	25.6	27.8
102.6	110.0	28.9	31.4	24.7	28.6
119.7	120.3	58.6	58.7	26.5	32.5
102.7	108.5	34.6	35.7	24.6	24.7
109.7	110.0	33.8	42.5	25.6	27.4
89.8	90.4	32.6	34.7	24.8	25.7
56.9	62.4	78.9	79.9	24.7	26.4

Bedroom		Kitchen		Sitting Room	
Dry	Rainy	Dry	Rainy	Dry	Rainy
110.7	111.8	72.8	72.8	24.5	26.5
124.7	124.9	55.80	55.9	24.20	24.6
89.7	90.9	51.80	52	39.30	45.4
78.4	78.6	56.80	56.9	28.60	24.5
75.6	75.7	24.90	25.7	36.00	37.5
101.6	102.8	25.70	27.9	23.50	24.5
67.9	68	45.90	54	23.70	25.6
79.6	79.8	46.80	53.6	28.10	31.7
70.9	72.6	47.60	53.6	26.10	26.2
57.9	57.9	45.80	48.9	31.10	32.3
59.5	60.1	46.80	49.4	25.50	56.3
117.6	117.9	34.80	37.5	34.50	63.4
79.8	79.9	26.80	29.5	33.90	54.5
91.7	92.8	25.80	27.6	31.70	45.6
110.8	110.9	34.70	36.5	24.50	32.5
73.7	74.9			34.00	45.2
107.8	110.6			26.90	32.4
45.7	48.8			24.50	26.6
104.8	114.7			25.6	27.8
108.6	110.5			24.7	28.6
41.8	41.9			26.5	32.5
120.5	120.9			24.6	24.7
52.6	53.7			25.6	27.4
40.8	41.8			24.8	25.7
55.8	58.9			24.7	26.4
115.8	115.9			88.9	93.8
55.5	56.5			56.9	57.8
54.8	55.8			76.9	78.9
67	67.9			28.9	31.4
54.2	54.9			58.6	58.7
54.2	63.4				
35.6	35.7				
55.6	63				
67.5	71.3				
78.9	79				
100.9	110				
24.6	25.3				
110.7	119.4				
89.4	92.8				
89.5	93				
34.3	43.4				
56.5	59.3				
34.8	36.3				
35.7	38.8				

102.5	110
34.7	36.3
26.7	29.7
33.7	36
34.7	42
99.7	100.4
92.3	98.4
94.7	100.4
98.7	100.9
95.6	97.4
97.7	110
96.7	98.8
87.6	90.3
67.8	71.3
65.8	65.8
78.9	89.8
67.8	67.8
56.8	56.8
67.8	67.9
34.6	35.7
33.8	42.5
32.6	34.7
78.9	79.9
65.7	66.8
103.6	107.6
102.6	110
119.7	120.3
102.7	108.5
109.7	110
89.8	90.4
56.9	62.4



**Appendix E: TABLE OF INDOOR ²²²Rn LEVELS IN DIFFERENT
TYPES OF DWELLINGS**

Dry season						Rainy season					
CM1	CM2	CM3	CM4	CM5	CM6	CM1	CM2	CM3	CM4	CM5	CM6
25.8	34.6	99.7	34.7	54.2	41.8	27.6	35.7	100.4	36.3	63.4	41.9
34.7	33.8	92.3	26.7	35.6	52.6	36.5	42.5	98.4	29.7	35.7	53.7
26.9	32.6	94.7	33.7	55.6	40.8	32.4	34.7	100.4	36	63	41.8
24.5	78.9	98.7	34.7	67.5	55.8	26.6	79.9	100.9	42	71.3	58.9
25.6	65.7	95.6	25.7	78.9	89.7	27.8	66.8	97.4	27.9	79	90.9
24.7	103.6	97.7	45.9	100.9	78.4	28.6	107.6	110	54	110	78.6
26.5	102.6	96.7	46.8	24.6	75.6	32.5	110	98.8	53.6	25.3	75.7
24.6	119.7	87.6	47.6	110.7	67.9	24.7	120.3	90.3	53.6	119.4	68
25.6	102.7	67.8	45.8	89.4	79.6	27.4	108.5	71.3	48.9	92.8	79.8
24.8	109.7	65.8	46.8	108.6	70.9	25.7	110	65.8	49.4	110.5	72.6
24.7	89.8	78.9	34.8	107.8	57.9	26.4	90.4	89.8	37.5	110.6	57.9
28.9	56.9	67.8	26.8		59.5	31.4	62.4	67.8	29.5		60.1
58.6	110.7	56.8	72.8		25.5	58.7	111.8	56.8	72.8		56.3
26.1	124.7	67.8	55.8		34.5	26.2	124.9	67.9	55.9		63.4
31.1	101.6	56.9	51.8		33.9	32.3	102.8	57.8	52		54.5
	115.8	76.9	56.8		31.7		115.9	78.9	56.9		45.6
	89.5	120.5	24.9		24.5		93	120.9	25.7		32.5
	102.5	117.6	34.3		34		110	117.9	43.4		45.2
	104.8	79.8	56.5		45.7		114.7	79.9	59.3		48.8
		91.7	34.8		54.2			92.8	36.3		54.9
		110.8	35.7					110.9	38.8		
		73.7	24.5					74.9	26.5		
		55.5	24.2					56.5	24.6		
		88.9	39.3					93.8	45.4		
			28.6						24.5		
			36						37.5		
			23.5						24.5		
			23.7						25.6		
			28.1						31.7		
			54.8						55.8		
			67						67.9		

Appendix F: TABLE OF INDOOR ^{222}Rn LEVELS IN DIFFERENT LOCATIONS IN TSAKPA

Dry Season			Rainy Season		
Bedroom	Sitting	Kitchen	Bedroom	Sitting	Kitchen
75.6	24.20	55.80	75.7	24.6	55.9
79.6	24.90	45.90	79.8	25.7	54
70.9	23.70	46.80	72.6	25.6	53.6
59.5	25.70	47.60	60.1	27.9	53.6
110.8	24.50	45.80	110.9	26.6	48.9
73.7	25.6		74.9	27.8	
45.7	24.6		48.8	24.7	
52.6	25.6		53.7	27.4	
40.8	24.8		41.8	25.7	
55.8	24.7		58.9	26.4	
34.7			36.3		
26.7			29.7		
33.7			36		
34.7			42		
39.30			45.4		
25.50			56.3		
31.70			45.6		
26.90			32.4		
46.80			49.4		
34.80			37.5		
26.80			29.5		
25.80			27.6		
34.70			36.5		
26.5			32.5		
24.7			28.6		

**Appendix G: TABLE OF INDOOR ²²²Rn LEVELS IN DIFFERENT
LOCATIONS IN AGBENOXOE**

Dry Season			Rainy Season		
Bedroom	Sitting	Kitchen	Bedroom	Sitting	Kitchen
124.7	28.60	72.8	124.9	24.5	72.8
89.7	23.50	56.80	90.9	24.5	56.9
67.9	31.10	88.9	68	32.3	93.8
117.6	24.50	58.6	117.9	32.5	58.7
91.7	34.00	76.9	92.8	45.2	78.9
104.8	32.6		114.7	34.7	
108.6	56.9		110.5	57.8	
41.8	34.6		41.9	35.7	
55.5	28.9		56.5	31.4	
67	33.8		67.9	42.5	
99.7			100.4		
92.3			98.4		
94.7			100.4		
98.7			100.9		
95.6			97.4		
97.7			110		
96.7			98.8		
87.6			90.3		
67.8			71.3		
65.8			65.8		
78.9			78.8		
67.8			67.8		
56.8			56.8		
67.8			67.9		
78.9			79.9		

**Appendix H: TABLE OF INDOOR ²²²Rn LEVELS IN DIFFERENT
LOCATIONS IN TORKOR**

Dry Season			Rainy Season		
Bedroom	Sitting	Kitchen	Bedroom	Sitting	Kitchen
110.7	24.5	51.80	111.8	26.5	52
78.4	36.00	54.8	78.6	37.5	55.8
101.6	28.10	54.2	102.8	31.7	54.9
57.9	26.10	54.2	57.9	26.2	63.4
79.8	34.50	55.6	79.9	63.4	63
107.8	33.90		110.6	54.5	
120.5	34.3		120.9	43.4	
115.8	34.8		115.9	36.3	
67.5	35.7		71.3	38.8	
78.9	35.6		79	35.7	
100.9			110		
24.6			25.3		
110.7			119.4		
89.4			92.8		
89.5			93		
56.5			59.3		
102.5			110		
65.7			66.8		
103.6			107.6		
102.6			110		
119.7			120.3		
102.7			108.5		
109.7			110		
89.8			90.4		
56.9			62.4		

**Appendix I: TABLE OF ANNUAL INDOOR RADON LEVELS IN
TORKOR, AGBENOXOE AND TSAKPA**

Torkor	Agbenoxoe	Tsakpa
26.5	26.6	21.7
36.8	22.5	42.4
29.9	31.7	24.7
36.2	28.5	40.9
49.0	39.6	38.7
44.2	99.8	47.3
119.2	101.6	53.2
127.9	41.9	41.3
115.9	72.8	57.4
51.9	56.9	55.9
111.3	104.8	25.3
88.7	90.8	75.7
102.2	58.0	79.5
57.9	103.8	71.8
89.9	92.3	59.2
55.3	56.0	110.9
63.6	67.5	74.3
68.8	91.4	45.5
45.7	100.1	28.2
59.3	90.4	47.4
69.4	97.6	38.4
88.6	99.8	56.8
105.5	96.5	50.0
24.9	103.9	50.2
125.1	125.9	50.6
91.1	89.0	117.9
91.3	69.6	48.1
48.9	65.8	36.2
57.9	78.9	28.2
45.6	67.8	46.7
37.3	56.8	35.6
106.3	67.9	29.7
66.3	57.4	25.6
105.6	77.9	26.7
106.3	30.2	26.7
122.7	58.7	29.5
105.6	35.2	24.7
119.9	38.2	26.5
90.1	33.7	45.7
89.7	79.4	25.6

Appendix J: LIST OF PUBLICATIONS AND CONFERENCE PRESENTATIONS

Paper submitted to Radiation Protection Dosimetry:

Manuscript ID: RPD-23-0043

Title: Assessment of natural radioactivity, radon gas, and soil characteristics along the Volta Lake in the Kpando Municipality of Volta Region, Ghana.

Paper submitted to PLUS ONE:

Manuscript ID: PONE-D-23-14119

Title: Assessment of indoor radon distribution and seasonal variation within the Kpando municipality of Volta Region, Ghana.

Conference Poster Presentation: AFRIRPA O6, 6TH African IRPA Congress, 10 – 13 October, 2022, Accra – Ghana.

Title: Studies of indoor radon levels within Kpando Communities in the Volta Region of Ghana.

